ENGINEERING OXYGEN TRANSPORT FOR IMPROVING CELL PERFORMANCE IN HEPATIC DEVICES

by

Gengbei Shi

A dissertation submitted to the faculty of
The University of North Carolina at Charlotte
in partial fulfillment of the requirements
for the degree of Doctor of Philosophy in
Mechanical Engineering

Charlotte

2012

Approved by:

_____
Dr. Robin N. Coger

_____
Dr. Mark G. Clemens

_____
Dr. Charles Y. Lee

_____
Dr. Praveen Ramaprabhu

_____
Dr. Thomas A. Schmedake

ABSTRACT

GENGBEI SHI. Engineering oxygen transport for improving cell performance in hepatic devices (Under the direction of Dr. ROBIN N. COGER and Dr. CHARLES Y. LEE)

The bioartificial liver (BAL) advancing medical technology aims to provide temporary liver substitution for patients in dire need of liver transplants and also for drug development. Yet despite nearly fifty years of development, the approval for this medical device from U.S. regulatory agencies (e.g., Food and Drug Administration) is still pending. The reasons for this have both clinical and fundamental aspects. Current clinical trial data does not convincingly demonstrate a higher survival rate of patients that received BAL treatment than non-BAL treated control. This issue may be attributed to the fundamental fact that, as a medical bioreactor, BALs still lack the effectiveness at the level of the natural liver. As oxygen (O_2) is a key substance to determine efficiency of the hepatocytes housed in the BAL, intensifying the O_2 conditions within the BAL cellular space will elevate overall BAL performance. This proposition has been substantiated by several studies. With higher efficiency the BAL may increase the liver patients' survival rate, benefit new drug development, and may ultimately attain the government approval in the U.S.

The work of this doctoral study focuses on methods of enhancing O_2 transport into three-dimensional (3D) customized hepatic devices. Firstly, enriched O_2 conditions were established within customized hepatic systems by applying an inert organic compound – perfluorocarbon (PFC). The PFC-treated hepatic cells demonstrated high cytochrome P450 (CYP 450) function performance especially when 3D gelatin sponge were used as the scaffold. They also exhibited less glucose consumption. Next the 3D

gelatin sponge scaffold was then characterized in a computational fluid dynamics (CFD)-based simulation to clarify the reasons for the performance improvement. The results of this simulation also suggest that using the new 3D cellular scaffold is an effective method for addressing the O_2 delivery problem previously reported for a novel BAL design, the four quadrant bioreactor (4QB) when using the 4QB for the support of larger cell numbers. Lastly, the effects of a previously custom designed flow device and the gelatin sponge scaffold, on the drug metabolism of rat primary hepatocytes (RPHs) were evaluated. The key results from the drug metabolism tests were confirmation of the benefits of combining the 3D gelatin sponge scaffold and flow condition in increasing the hepatocytes drug metabolism enzyme performance. Surprisingly, the results also demonstrated the suppression of the RPHs drug metabolizing ability in flow devices and relevant analysis to this phenomenon was also conducted.

This doctoral study has thus provided valuable information on experimental and numerical approaches for improving the fundamental performance of future BAL designs. It mainly highlights that in BALs, the 3D cell cultures and efficient flow perfusion are key to O_2 delivery for the scaffold interstitial region (extracellular space). The work thus helps moving toward their development one step closer to establish the future clinical trial and industrial application of BAL devices.

ACKNOWLEDGMENT

First and foremost I give my deep gratitude to my main Ph.D advisor Dr. Robin Coger. As a role model to students and the Harshini V. de Silva Graduate Mentor Award winner, all her great shining aspects in a mentor's personality: the curiosity, diligence and commitment to scientific research, the devotion to service as former director of the Center for Biomedical Engineering and Science (CBES, formerly Center for Biomedical Engineering Systems) and to service as former interim chair of Mechanical Engineering department in UNC Charlotte, the sense of responsibilities to general daily work affairs, the openness to all kinds of discussions in not only study but life, the patience on listening to speech of any international student that has a vastly distinct culture background and so forth, strongly inspired me, encouraged my whole Ph.D study and will resume to impact my life post-graduation. I would also like to give sincere thanks to my co-advisor Dr. Charles Lee, who continuously and selflessly provided valuable guidance, dedication of time and manuscript review, animal surgery assistance and lab-cost material support during mentoring the rest time of my Ph.D study.

To the rest of my committee members: Dr. Mark Clemens, Dr. Tom Schmedake and Dr. Praveen Ramaprabhu, I would like thank you for your mentoring and support along the odyssey, for your dedication on reviewing, your valuable comments and advices to revise this dissertation into a better one.

The group my special thanks given to certainly also include many other people – without their help accomplishing this dissertation is impossible. They are: my lab member Balasubramanian Karthik Kumar, former lab members Dr. Mei Niu, James P. Cassell and Umar Faraz for their stimulating discussions and assistance in many days and

nights of the past 6 years; Marvaleeta Blye for her assistance in student-related business and conference paperwork preparation; Cathy Culberson and Eric Norris in Dr. Clemens lab for their general guides on liver biology assays and isolation surgery; Dr. Nilay Chakraborty for his assay training, career advice as a friend, Dr. Aniket for the dissertation proofreading and mental support as a friend too; Dr. Martin Garry Hodgins, Franklin Green, Dr. James Miller and Karthik Muthuraman from the Department of Mechanical Engineering and Engineering Science for their experimental and numerical techniques assistance, Dr. Helen Gruber and Gretchen Hoelscher in Carolina Medical Center for their techniques assistance, Dr. Richard Kiral of Oxygen Biotherapeutics Inc. for supplying the Oxycyte® PFC product,.Dr. James H. Kelly of Stem Cell Innovation Inc. for his responses to technical inquiries, Jonathan Halter and Dr. Charles Price of UNC Charlotte's Campus Computing for cluster usage support and ANSYS FLUENT configuration on the parallel computing cluster, Jennifer Shoe for her isolation surgery and fine lab maintenance.

Finally I would conclude this acknowledgement by thanking the financial supports from National Institute of Health (NIH #1R21 EB004982-01A11), travel grant from the Center for Biomedical Engineering and Science (formerly Center for Biomedical Engineering Systems) of UNC Charlotte, as well as UNC Charlotte Graduate Assistant Support Plan (GASP) award. All this work cannot be accomplished without these aids.

DEDICATION

To my beloved parents, Chen Lihua and Shi Bolong.

TABLE OF CONTENTS

LIST OF TABLES

LIST OF FIGURES

LIST OF ABBREVIATIONS

3-MC	3-Methylcholanthrene
7-HC	7-Hydroxycoumarin
ANOVA	Analysis of variance
BALs	Bioartifical liver devices
CFD	Computational fluid dynamics
CFL	Courant-Friedrichs-Lewy
CYP450	Cytochrome P450
DMEM	Dulbecco's modified eagle medium
DMEs	Drug metabolism enzymes
DO	Dissolved oxygen
ECOD	7-ethoxycoumarin-O-deethylase
EGF	Epidermal growth factor
ELISA	Enzyme-linked immunosorbent assay
ER	Ethoxyresorufin
EROD	7-ethoxyresorufin-O-deethylase
FBS	Fetal bovine serum
FHF:	Fulminant hepatic failure
HPHs	Human primary hepatocytes
LETFs	Liver enriched transcriptional factors

MAP	Metabolicly active population
MEM	Minimum essential medium
mRNA	messenger ribonucleic acid
NADH	Nicotinamide adenine dinucleotide, reduced
NADPH	Nicotinamide adenine dinucleotide phosphate, reduced
OLT	Orthotopic liver transplant
OUR	Oxygen uptake rate
pO_2	Oxygen partial pressure
PAHs	Polycyclic aromatic hydrocarbons
PFCs	Perfluorocarbons
PFOB	Perfluorooctyl bromide
PPHs	Porcine primary hepatocytes
PTBCH	Perfluoro-t-butylcyclohexane
PTFE	Polytetrafluoroethylene
RPHs	Rat primary hepatocytes
TCDD	2,3,7,8-Tetrachlorodibenzo-p-dioxin
UV	Ultraviolet

LIST OF SYMBOLS

Symbol	Description	Unit
$[O_2]$	O_2 concentration	kg O_2/kg mixture
C_1, C_2, C_3, C_4	notations of computational layers in cartridge space	-
C_{ij}	the *i*-*j*th components of coefficient matrix C	-
D_0	O_2 diffusivity in free medium	m^2/s
DO_{in}	O_2 concentration at inlet	mg/L
DO_{out}	O_2 concentration at outlet	mg/L
D_c	rat hepatocytes intracellular O_2 diffusivity	m^2/s
D_s	O_2 diffusivity at air-water interface	m^2/s
D_e	effective O_2 diffusivity in porous material	m^2/s
D'_e	cell presence-modified effective O_2 diffusivity	m^2/s
D_{ij}	the *i*-*j*th components of coefficient matrix D	-
$\vec{F}$	body force (vector)	N (with direction)
K_{T_0}	Henry's constant at temperature T_0	mol/(L·atm)
K_T	Henry's constant at temperature T	mol/(L·atm)
K_c	collagen permeability	m^2
K_g	Gelatin sponge permeability	m^2
K_M	Michaelis-Menten constant (O_2 concentration when the OUR is half V_{max})	kg O_2/kg mixture or mmHg
K_m	Membrane permeability	m^2
l_s	air-water O_2 exchange surface layer thickness	m
$\dot{M}$	Medium mass flow rate	kg/s

R_h	O_2 hydrodynamic radius	m
R_{max}	maximum lumen radius	m
R_{min}	minimum lumen radius	m
S_{O_2}	volumetric O_2 uptake rate	kg/(s·m^3)
S_m	mass source	kg
$\dot{V}$	medium volumetric flow rate	cm^3/s
V_{max}	maximum OUR that can be achieved	kg/s
k_B	Boltzmann constant	J/K
$\bar{u}$	average velocity	m/s
$\vec{u}$	velocity (vector)	m/s (with direction)
x_g	gas volume fraction in a gas-liquid system	-
x_l	liquid volume fraction in a gas-liquid system	-
μ_0	Viscosity of an emulsion's continuous phase	kg/(m·s)
μ_1	Viscosity of an emulsion's dispersed phase	kg/(m·s)
μ_e	Effective viscosity of an emulsion	kg/(m·s)
ρ_{cell}	cell density	10^6/m^3
ρ_l	density of liquid phase	kg/m^3
ρ_m	medium density	10^3kg/m^3
τ_{max}	maximum shear stress	Pa
τ_{min}	minimum shear stress	Pa
ϕ_c	cell volume fraction in collagen space	-
ϕ_c	rat hepatocytes volume fraction in collagen space	m^3

ΔL	the distance fluid flows through	m
ΔP	the pressure difference along ΔL fluid flows through	Pa
Δt	time step	s
$\Delta x, \Delta y, \Delta z$	segments at x, y, z direction in Cartesian coordinate	m
∇	gradient operator	-
Δn	Membrane thickness	μm
ϕ	Volume fraction (PFC, collagen fiber etc.)	-
A	cross-sectional area	m^2
C	constant	-
Cou	Courant number	-
N	cell population	10^6
Q	volumetric flow rate	m^3/s
R	lumen radius	m
S	momentum source	kg·m/s
T	temperature	K
a	PureCol® collagen fiber diameter	nm
b	Collagen average pore size	μm
g	gravitational acceleration	m/s^2
k	geometric factor	-
r	radial distance from lumen axis	m
t	time	s
u, v, w	Velocities (scalar) at x, y, z directions in Cartesian coordinate	m/s

U	velocity vector	m/s
α	proportionality	-
ε	porosity of collagen, $\varepsilon + \phi = 1$	-
μ	dynamic viscosity	kg/(m·s)
ρ	Density (general)	kg/m^3
ω	saturated oxygen mass fraction in aqueous medium	ppm (10^{-6})
τ	shear stress matrix for 3D case	Pa

CHAPTER 1: INTRODUCTION

Liver is the largest internal organ in human body[1] that performs multiple essential functions to sustain an individual's life[2]. For example, it synthesizes albumin which is a protein in serum modulating blood oncotic pressure[3], produces urea to cleanse ammonia as part of human body nitrous metabolism, secretes bile to facilitate fatty acid digestion, composes or decomposes glucose to store or release energy, detoxifies heavy metal ions and xenobiotics such as drugs and toxins[4], et cetera. These vital functions are vulnerable to liver injury and chronic or severe liver diseases, including hepatitis, cirrhosis or hepatoblastoma. When these pathological disruptions overwhelm the liver recovery rate, failure of this organ may occur. A devastating case is the fulminant hepatic failure (FHF, also: Acute Liver Failure), prognosis of which is difficult and has more than 50% mortality [5, 6]. Due to the dangerous situation that sepsis and multiple organ failure could be triggered via FHF, it is imperative to take all possible treatments to save the patient using immediate and effective methods.

To date, the most effective therapy to cure liver failure is to perform the orthotopic liver transplant (OLT)[5]. This requires one transplant recipient ideally to have one matched liver donor. However, the shortage of suitable liver donors continues to exclude this option for many liver patients [6, 7]. The discrepancy between number of donors and the patients is huge: based on OPTN (Organ Procurement Transplantation Network) data as of July 25, 2012 for United States, there are 15,997 patients on the liver transplant waiting list nationwide, while total patients successfully received liver

transplant surgery during year 2011 were merely 6,932. Animal liver (e.g., porcine liver) has greater availability and it seems to be a solution for this gap. However, transplantation across different species raises the regulatory agency's concern of graft biocompatibility and xenozoosis[8], leaving the problem unsolved.

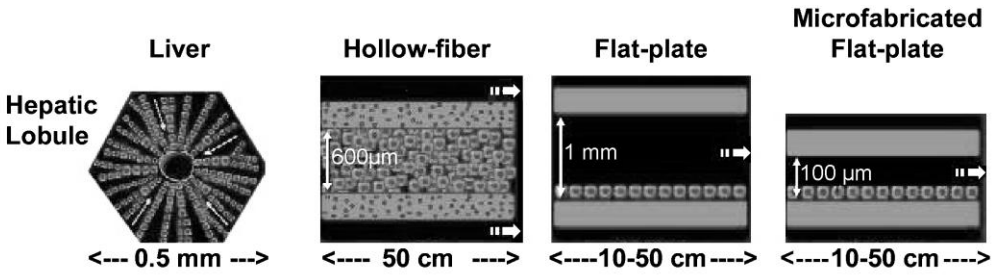

FIGURE1.1 Natural liver structure and several configurations of popular BALs, comparisons of their cell number, density (in terms of "cell number/blood or medium volume"), transport area and cell fraction on surface. Reproduced from [9].

This medical challenge drives scientists and engineers to find an alternate solution to bridge patients who are waiting for liver replacement, or their own liver to recover. Such an artificial organ surrogate must firstly mimic natural liver functions at competitive levels. It should also have stable manufacturability and independent of limited human liver resources[8]. Depending on whether there are biologically viable cells present, this type of "hepatic assist device" (or "liver support system") can be divided into two subgroups: artificial liver devices, or bioartifical liver devices (BALs). For the cell-free

artificial liver, dialysis, filtration and adsorption are mainly the techniques that had been used for toxin clearance. Because of its many shortcomings (e.g., causing thrombocyte loss and coagulation disorder, unable to remove protein-bound or hydrophilic toxins, unable to perform synthetic function [10, 11]), research advanced to develop a more complicated, cell-encapsulated system – the BALs. Since cells are present in BALs, such devices do not only have the ability to perform better detoxification, but they also can achieve synthetic and metabolic functions.

Various BAL prototypes have been fabricated, where designs feature direct perfusion, flat membrane, or hollow fiber exchange (Fig. 1.1). Some promising candidates started to enter the stage of clinical evaluation and/or industrial collaboration. These milestones include the HepatAsssist™ device (Arbios Systems Inc., Allendale, NJ), the Extracorporeal Liver Asssist Device (ELAD®) (Fig. 1.2), the Bioartificial Liver Support System (BLSS™), and the Academic Medical Center Bioartificial Liver (AMC-BAL) [12]. Nevertheless, none of these BAL has successfully earned FDA approval. Thus far, the available clinical trial reports indicate that the designs failed to substantiate a significant improvement in FHF patients survival rate [12]. Limitations in the functional levels that a single device can achieve are considered one of the common reasons to this result. This may be due to the limited cell mass that each device can accommodate compared to the capacity of the natural liver (see total cell number comparison in Fig. 1.1). Given the limited space and cell mass that a single therapeutic device can house, the individual cell's mean efficiency determines the whole BAL's output.

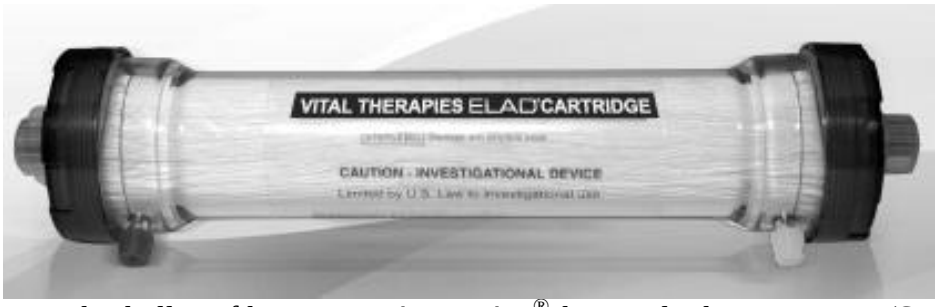

FIGURE1.2 The hollow fiber type BAL ELAD® by Vital Therapies Inc. (San Diego, CA). Using C3A hepatoma cell line, four of such cartridges with about total 800 g hepatocytes [11] were used in a pilot clinical trial starting from 2007 and containing 49 patients in China [12]. Image courtesy: Vital Therapies Inc. official website.

Recalling that the liver is the main site for drug metabolism in the human body, pharmaceutical industries will also benefit from successful BALs[13-15]. Conventional drug screening relies heavily on *in vitro* static multi-well plate cell culture and animal models. However, though effective in phase I drug metabolism, static primary hepatocyte cultures lack further predictability in phase II drug metabolism and clinical trials, partly because human physiological environment such as three-dimensional (3D) cell architecture, blood flow perfusion, and signal transductions from extrahepatic organs are absent in this simple model [16]. While animal models (rodents, pigs, monkeys etc.) with integral physiological systems are applied, they do not guarantee successful screening due to the genetic difference. Both conventional screening methods have cases that failed in the later stage drug developing pipeline, resulting costly withdrawal of drug candidates[8, 16].

BALs that integrate hepatic cells (either hepatocytes alone, or multi-type co-culture) are designed to perform drug clearances that mimic the natural liver and its preliminary drug screening effectiveness was demonstrated by several studies [14, 17, 18]. The effectiveness could be attributed to BAL's many features that are absent in other

methods: for example, static plate culture using in conventional drug screening does not have blood perfusion-like flow condition, which encourages hepatocytes functionality. Besides, BAL's 3D configuration easily enables the multi-cell type co-culture as in natural liver, which is important to regulate hepatcoytes function (e.g., co-culturing Kupffer cells which mediates hepatocytes functioning via cytokine)[19, 20]. Minimally, BALs as drug testing devices should help predict the cytotoxicity of drugs and the long-term goal focuses predicting hepatoxicity (organ-level). It is believed that with further optimization and experimental efforts, the BALs will emerge and recognize as cost-effective *in vitro* drug testing devices. One example of a product candidate is the multi-well plate BAL device with pneumatic force-driven flow [16, 21] that is currently developed for commercialization by HemoShear, LLC (Charlottesville, VA).

Regardless of its medical or pharmaceutical application, the BAL's functional output level is the key to success. In the natural liver, hepatocytes are in spheroidal shape and attached to surrounding extracellular matrix [22]. For many comprehensive metabolic tasks they have an aerobic profile with high oxygen (O_2) uptake rates (OUR) [23]. Molecular O_2 is essential as it mediates many fundamental aspects of liver metabolism [24]. It is the electron receptor in phosphorylation cycles that provides energy[25]. O_2 is also the oxidant for the key step of drug and steroids hydroxylation that facilitates drug excretion[25, 26]. O_2 delivery to hepatocytes is achieved by the natural O_2 carrier – hemoglobin – within erythrocytes, the highly organized hepatic sinusoids architecture (Fig. 1.1: hepatic lobule) and hepatic vasculature. The hepatic cellular component as BALs functioning portion also has high O_2 demand. Besides aforementioned O_2 importance, increased O_2 also magnifies hepatocytes attachment and

spreading area of *in vitro* culture [27]. BAL mainly used aqueous medium in circulation for nutrient and O_2 supply, whereas the aqueous medium has a low O_2 solubility[28] and O_2 also has a short diffusion distance within[29, 30]. Artificial vascularization in 3D tissue equivalent of BAL could help better O_2 delivery. But this technique is a challenge too[31]. Thus, O_2 transport in current BALs is still inadequate and far from clinical use[32]. Helping to solve this problem becomes the objective of this dissertation.

In this dissertation, the functional responses and viability of HepG2/C3A hepatoblastoma cell line and primary rat primary hepatocytes (RPH) at different O_2 levels in flow-perfused 3D cultivation were investigated. Also, the underlying O_2 interstitial transport in conventional cell scaffold and its replacement have been numerically simulated to reveal the material-dependent mechanistic control for O_2. Specific to each chapter, in CHAPTER 2 and 3, the O_2-dissolving capability of a commercial perfluorocarbon O_2 carrier "Oxycyte®" has been characterized and it was supplemented to 3D thick flow-perfused C3A hepatoblastoma cell line culture. Chapter 2 results demonstrated that PFC-medium mixture with different PFC volume fractions can dissolve different O_2 contents. Chapter 3 results demonstrated that the PFC supplemented medium allowed each C3A cell to consume less glucose while synthesizing the same level of albumin as control in dynamic condition. The same condition – PFC-medium and dynamic flow condition – also encouraged cell population growth (7 times of PFC-free control at endpoint) under toxic drug inducer condition for cytochrome P450 activity assay. In CHAPTER 4, O_2 transport in the four quadrant bioreactor (4QB) was computationally simulated via ANSYS FLUENT®. The primary goal of the simulation was to identify how manipulating the scaffold affects O_2 diffusion to the RPHs

maintained in the 4QB on a computational basis. Results of this chapter indicate that while O_2 condition in 4QB at housing double cell population becomes inadequate, replacing the scaffold from collagen gel to gelatin sponge as well as doubling the flow rate can improve the O_2 level cells in 4QB receive. In CHAPTER 5, the use of two hepatic 3D bioreactors as initial drug screening devices was explored. Activities of two key drug metabolism enzymes (DMEs): ethoxycoumarin-O-deethylase (ECOD) and ethoxyresorufin-O-deethylase(EROD) of RPHs for each device were investigated in various culture configurations. These culture types include conventional multi-well sandwich, static 3D and 3D flow-perfusion cultures. Results of this chapter demonstrated the effectiveness of gelatin sponge and flow device on DMEs activities of RPH, and also suggested potential overdosing effects of medium volume changed in different flow devices compared to that in static culture. Overall, this dissertation explored three general ways to enhance O_2 transport for hepatic cells functional improvement: (1) by ECM manipulation (e.g., replacing collagen gel with gelatin sponge) for allowing more O_2 delivered to cellular space, (2) by medium supplementation (e.g., adding PFC to aqueous medium) for carrying more O_2 in hepatic device circulation, and (3) by flow device design to regulate flow pattern and deliver O_2 into interstitial space more effectively (e.g., ineffective circumventing flow pattern in plate device compared to effective perfusion flow pattern in tube device). The methods investigated in this dissertation can be modified and applied to more other BAL devices, for their functional improvement and potentially better therapeutic efficacy.

CHAPTER 2: THE OXYGEN CAPCITIES OF PERFLUOROCARBON-SUPPLEMENTED MEDIUM AT DIFFERENT CONCENTRATIONS

2.1 Introduction

As seeking engineering solutions to improve O_2 availability in BALs, perfluorocarbons (PFCs) are of great interest. PFCs are a family of highly inert compounds that were originally synthesized during World War II for the Manhattan project by replacing all hydrogen (H) atoms with fluorine (F) atoms [and possibly other halogen atom such as bromine atom in PFOB (perflubron)[*]] in hydrocarbons (C_nH_m). Because PFCs have extraordinary O_2 solubility due to their molecular affinity for O_2 [33-38], they are utilized in clinical applications [39, 40] such as the partial liquid ventilation for patients with respiratory disease [41]. They have even been used in diagnostic imaging [42]. When used in *in vitro* cell cultures, a variety of effects have been reported: for non-hepatic cell cultures, one of the PFCs – PFOB – "permanently inhibited human fibroblast cell proliferation and decreased mitochondrial activity" when added to culture medium[43]. In addition PFOB was found to "attenuate oxidative damage" for rat pulmonary artery endothelial cells[44]. Another PFC – perfluorodecalin[†] – was shown to have positive effects on the human Hela cell line [45]. In hepatic culture studies of rat primary hepatocytes (RPH) cultivated in PFOB-embedded collagen gel, albumin secretion, ureagenesis (for the first 24hours) and CYP1A1 activity of were improved [34]. Contrastingly, the glycolytic activities of porcine primary hepatocytes (PPH) treated by

i. [*] PFOB (perflubron): perfluorooctyl bromide, $C_8F_{17}Br$
ii. [†] perfluorodecalin: $C_{10}F_{18}$

PFOB in a bioreactor were lower than its control [46]. When the HepG2 hepatoblastoma cell line was treated by PFTBA[‡]-PFOB blend, increased cell growth rate and improved glucose utilization were discovered[36]. It was also reported that HepG2 cells had 47-104% higher metabolic activity in PFOB-encapsulated alginate matrix[47]. The promise of these studies founded the basis for investigating the effects of a PTBCH[§]-based, second generation O_2 carrier "Oxycyte®" on hepatic cells as a possible way to further enhance O_2 transport in BALs. To achieve this, it was first necessary to characterize its O_2 dissolution profile.

2.2 Materials and Methods

2.2.1 PFC Fraction and O_2 Concentration Calibration

The Oxycyte® PFC emulsion (Oxygen Biotherapeutics, Durham, NC, formerly "Synthetic Blood International", Costa Mesa, CA) contains 60% (w/v) PTBCH plus other supplements (Tab. 2.1, because PFCs are hydrophobic and thus immiscible in water, for use they are emulsified by surfactant, e.g., egg phospholipid). Previously this commercially prepared PTBCH product was used in treatment for rat brain injury [48], or as the perfusate in cardiopulmonary bypass machines [49, 50]. Positive effect of rat cognitive function improvement was reported, but adverse effect such as increased rat inflammatory reaction did appear too.

iii. [‡] PFTBA : perfluorotributylamine , $C_{10}F_{21}N$
iv. [§] PTBCH: perfluoro-t-butylcyclohexane, $C_{10}F_{20}$

TABLE 2.1. Percentage of main ingredients in Oxycyte®[51].

Essential Oxycyte® ingredients	Function	% (w/v)
PTBCH	effective ingredient	60
egg yolk phospholipid	surfactant/emulsifier	-

TABLE 2.2. Actual PTBCH weight/volume fractions (w/v) in 0%, 5% and 10% PFC-media

% Oxycyte® (v/v)	% PTBCH (w/v)	% PTBCH (w/v) in tested media
0	60	0
5	60	3
10	60	6

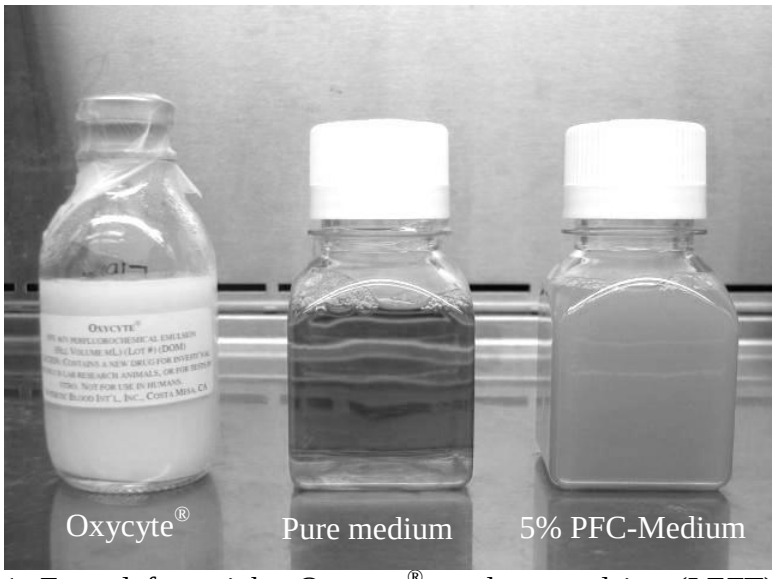

FIGURE 2.1. From left to right: Oxycyte® product emulsion (LEFT); pure 10% FBS supplemented MEM-based cell culture medium (MIDDLE), and such medium supplemented with 5% Oxycyte® (RIGHT).

To quantify the effects of PFCs on the quantity of O_2 aqueous solutions can dissolve, a series of calibration experiments were completed: emulsions of 0%, 5% and 10% (v/v) Oxycyte® PFC emulsions in normal cell culture medium were prepared. For the remainder of this study, 0%, 5% and 10% Oxycyte® (v/v) in media, will be referred to

as “0% PFC-medium” (or “normal medium”), “5% PFC-medium” and “10% PFC-medium”, respectively. The actual PTBCH weight/volume fractions for these three emulsions are shown in Tab. 2.2.

The dissolved O_2 (DO) concentrations of the PFC-media were measured at 37^{o}C using the single-loop flow circuit shown schematically in Fig. 2.2. As illustrated, 100 mL of the target PFC-media from reservoir (Fig. 2.2-b) in 37 ^{o}C incubator (Fig. 2.2-a) was pumped through a 95% O_2/5% CO_2 (Fig. 2.2-d) pressurized gas exchanger (Fig. 2.2-c), at the rate of 4.1 mL/minute using an Ismatec BVK peristaltic pump (Cole-Parmer, Vernon Hills, IL) (Fig. 2.2-e). This gas exchanger (Fig. 2.2-b) consists of a Pyrex® 500 mL glass bottle (Corning, Lowell, MA) with a threaded cap and a pair of press-fit gas inlet and outlet on the cap. A 0.5 m long, gas-permeable silicone tubing (inner diameter≈1.6mm) (Nalge Nunc, Rochester, NY) was coiled in the bottle. Conventionally used in sterile gas exchange, this tubing allows O_2 diffusion into the flowing liquid. Gas gauge pressure was adjusted at 50 kPa and gas influx is controlled by an air flow meter (Cole-Parmer, Court Vernon Hills, IL). Gas flow rate was initially set at 0.1 L/minute until equilibrated. Given ideal equilibrium the estimated absolute O_2 partial pressure (pO_2) inside the Pyrex® glass bottle was over 1000 mmHg. The DO value was measured using a polarographic AccumetXL60 DO meter (Thermo Fisher Scientific, Waltham, MA) with an electrolytic solution-filled, membrane-capped cell. For sampling, 5 mL of media from the bulk flow was released every 5 minutes (Fig. 2.2-f) beginning 1 minute after pump flow was initiated and read by the probe. The tested sample was returned to the circuit for volume maintaining. DO measurements continued until the readings approached steady state.

2.2.2 Media Viscosity Measurements

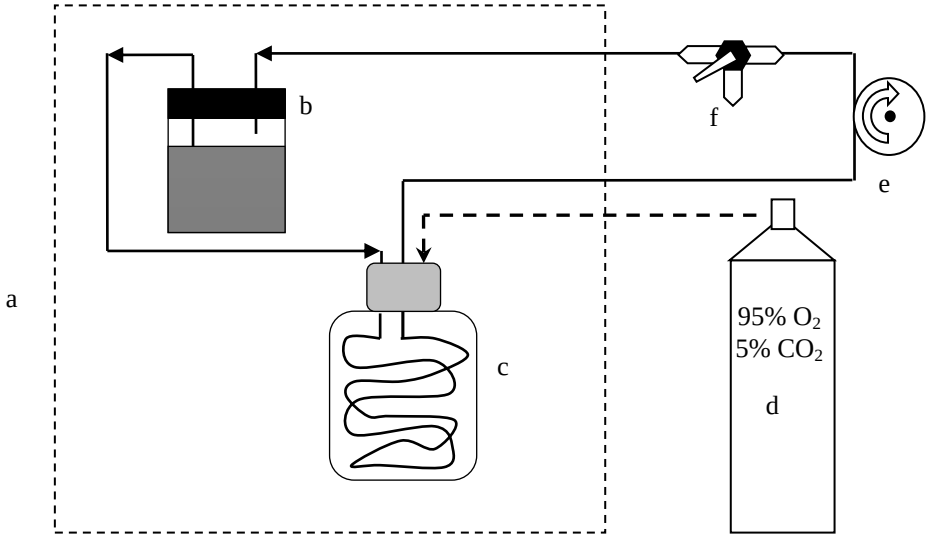

FIGURE 2.2. Schematic diagram of the flow circuit used to determine the DO characteristics of the PFC-medium emulsions: (a) Incubator; (b) PFC emulsion reservoir; (c) Gas exchanger; (d) O_2 tank; (e) Peristaltic pump; (f) Sampling point by a 3-way connector.

The viscosities[**] of 0%, 5% and 10% PFC-medium at 37^{o}C were measured using a Cannon-Fenske viscometer (Cannon Instrument, State college, PA). Sample temperature was maintained throughout the measurement using a 37^{o}C water bath.

v. [**] Viscosity is a physical property of fluid that measures the resistance to deformation of such fluid.

2.3 Results

2.3.1 Dissolved O_2 Concentration of PFC-medium

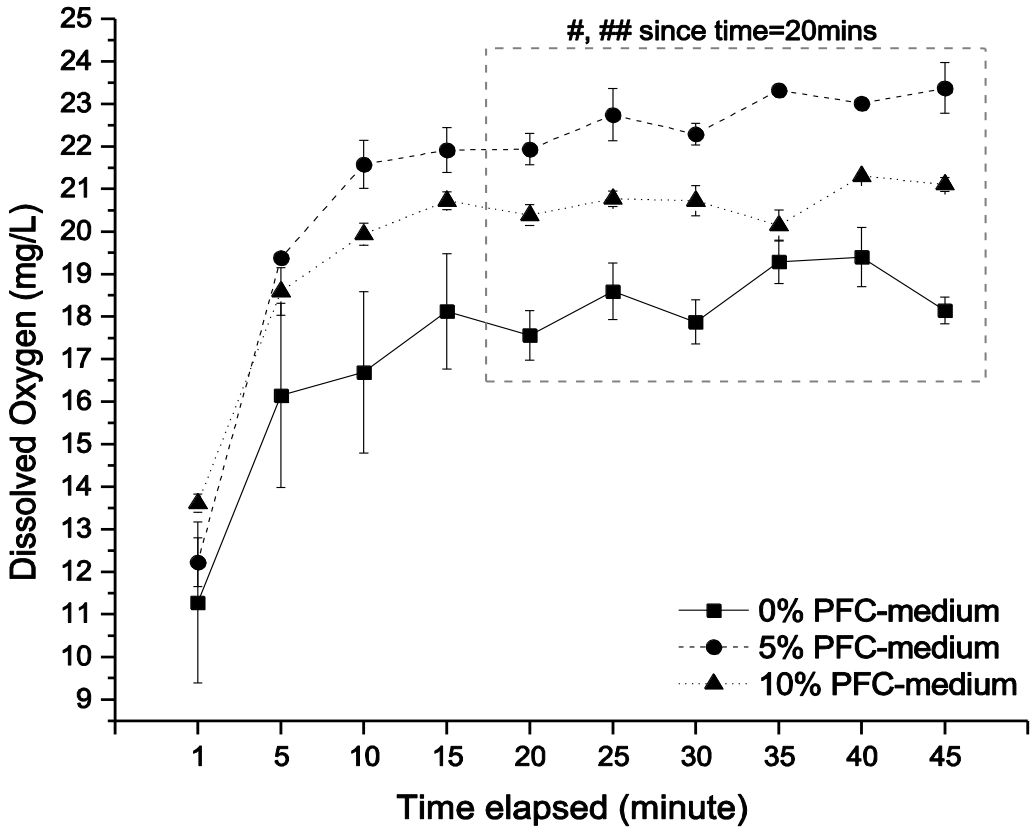

FIGURE 2.3. Dissolved O_2 characteristic curves of pressuring oxygenated PFC-media with different fractions of PFC at 37^{o}C. #:5%PFC >0%PFC at each data point in dashed-line box, $p<0.05$; ##: 5%PFC>10%PFC at each data point in box, $p<0.05$. n=3. Mean±SE.;

Before one could quantify whether PFC supplementation increases the functional performance of 3D hepatic tissue equivalents, it was first necessary to quantify the effects of PFC on the DO concentration of nutrient medium. The results of this are shown in Fig. 2.3. Of the three PFC concentrations indicated (0, 5, and 10% v/v PFC), 5% PFC-medium maintained the highest DO level for majority of the experiment's duration. As previous cell culture results indicated 10% PFC started to demonstrate cytotoxicity, 5%

PFC-medium will be the concentration to supplement medium in the associated cell function study (see CHAPTER 3). Surprisingly, Fig. 2.3 also indicates that the 10% v/v PFC fraction experienced a lower DO concentration than the 5% fraction under the same O_2-pressurizing condition. This could be due to other material properties affected by the PFC volumetric fractions. Therefore the viscosities of the 3 PFC emulsions based on medium and water were measured and results were graphed in Fig. 2.4. In this figure, 10% PFC-medium is the most viscous solution of the three, while the viscosity of 5% PFC-medium is fairly indistinguishable from that of normal medium (0% PFC).

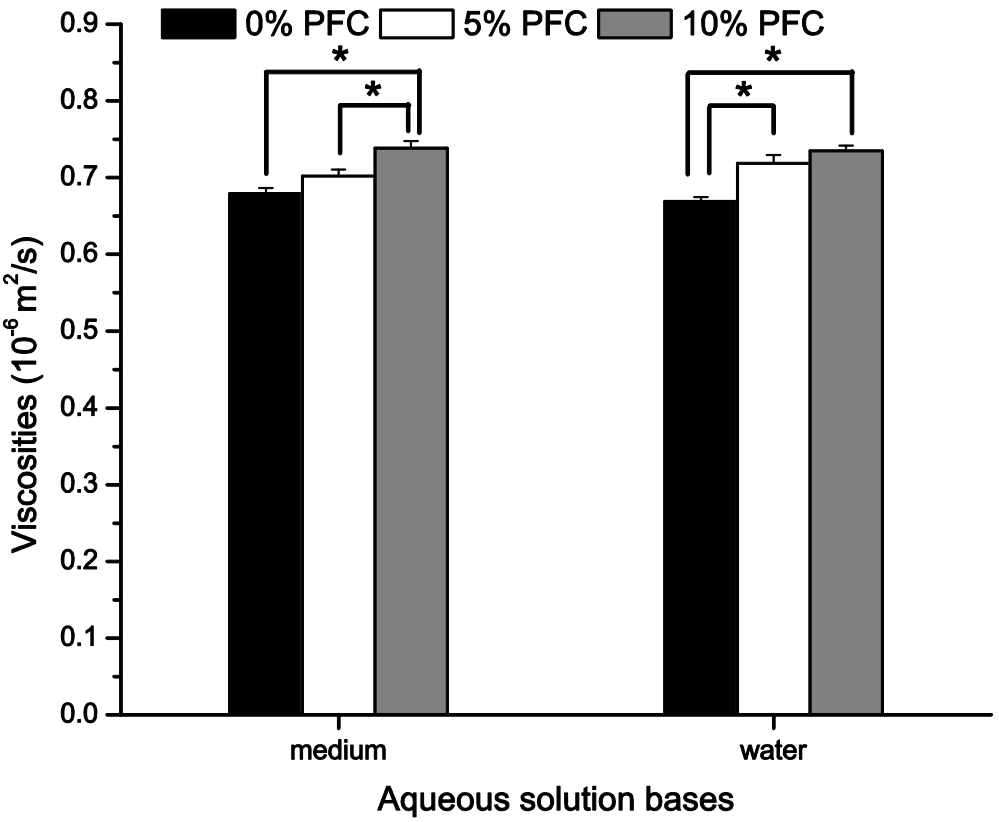

FIGURE 2.4 Viscosities of 0%, 5% and 10% (v/v) PFC-medium and PFC-water at 37ºC.*: $p<0.05$. n=3. Mean±SE

2.4 Discussion

The O_2 capacities of three PFC-medium concentrations were quantified within this study (Fig. 2.3). This is the first time this has been measured for a commercially prepared PFC product Oxycyte®. A PFC product – Oxygent® – in perfusate at concentration 6.4% (v/v) were computationally predicted to increase delivered O_2 than 3.2% PFC supplemented perfusate [52]. Another PFC (species not specified) numeric model in hepatic hollow fiber bioreactor predicted that O_2 transfer flux in bioreactor increases with climbing PFC volume fraction [53]. These simulated results seemingly suggest that larger PFC volume fractions necessarily result in higher O_2 capacities of the overall emulsion. While these models considered the viscosities, their impact on the dissolved O_2 concentration of the perfusate was overlooked.

The immiscible PFC disperses as nanodroplets in aqueous medium [43], forming a biphasic emulsion system. Thus mathematical relation between its volume fraction and the overall viscosity for a dilute emulsion is [54, 55]:

$$\frac{\mu_e}{\mu_o} = \frac{1}{1 - \sqrt[3]{\phi}} \qquad (2.1)$$

where μ_e is the effective viscosity of emulsion, μ_o is the viscosity of the continuous phase (e.g., aqueous medium), and ϕ is the volume fraction of dispersed phase (e.g., PFC). A more complex representation – Taylor's equation – describes this relation as [56]:

$$\frac{\mu_e}{\mu_o} = 1 + \left(\frac{\mu_o + \frac{5}{2}\mu_1}{\mu_o + \mu_1} \right) \phi \qquad (2.2)$$

where μ_1 is the viscosity of dispersed phase (i.e., viscosity of PFC). Both equations indicate that PFC-medium viscosity is expected to increase with PFC additions. This theory is substantiated by the results of Fig. 2.4. Connecting this to the results of Fig. 2.3-a suggests that the statistically significant viscosity increase of the 10% (v/v) PFC-medium, as compared to 5% v/v, interferes with its O_2 solubility. This conclusion is consistent with work reported for the custom PFC emulsion "Fluroxygen", where the 25% volume fractions did not achieve higher O_2 solubility than the 15% limit [57]. Similar phenomenon was also reported in fermentation process when the viscosity of fermenting liquid increases[58, 59]. It was believed the increased viscosity adversely slows down water-PFC interfacial O_2 exchange rate. This transport impedance is believed subsequently curtailing the overall O_2 delivery efficiency and O_2 solubility in emulsion [57]. However, such interfacial O_2 exchange rate was regarded not obstructed in previous modeling analysis and thus led to totally different conclusions [52, 53].

Further investigation of mass transfer in emulsion elaborates why viscosity thresholds O_2 transfer efficiency. The biphasic mass transfer of a single viscous droplet (dispersed phase) moving in continuous-phase liquid was numerically modeled [60]. The results showed as the viscosity ratio μ_e/μ_o in Eqn. 2.1&2.2 (specifically $\mu_{\text{PFC-medium}}$ / $\mu_{\text{pure medium}}$in this study) increases, the overall convective mass (including O_2) transfer (represented by Sherwood number[††]) decreases [‡‡][60]. Such limited O_2 convective transfer hinders PFC O_2 transport efficiency. As a result, more viscous PFC-medium will have a lower O_2 transfer rate.

vi. [††] Sherwood number is the ratio of convective mass transfer coefficient to the diffusive mass transfer coefficient.

vii. [‡‡] Given Reynolds number[‡‡] (Re) and Péclet number[‡‡] remain constant within the range Re < 1000, Pe <500, as premises.

Another cause for the 5% and 10% PFC-media DO difference in results of Fig. 2.3 could be from the measuring DO probe itself. From theory appendix of its user manual, the DO probe measures pO_2 according to the current strength between its gold cathode and silver anode. The O_2 concentration value was calculated by device program based on the assumption that measured solution is totally aqueous. However, this preset condition does not apply to the PFC emulsion in this dissertation.

The composite solubility of PFC emulsions is [61]:

$$Solubility_{emulsion} = Solubility_{aqueous} \times vol\%_{aqueous} + Solubility_{PFC} \times vol\%_{PFC} \quad (2.3)$$

and the DO concentration then is calculated as:

$$DO\ concentration = pO_2 \times Solubility_{emulsion} \quad (2.4)$$

The 5% and 10% PFC-medium emulsion should have different O_2 solubility due to different PFC volume fractions, which however was preset as the same value that only applies to aqueous solution in the Clark type DO probe device. But the pO_2 values it measured can be used to calculate the actual O_2 concentration in PFC-media. The Oxycyte® O_2 solubility is 0.566 mL O_2/(L pure PTBCH·mmHgO_2) at 37ºC [51], while the rest part in PFC-medium is assumed as pure water for simplified calculation and its O_2 solubility at 37 ºC is 0.0337 mL O_2/(L water·mmHgO_2)[62]. Through water weight/volume fraction (confidential product information) and PTBCH weight/volume fraction, the final PTBCH volume fraction in PFC-medium (instead of its weight/volume fraction as in Tab. 2.2) can be obtained and the composite O_2 solubility of PFC emulsion in Eqn. 2.3 is evaluated. Fig. 2.5 shows the recalculated DO values presented in 0% (purely aqueous), 5% and 10% PFC-media. This calibration study of this dissertation

work thus has clarified different PFC fractions result in emulsion's different DO concentrations. Because previous preliminary cell culture showed the cytotoxicity of 10% PFC in medium and its O2 solubility is close to that of 5% PFC-medium (Fig. 2.5), it is the 5% PFC-medium that will be applied to following hepatic cell culture (see CHAPTER 3). Though generally regarded as not acutely toxic [63, 64], various levels of cytotoxicity by different PFCs to non-hepatocytes had been confirmed in the literature [43, 65, 66]. The hepatic cytotoxicity of the specific PTBCH that Oxycyte® contains must be evaluated in the future if it is to be applied as a supplement in BALs.

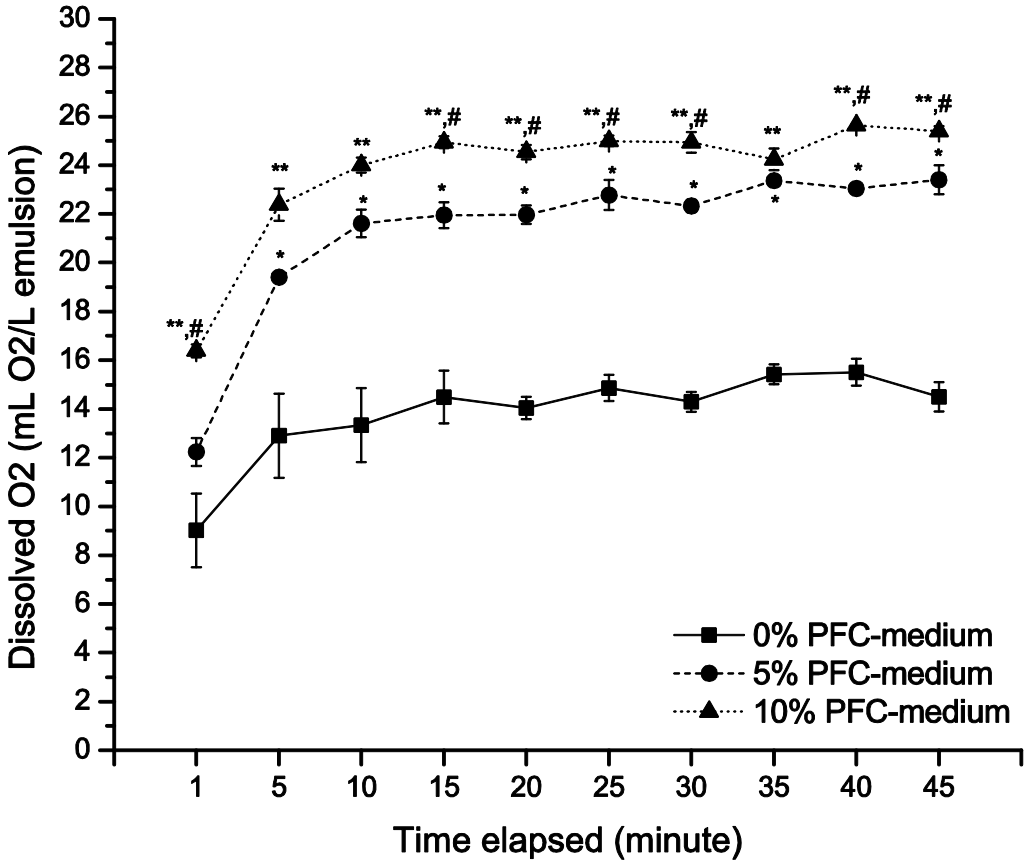

FIGURE 2.5. (Converted from Fig. 2.3) DO concentrations of O_2-pressurized PFC-media with different fractions of PFC at 37°C. *:5%PFC>0%PFC, $p<0.05$; **: 10%PFC>0%PFC, $p<0.05$, #: 10%PFC>5%PFC, $p<0.05$. n=3, Mean±SE.

CHAPTER 3: USE PERFLUORONCARBONS TO ENHANCE OXYGEN DEVLIERY IN 3D THICK HEPATIC TISSUE EQUIVALENT

3.1 Introduction

Incorporating PFCs within the perfusate of BALs is expected to benefit its O_2 delivery and elevate functionality. Yet to date this has not been investigated in thick 3D hepatic tissue equivalents study, nor has it been presented for the commercially prepared PFC emulsion Oxycyte® (Oxygen Biotherapeutics, Durham, NC) characterized in CHAPTER 2. "Thick 3D hepatic tissue equivalent" here refers to hepatic culture that has significant larger size or dimension than regular multi-well plate culture, such that O_2 delivery to its cellular space will be challenged. There are many hepatic cell candidates for BALs [4, 32, 67, 68] and which kind of cells are used for the Oxycyte® efficacy evaluation must be determined. The HepG2/C3A cell line subcloned from its parental HepG2 hepatoblastoma cell line was selected, because it retains many human primary hepatocytes (HPH) phenotypes. These phenotypes include: high albumin and low α-fetoprotein secretion, strong glucose metabolism, urea production (although not due to removal of ammonia[69]), and cytochrome P450 activity [70, 71]. With these key functionalities and its proliferative ability, the C3A cell line has been used in clinical trials since the 1990s [72, 73] and includes being used in the ELAD® BAL(Vital Therapies Inc., San Diego, CA) [11]. Thus, in this chapter, the effects of PFC-supplemented medium on HepG2/C3A cells function and viability were evaluated for thick 3D hepatic tissue equivalent under static and dynamic flow conditions.

3.2 Materials and Methods

3.2.1 Cell Culture

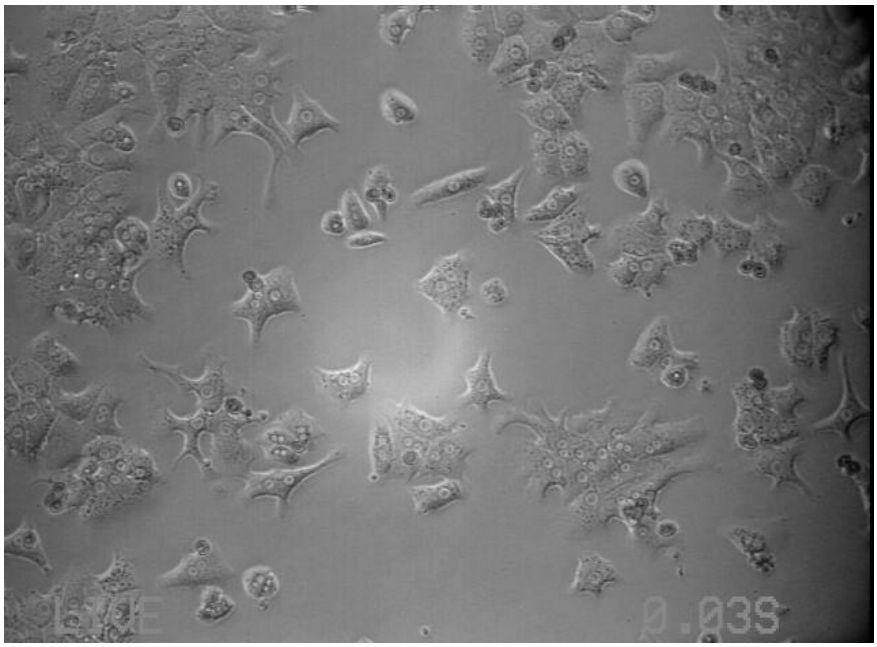

FIGURE 3.1. Proliferating HepG2/C3A cells monolayer cultured in a protein-coated T75 cell culture flask.

The human hepatoblastoma cell line HepG2/C3A from American Type Culture Collection (ATCC #CRL-10741, Manassas, VA) was used. In the current work, C3A cells were cultured in T-75 flasks (Cellstar, Greiner Bio-One, Monroe, NC) and incubated with humidified, air-balanced 5% CO_2 at 37ºC (Fig. 3.1). The C3A full growth medium, based on Eagle's Minimum Essential Medium (MEM) (Mediatech, Manassas, VA), was supplemented with 0.11 g/L (1mM) sodium pyruvate (Sigma-Aldrich, St. Louis, MO), 1.5 g/L sodium bicarbonate (Sigma-Aldrich, St. Louis, MO), 10% v/v Fetal Bovine Serum (FBS) (Hyclone, Logan, UT) and 1% v/v antibiotic/antimycotic solution (10,000 Unit penicillin G, 10,000µg streptomycin and 25 µg/mL amphotericin B, JR Scientific,

Woodland, CA). Oxycyte® was supplemented to this full growth medium at 5% for following PFC-treatment. The culture medium of each T-75 was changed every other day, as well as 24 hours prior to subculture (i.e., passaging). Once 90% confluency was attained, cells were trypsinized using 0.25% Trypsin-EDTA solution (Sigma-Aldrich, St. Louis, MO) and centrifuged at 800 rpm (~130*g*) for 5minutes. Cells with passage number of no more than 7 were used in this study. After aspiration, cells were further trypsinized with 5 mL of the same Trypsin-EDTA solution then incubated for 25 minutes to facilitate cell monolayer detachment and cell aggregate dissociation.

3.2.2 Extracellular Matrix (ECM) Preparation

3.2.2.1 Collagen gel as ECM

Collagen gels have been extensively used as the ECM for *in vitro* 2D hepatic cultivation [74-76] in which primary hepatocytes polarize themselves and demonstrate phenotypes as *in vivo*. To establish a reliable function control to calibrate effects of the Oxycyte® PFC, PureCol® Type I collagen purified from bovine source (Advanced BioMatrix, San Diego, CA) as ECM was used in 2D double gel (sandwich) cultures. Its collagen density was originally ~3 mg/mL yet diluted down to 1.1 mg/mL using 0.1 M NaOH solution, 10× Minimum Essential Medium (MEM) and deionized water for this work.

3.2.2.2 Gelatin sponge as ECM

Since goal of this work is to clarify the effects of PFCs in improving O_2 delivery to thick 3D tissue equivalents under flow conditions, it was necessary to establish an ECM environment amenable to cell attachment and able to withstand aqueous flow. Unfortunately the low permeability [77] and weak mechanical properties [78] of collagen

impaired its reliable use as the 3D ECM for thick tissue equivalents. Since Gelfoam® gelatin sponge (Pharmacia & Upjohn, New York, NY) had demonstrated effectiveness in supporting mammalian cells [79-82] and exhibited adequate pore sizes (30-700 μm [80]) for transport [83], it was chosen as the ECM substrate for the 3D tissue equivalent design of this study. To prepare for culture, the Gelfoam® sponge with vendor thickness of 1 cm was first cut into 1×1×1 cm cubes (for the static flow study in multi-well plate) and 3.5 cm diameter discs (for the dynamic flow study). The prepared sponge scaffolds were then sterilely pressed in Redi-Pak® straight wall glass jars (VWR, West Chester, PA) to remove air from the sponge scaffolds. The sponge scaffolds were then transferred into standard 12-well plates (cube) or 6-well plates (disc). Each well was added 2 mL (cube) or 6 mL (disc) of 1× Hank's Buffered Salt Solution (HBSS). After 25 minutes, HBSS was aspirated and the rinsing cycle was repeated. Following thorough aspiration, 2 mL (cube) or 5mL (disc) of the C3A full growth medium (or PFC-medium) was then added into each well, and the 3D gelatin ECM was incubated for another 1 hour prior to cell seeding.

3.2.3 Cell Culture Preparation

3.2.3.1 Static Cultures

For the static flow culture study, collagen gel and gelatin sponge were both utilized, where cells sandwiched between layers of collagen gel served as function control. For the sandwich cultures, each well of a standard 12-well plate (Greiner Bio-One, Monroe, NC) was coated with 0.34 mL collagen and incubated 2 hours for fully gelation. After viability was confirmed by Trypan Blue (Sigma-Aldrich, St. Louis, MO) exclusion assay following trypsinization, 1×10^5 viable C3A cells were plated into each

collagen-coated well and were gently shaken to spread evenly. After 2 hours incubation for cell anchorage, supernatant of each well was aspirated and 0.34 mL same collagen was placed on top of cells. After this top layer fully gelled in 4 hours incubation, 2 mL cell culture medium (normal full growth medium or 5% PFC-medium) was added into each well. For the gelatin sponge cultures, 1×10^5 viable C3A cells were inoculated into each prepared 1×1×1 cm sponge cube which afterwards were added to standard 12-well plate 1 hour later and 2 mL of culture medium (normal medium or 5% PFC-medium) was added to each well. Both static sandwich culture and gelatin sponge culture were maintained for 10 days at 37°C in 95% air/5% CO_2, where their culture media were replaced every 48 hours (i.e., day 2, 4, 6, 8, 10).

3.2.3.2 Dynamic Cultures

Culture preparation for dynamic study is very similar to static culture excepted that each sponge disc was inoculated 5×10^5 viable C3A cells and there were multiple pipetting-inoculations to achieve even cell distribution. Cell leakage was examined to confirm inoculation success, by microscopically evaluating the remnant medium left by displaced sponge. Cell-loaded sponge discs were incubated at 37°C in 5% CO_2/95% air for 24 hours prior to use in the custom flow device, for stabilizing cell attachment.

3.2.4 Dynamic Flow Culture Conditions

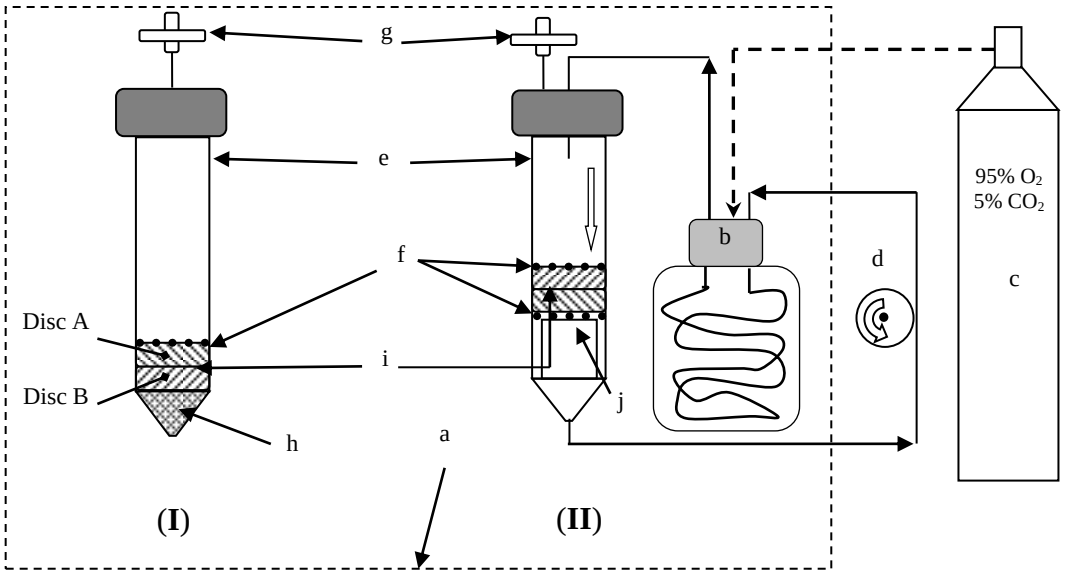

FIGURE 3.2. Schematic diagram of the dynamic flow device (II) and its static flow culture as control (I): (a) Incubator; (b) Gas exchanger; (c) O_2 tank; (d) Peristaltic pump; (e) Flow device and its static control device, with cell loaded sponge discs; (f) Stainless steel mesh; (g) Sterile venting filter; (h)Teflon® filled cone bottom; (i) Double stacked sponge discs; (j) Supporting sectioned syringe barrel. The open downward arrow in (II) indicates flow direction in the device.

The custom flow device designed for this study is schematically shown in Fig. 3.2. Its main part consists of a 50 mL polypropylene tube (Greiner Bio-One, Monroe, NC) able to accommodate two stacked 3.5 cm-diameter sponge discs (hatched region in Fig. 3.2). The stacked sponge culture in flow device (Fig. 3.2-i) was sandwiched between 2 trimmed stainless steel #316 meshes for immobilization against buoyant force (Fig. 3.2-f) (Small Parts, Miramar, FL). Since flow through the base of the stacked discs is required, the bottom mesh rests on a cylindrical shell platform (Fig. 3.2-j). It was sectioned from a 30 mL polypropylene syringe barrel (BD Science, Franklin Lakes, NJ,) and effectively suspended the stacked discs ~25mm high from the flow device outlet meanwhile

allowing flow though. The use of 2 stacked cell-loaded sponges (Fig. 3.2-i) established the thick culture thickness (~ 1.2 cm) required for clarifying PFC's effects on cell viability along the Z-axis depth through this 3D culture. Furthermore, it did not interfere with the perfusion of the medium through the 3D culture volume. The priming volume for the flow device was 20 mL. The medium inflow to the device was oxygenated with 95% O_2/5% CO_2 via the same gas exchanger (Fig. 3.2-b) as in Fig. 2.2-c (CHAPTER 2). To establish a suitable control for the flow device, a complementary system was engineered (shown schematically in Fig. 3.2-I) that differed from the flow system in a single feature – it did not have media flow. This static tube thus allows only unidirectional passive diffusion to dominate O_2 transport to the volume of the cellular space. Main difference of such diffusion pattern from static flow's sponge cube culture is that for sponge cube the diffusion occurred on its entire sides and top as there were gaps between culture and wall (see Fig. 5.4), while in this static tube medium can only directly access top of sponge discs.

3.2.4.1 The Dynamic Flow Experiment

As previously mentioned, the cell-loaded sponge discs were added to the dynamic flow device (Fig.3.2-II), and its static control (Fig. 3.2-I) 24 hours after preparation. After 20 mL medium (normal or PFC-supplemented) was added to the culture-loaded dynamic flow device, its pump started at the rate of 0.25 mL/minute. The static control (Fig. 3.2-I) was added 20 mL medium (normal or PFC-supplemented) while dynamic flow device began operating. Both cultures in Fig. 3.2-I and Fig.3.2-II were maintained for 48 hours from flow initiation. During the whole culture period, color of phenol red-contained medium in dynamic flow device and static control was monitored and stable color

through the culture indicating pH ~7.4 was observed. At the end, the viability, albumin secretion, glucose reduction, CYP450 activity (EROD) and propagated population of the cells in each sponge disc were assessed.

3.2.5 Function and Metabolic Activity Studies

3.2.5.1 Albumin Secretion

One of the key HPH functions retained by C3A cells is albumin secretion. The albumin concentrations of day 2, 4, 6, 8, 10 (static study) or end of culture (dynamic study) were measured using a standard enzyme-linked immunosorbent assay (ELISA) as per vendor's protocol (Human Albumin ELISA Quantitation Kit, Bethyl Laboratories, Montgomery, TX). Measurements were quantified using a Synergy HT microplate reader (Bio-Tek, Winooski, VT) read absorbance at 490 nm wavelength. The total secreted albumin values were calibrated against standard curves.

3.2.5.2 Glucose reduction

Energy of metabolism mainly comes from the glucose breakdown (glycolysis). To monitor the energy consumption of the cultured cells, the glucose concentrations of the spent culture medium (static study: day 2, 4, 6, 8, 10; dynamic study: end of culture) were read at absorbance of 630 nm using the QuantiChrom Glucose Assay Kit (BioAssay Systems, Hayward, CA). The glucose reduction was calculated as the quantitative difference between the glucose level of spent sample medium and that of the cell-free stock medium. The total glucose reduction was calibrated against standard curves.

3.2.5.3 Cytochrome P450 (CYP450) activity

In human liver, cytochrome P450 (CYP450) is a large family of isoenzymes that play key roles in phase I drug metabolism. Among such enzymes, CYP1A1 and CYP1A2

catalyze the ehoxyresorufin o-deethylase (EROD) and their activities are typically tested through EROD assay where ethoxyresorufin (ER) (Molecular Probes, Eugene, OR) is the substrate [84-86]. In this study, the EROD assay applies to the ability of C3A cells to retain CYP1A2 function.[71] C3A cell-loaded cultures were dosed with 2μM 3-Methylcholanthrene (3-MC) (Sigma-Aldrich, St. Louis, MO) medium for 48 hours prior to the EROD evaluation [71].

The product of the EROD assay is resorufin and its production rate – the level of resorufin produced over a specified time period – is an indicator of CYP450 activity. Since this assay requires inducing medium containing the drug 3-MC, it cannot run parallel with albumin and glucose assays. In the static study the EROD activities of independent C3A cell groups were tested on day 3, 6 and 9. In the dynamic flow study, cell culture for EROD assay was tested at end of culture. For the static flow study, to remove residual 3-MC medium at the endpoint of dosing each culture was rinsed using 3 mL HBSS for 30 minutes incubation. Later 2 mL 5 μM ER in 50 mM HEPES buffer solution was added followed by 3 hours incubation at 37°C. For the dynamic flow study, 3-MC medium was drained at the end of 48 hours, when perfusion flow was stopped. Each sponge disc was relocated from flow device into a new standard 6-well plate. Each disc was then added 6 mL HBSS and the sponge discs were incubated at 37°C for 30 minutes to remove excess 3-MC medium, then the excessive supernatant aspirated. Subsequently, 5 mL of 10 μM ER in phenol red-free medium (Mediatech, Manassas, VA) was added to each well and incubated for 6 hours.

3.2.5.4 Resazurin Metabolism Assay

Resazurin (Sigma-Aldrich, St. Louis, MO) is the main functioning component of the commercial dye alamarBlue® [87] which is widely used in cell viability and cytotoxicity determinations [87-92]. In this study, resazurin (Sigma-Aldrich, St. Louis, MO) was used to determine the metabolically active population (MAP) of the cell loaded sponge during continuous proliferation, and such population results were used in normalization of function results. Resazurin was prepared as 3 mM stock solution by being dissolved in HBSS. Such stock solution was then diluted in phenol red-free culture medium (Mediatech, Manassas, VA) to achieve a 10% (v/v) resazurin-medium solution. In static flow study, 2 mL of 10% resazurin-medium was added to each sandwich culture/sponge cube within 12-well plates and incubated for 2 hours. For dynamic flow study, after perfusion ended and discs being relocated to the new 6-well plate, 5 mL 10% resazurin-medium was added to each 3.5 cm-diameter sponge disc and incubated for 2 hours. Each well was sampled 3 aliquots of 100 μL solution from each well were transferred to a 96-well plate (Nunc, Rochester, NY). Standard resorufin solution (concentrations ranging 0-20 μM) was then pipetted into the same plate, and the fluorescence signal of each well was read by Synergy HT microplate reader (Bio-Tek, Winooski, VT) at the excitation/emission of 530/590 nm. Resorufin production was determined from standard curves. Following the completion of the metabolic assay, each sponge disc was exposed to 2 cycles of a 30 minutes HBSS rinse, to minimize remaining fluorescent noise and prepare for fluorescent viability study.

3.2.6 Evaluation of Cell Viability

It was important to quantify whether cell viability varies with Z-position along the thick tissue equivalent at the conclusion of experiments. In this study, C3A cell viability was determined through using nuclei fluorescence dyes: 1 μg/mL concentration of Hoechst 33342 and 1 μM Ethidium Homodimer-1 (EthD-1) (Molecular Probes, Eugene, OR). Since EthD-1 is sensitive to serum, it was necessary to first remove the FBS in the medium before viability could be assessed. This was achieved by placing each cell-loaded sponge disc tissue equivalent in the well of a 6-well plate, followed by twice soaking in 1×HBSS, where each soak was of 20 minutes duration. To ensure that FBS was removed from the sponge interstitial space, each sponge disc in dynamic study was rinsed by 6 mL HBSS. After aspiration of HBSS supernatant, the hybrid Hoechst-EthD HBSS was added to each sponge tissue equivalent and incubated at 37°C for 1 hour. After aspiration, the cell-loaded sponge discs were fixed by equilibrating each cell loaded cubic and disc sponge with 5 mL of 10% formalin (VWR, West Chester, PA) to prevent Hoechst efflux by transport protein [93-96]. The excess formalin was then aspirated and HBSS was added for another 30 minutes incubation. After the last aspiration the fixed tissue equivalents were stored at -80^{o}C until the microtome work was initiated.

Since the 3D sponge disc cultures were too thick and opaque to be viewed readily via confocal microscopy, it was necessary to slice each fixed tissue equivalent using a HM550 Microtome cryostat (Microm, Walldorf, Germany) at 3 designated positions (Fig. 3.3, I, II and III). Prior to slicing, the frozen and fixed tissue equivalent sample was chilled in the -20^{o}C chamber of the cryostat. It was then thoroughly coated with Tissue-Tek® Optimal Cutting Temperature compound (Sakura Finetek, Torrance, CA), then

sliced to 100 μm thick segments, thickness of which is to ensure its full integrity (thick black lines in Fig. 3.3-a represent such layers). Each layer was then positioned on a 75×50×1 mm microscope glass slide (Fisher Scientific, Pittsburgh, PA). Since the total

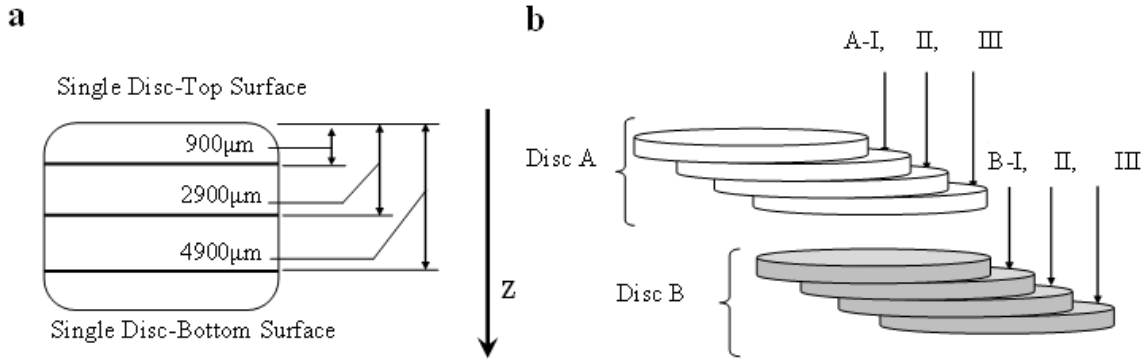

FIGURE 3.3. Schematic demonstrating: (a) The slice thicknesses used in the cell viability evaluation procedure for each 3D sponge disc (A and B); (b) the positioning of cell-loaded sponges A and B, and the positions of their cryostat slices for confocal imaging (totally 6 positions, while A-I, II&III are different cryostat slice of one sponge disc A, same as B-I, II&III), within the thick 3D tissue construct of the dynamic flow condition in this study.

height of each frozen sponge disc was ~6000 μm, it was sliced at 900 μm, 2900 μm and 4900 μm away from top surface (Fig. 3.3). The viability of the prepared tissue equivalent slices was then quantified using an Olympus IX70 laser scanning confocal microscope, and documented using FluoView 5.0 (Olympus America, Center Valley, PA). Each sample slice was imaged 5 random fields. The results were averaged to quantify the overall viability of one single slice. Because Hoechst 33342 stains all cell nuclei, while EthD-1 stains dead cells, the number of viable cells was obtained by subtracting the dead cells (EthD-1 marked) from the total cells (Hoechst marked).

3.2.7 Plot and Statistical Analysis

Plotting of the O_2 concentration, viscosity, population-normalized function results (Fig. 3.2-3.6) and the statistical analysis were completed using OriginPro (OriginLab, Northampton, MA). One-way Analysis of Variance (ANOVA) is used to determine significance of differences between mean values. Unless otherwise specified, $p<0.05$ is regarded as statistically significant. For the PFC O_2 concentration calibration, 3 independent samples were analyzed (n=3), such that each 100ml sample was only used once in the calibration. In evaluating the viscosity of each condition (e.g., PFC media, normal media) 3 samples (n=3) were used, where each sample was measured three times via the viscometer. For the function studies, experiments were conducted on triplicate separate samples, where each experiment was independently repeated three times.

3.3 Results

3.3.1 Effects of PFC on Liver Function

Since adding 5% v/v PFC to normal medium significantly enriched its O_2 concentration (CHAPTER 2), it was necessary to ensure that this addition would not negatively affect the cells functionalities. In all figures and discussions beyond this point, 5% Oxycyte® PFC-medium will be referred to as "PFC-medium". C3A cells were then cultured in the presence of PFC-medium under traditional static conditions, which include two ECMs: collagen double gel and gelatin sponge 3D scaffold to evaluate PFC's effect.

3.3.1.1 Static collagen sandwich culture

Functional results in collagen sandwich culture were recorded into Fig. 3.4-I, including albumin secretion, glucose reduction, and EROD activity. The normalized

results via resazurin assay-determined cell population are presented, to elucidate PFC's effect on such a dynamically proliferating cell line. While in sandwich culture both normal and PFC-medium treated cells had a decreasing trend of albumin secretion per cell (Fig. 3.4-Ia), there was no statistical difference between these two groups through the cultured period. Meanwhile their glucose reduction results through the same period entailed that through 10 days culture, both normal and PFC-medium treated cell group had stable and same level of energy consumption per cell (Fig. 3.4-Ib). For CYP450 assay, only normal medium-treated C3A cell had an increasing EROD activity from day 3 to day 9 (Fig. 3.4-Ic), and on day 6 normal medium-treated group had higher resorufin production rate than PFC-medium treated group per cell (Fig. 3.4-Ic).

3.3.1.2 Static gelatin sponge 3D culture

Fig. 3.4-II illustrates PFC's effects on the same three functionalities of C3A cells in sponge culture: albumin, glucose reduction and EROD activity as compared to that of normal medium Cells cultured in static PFC-medium performed equivalently to those cultured in normal medium except day 6 and day 8 with respect to albumin secretion (Fig. 3.4-IIa). Their glucose reductions (Fig. 3.4-IIb) throughout the 10 day period were also not significantly different through the 10 day culture period. The effects of PFC-medium having more O_2 available to the sponge-cultured cells revealed its most pronounced effects on CYP450 activity – where cells exposed to PFC-medium yielded significantly higher EROD activity than cells in normal medium by day 6 of the culture (Fig. 3.4-IIc), but this effect was not seen on day 9.

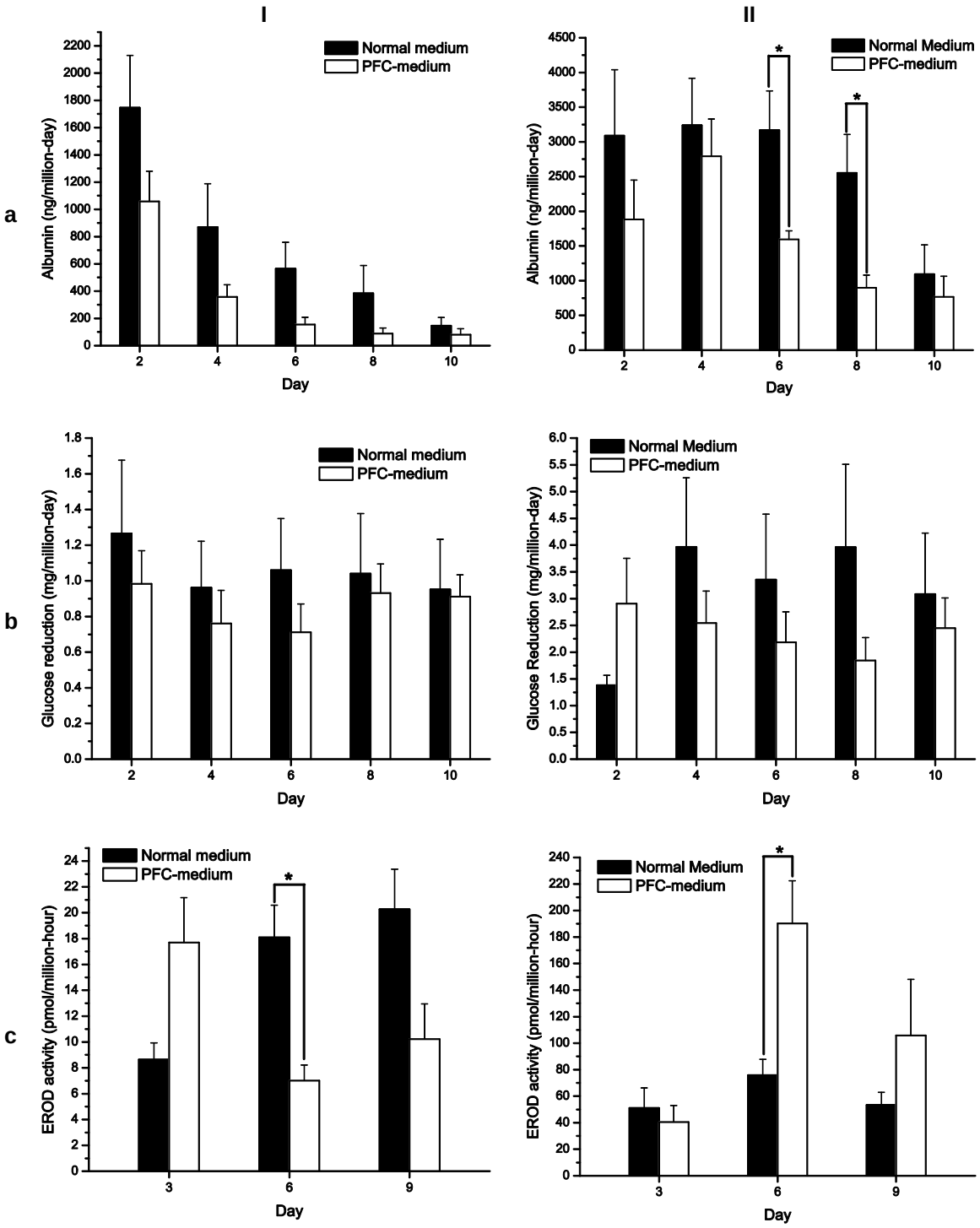

FIGURE 3.4. Population-normalized albumin (row a), glucose reduction (b) and EROD activity (c) of initially 1×10^5 C3A cells cultured in collagen gel sandwich (column I) and sponge cube (II) in static multi-well plate. n=9.*: $p<0.05$. Mean±SE.

3.3.1.3 Dynamic gelatin sponge 3D culture

Fig. 3.6 presents the normalized results of PFC-medium exposure on C3A cells under dynamic flow and static conditions. The functional performance is compared to that in normal medium. As illustrated in Fig. 3.6-a, under dynamic flow conditions C3A cells cultured in PFC-medium secrete albumin at equal level of cells in normal medium, while consuming less glucose (Fig. 3.6-b). The exposure to PFC-medium seemed not to directly enhance single cell's ability of accomplishing EROD activity, but to encourage the cell population growth under flow condition though not statistically significant (Fig. 3.5-a). As shown in Fig. 3.5-b, the MAP of C3A cells in flow device with 3-MC dosing proliferated from 1×10^6 to ~4×10^6 after 48 hours. Such a change is significantly different from its normal medium-treated counterpart (Fig. 3.5-b).

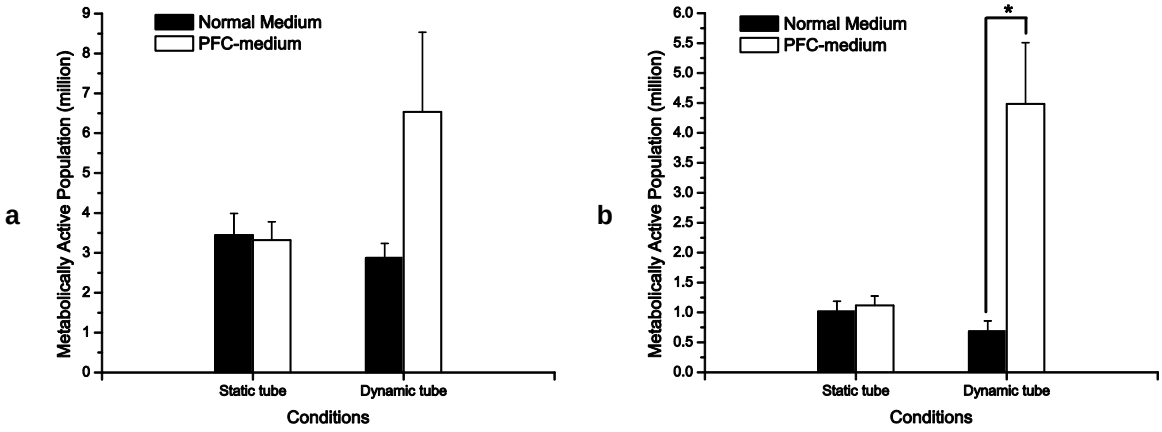

FIGURE 3.5 Metabolically active populations (MAPs) of C3A cells at endpoint of albumin and glucose reduction assays (a) and EROD activity assay (b) (population used to obtain normalized results in FIGURE 3.6). n=3.*: $p<0.05$. Mean±SE

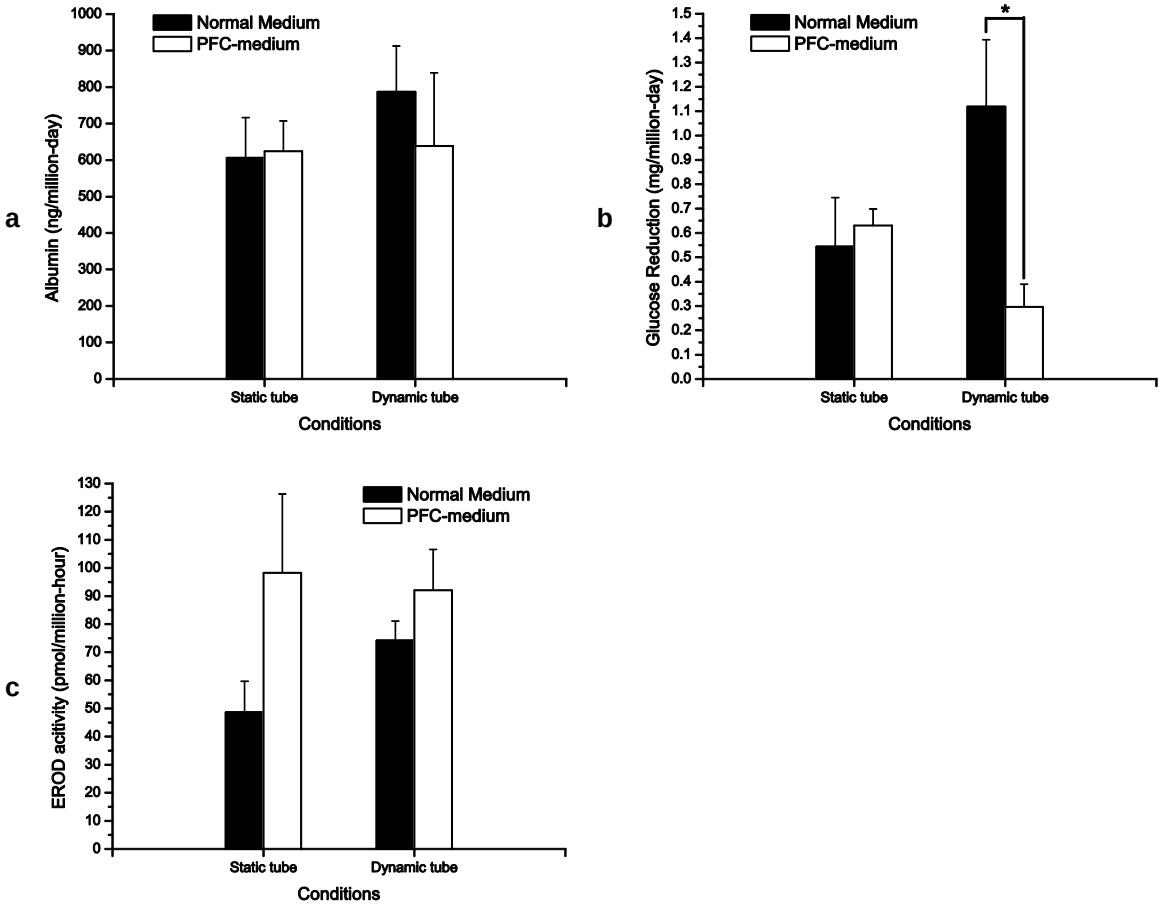

FIGURE 3.6 Population-normalized albumin (a), glucose reduction (b) and EROD activity (c) of initially 5×10^5 C3A cells cultured in dynamic flow tube device and static tube as control. n=3.*: $p<0.05$. Mean±SE

3.3.2 Cell Viability through Z-axis of Thick 3D Tissue Equivalents

It is necessary for O_2 to be transported effectively throughout culturing thick 3D tissue equivalents. Since the normal function of hepatic cells, including C3A cells, are highly O_2 dependent, it was necessary to quantify the viability of the cells within the cell-loaded sponge cultures of the current work. The viability results for different layers of the thick tissue constructs are shown in Tab. 3.1. The position of each layer along the z-axis is shown in Fig. 3.3. The results indicate that for normal and PFC-medium conditions,

cell viability was very high (> 98%) throughout the duration of the culture for both normal and PFC-medium treated cells in flow device.

TABLE 3.1: Cell viability results for 3 incremental positions along the Z-axis of the 3D tissue equivalents 48 hours after flow system start (i.e. 72 hours after cell seeding). No statistical difference detected. Results listed as Mean ± SEM. n=6.

	Conditions[§§]			
Z Positions	NM-S	NM-D	PFC-S	PFC-D
A-I	98.63±0.69%	99.11±0.64%	99.57±0.37%	99.51±0.33%
B-I	99.67±0.71%	97.64±1.18%	98.89±1.04%	100±0%
B-III	98.67±0.82%	100±0%	99.84±0.15%	99.86±0.14%

3.4 Discussion

3.4.1 PFC's Effects on Cell Functionalities and Viabilities

A successful method for enhancing O_2 transport through 3D tissue spaces of BAL and other applications must minimally establish an environment that supports viable functioning cells. The results of the current study demonstrate that together with the custom designed flow device and Oxycyte® PFC, this was successfully achieved for C3A cells-seeded 3D thick tissue constructs. The work shows that the use of 5% v/v PFC-medium is slightly effective in static culture, and more effectively improving C3A cells functional performance under perfusive flow condition.

viii. [§§] Condition abbreviations: NM = Normal Medium, PFC = PFC-medium, S = Static, D = Dynamic.

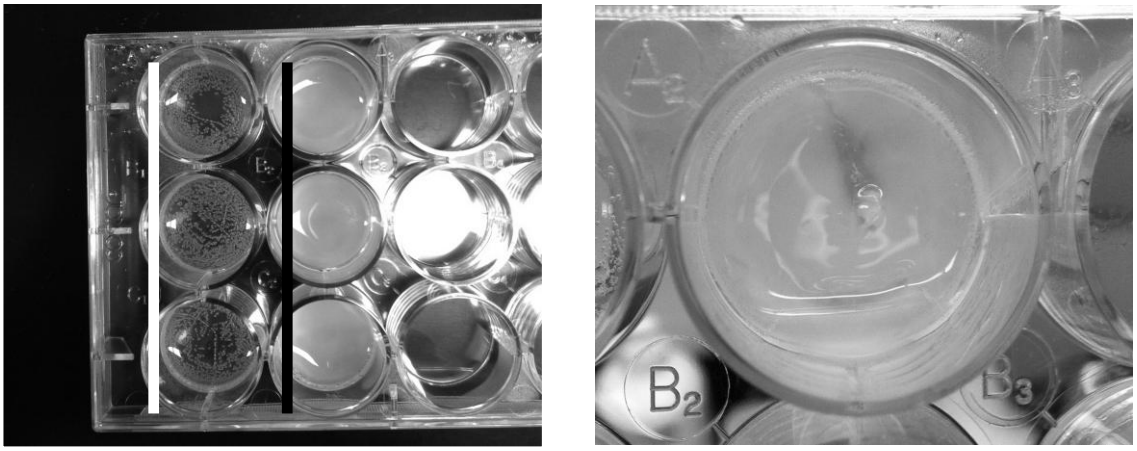

FIGURE 3.7 In a standard 12-well plate (LEFT), normal medium treated, clear collagen gel (white line marked) and 5% PFC-medium treated collagen gel for 3 days (black line marked), where a closer view shows that PFC sediment gives collagen a cloudy look (RIGHT).

The benefits of enhanced O_2 availability on the functional performance of primary hepatocytes have been previously reported [24, 30, 34, 38, 97, 98]. Yet the responsiveness to enhanced O_2 conditions of human hepatic cell line albumin synthesis appears to be method and cell source dependent. The PFC-treated porcine primary hepatocytes (PPHs) in their perfusion system had equivalent glycolytic activity as normal medium treated control (ambient condition) and are even less glycolytic at 5% O_2 [46]. In a bovine erythrocyte-conditioned hollow fiber bioreactor, over 7 days were taken to demonstrate effect of increased O_2 on the inoculated C3A cells' albumin production [99, 100]. Contrastingly, when a C3A loaded bioreactor perfusate was supplemented by a Russian commercial PFC Perftoran® [***] (Pushchino, Moscow, Russia), the initial population-normalized albumin production increased significantly above its control [35]. However, the results of each study aforementioned were not quantified by immediate cell

ix. [***]Perftoran® is a blend of perfluorodecalin ($C_{10}F_{18}$) and perfluoromethylcyclohexylpiperidine ($C_{12}F_{23}N$).

population (instead of “initial population” as population beginning of cultivation). For example, it was not clear in the Perftoran® PFC study[35] whether the improved albumin production was achieved through enhanced protein synthesis per cell or more populated cells, or both under increased O_2 condition. In another PFC-free 3D perfusion conditioned study, the albumin secretion of C3A cells in alginate-based 3D culture (scaffold pore size at 65-85 μm, flow rates at 60 mL/min or 100 mL/min) was also normalized via population of day 0 (literally “initial population”), not the actual population at the assay moment.[18] In order to portray more precise normalized function results, the resazurin assay is introduced for obtaining the key number of MAP.

Subcloned from its parental cell line HepG2, available literature data of C3A cell line are more limited than the vastly investigated HepG2. Borrowing intelligence of HepG2 cell line could assist the analysis for C3A cells – after all, these two are genetically related [70]. The albumin regulations of HepG2 cells and RPH using hepatocytes growth factor are different [101]. In addition, hypoxia condition does not inhibit the HepG2 albumin gene sequence expression.[102] These indicate that albumin expressions of HepG2 cells may be notably different than that of primary hepatocytes. Such a difference may contribute to the fact that HepG2 cells secreted more net albumin than RPH 24 hours after inoculated in bioreactor [103]. Moreover, due to altered CYP450 expression, HepG2 cells are also known to have weaker EROD activity as compared to RPH [86] and HPH [104, 105]. This also elucidate why the EROD levels achieved by C3A cell line here are lower than that previous RPH-based study using normal medium [106]. It should be concluded that the C3A cells response to O_2 exposure can only be poorly predicted from primary hepatocytes behavior.

In static collagen sandwich culture, PFC's effect to C3A cells was not obvious (Fig. 3.4-Ia, Ib & Ic). The PFC-medium conditioning did not create a difference from the normal medium at both albumin secretion and glucose consumption. Rather, in EROD activity study normal medium treated cells had even higher EROD activity than PFC-medium treated cells on day 6. This could be attributed to the PFC deposition on collagen gel. Heavier than water, if statically placed PFC droplets in PFC-medium emulsion sink to the bottom and precipitate. Medium refreshing only removes supernatant yet the PFC deposition stays (Fig. 3.7), leaving an oil-like film hindering other nutrients (glucose, growth hormone, amino acids etc.) transport from medium through collagen. This side effect may contradict PFC's O_2 benefit to cell functioning in following cultivation.

On day 6 of static gelatin sponge culture PFC-conditioned CYP450 activity per cell is significantly higher but this did not recur on day 9 (Fig. 3.4-IIc). A reasonable answer is that expression of EROD enzyme had remarkably decreased before day 9 due to its continuously degrading mRNA, probably as a result of cell line's altered liver enriched transcriptional factors (LETFs) [86, 107]. While Fig. 3.6-a shows that under flow condition, albumin productions of cells treated by normal and PFC-medium are equal, the glucose consumption of the PFC-medium treated (Fig. 3.6-b) is less. Together, this lower cell glucose consumption suggests that under PFC and flow condition, higher energy per glucose molecule was released such that each cell cost less glucose to secrete equivalent level of albumin, or increased gluconeogenesis. Fig. 3.5-b indicates that when the 3-MC perfusate in C3A-loaded flow system was supplemented by PFC, more metabolically active C3A cells proliferated, with each cell still able to maintain the same level of EROD activity as control (Fig. 3.6-c).

3.4.2 Conclusions

To summarize, this study presents the effects of adding PFCs to normal medium on the functional performance output of thick 3D hepatic tissue constructs, under flow and static culture conditions. The results also demonstrate that the increased O_2 concentration of PFC-medium significantly reduces the glucose consumption during albumin secretion per cell and stimulates cell growth under flow conditions. As such the results of this work can be applied to the design and support of future BALs in which the support of sizable 3D tissue spaces is critical. As a conclusion, by delivering more O_2 into the 3D gelatin sponge ECM interstitial space, the PTBCH-based PFC-medium ensures high viability and improves key functionalities of the human hepatoma cell line HepG2/C3A into cellular spaces.

CHAPTER 4: PREDICTING OXYGEN TRANSPORT IN A NOVEL HEPATIC BIOREACTOR NUMERICALLY FOR ITS MELIORATION

4.1 Introduction

A novel prototype of Four-Quadrant Bioreactor (4QB) was designed and fabricated for hepatic support [106]. Such study verified that the 4QB created a unique dynamic flow environment for the rat primary hepatocytes (RPHs) it housed and enabled RPHs to achieve improved functional performance. It also revealed that as RPHs population increased to 32 million per quadrant, oxygen (O_2) deficient regions appeared in the cellular spaces. This implies that the total functional output of the 4QB could be even further elevated along with O_2 enhancement. Considering numerical methods based upon computational fluid dynamics (CFD) theory have been widely applied to modeling flow in bioreactor [29, 53, 108, 109], such computation has the potential to resolve the O_2 delivery issue in 4QB at high cost-efficiency. In this study, prediction of O_2 transport within the 4QB was established by a simplified 3D model capable of representing otherwise complicated real multiphase flow. A number of variables (e.g., flow rate, cell populations, the spatial flow pattern dictated by cartridge arrangement etc.) presumably influence the cellular O_2 accessibility in 4QB jointly. Computational results have successfully shown that of these variables, local O_2 diffusivity in extracellular space is a factor as important as the flow rate, while increasing the latter yields higher shear stress. The model answers the question that in order to meliorate the local O_2 diffusivity for amplifying the overall 4QB cellular O_2 level without altering original medium formula,

ECM material selection is the key. This model also suggests that in CHAPTER 2, prior to PFC usage the gelatin sponge 3D scaffold may have already establish the 1st step toward O_2 transport enhancement.

4.2 Theory

The total O_2 mass flow within a bioreactor universally obeys the law of mass conservation: (adapted from [110])

$$\frac{\partial \rho}{\partial t} + \nabla \cdot (\rho \vec{u}) = S_m \quad (4.1)$$

where $(\nabla \cdot)$ is the divergence operator, $\vec{u}$ is velocity vector, S_m is the mass source (positive if mass is generated, negative if mass is consumed). Particularly, if flow involves both gas and liquid, the mass conservation governing equation for the dual phase flow is:

$$\frac{\partial (x_l \rho_l)}{\partial t} + \nabla \cdot (x_l \rho_l \vec{u}) = S_m \quad (4.2)$$

where x_l is volume fraction of liquid, ρ_l is density of liquid. In a computational grid, volume fraction of gas is calculated as: $x_g = 1 - x_l$. Similarly, the momentum of the O_2-contained flow of 4QB also conserves as: (adapted from [110])

$$\frac{\partial}{\partial t}(\rho \vec{u}) + \nabla \cdot (\rho \vec{u} \vec{u}) = -\nabla P + \nabla \cdot \mu(\nabla \vec{u} + (\vec{u})^T) + \vec{F} + S \quad (4.3)$$

where ∇ is the gradient operator, $\rho \vec{u} \vec{u}$ is the momentum of interested mass flow (i.e. $\dot{m}\vec{u}$ where $\dot{m}$ is mass flow rate), μ in viscous term $\mu(\nabla \vec{u} + (\vec{u})^T)$ is the dynamic viscosity, $\vec{F}$ is the body force term (such a gravitational force $\rho \vec{g}$), and S is momentum source term. The entire device during previous experiments was placed in a 37ºC incubator such that the device temperature was equilibrated at 37ºC. Thus there was no net heat exchange in the system and energy-affected mass transport is minimal in simulation.

4.2.1 Momentum Loss in Porous Structure

PureCol® collagen (Advanced BioMatrix, San Diego, CA) had been applied in 4QB as the extracellular matrix (ECM). Collagen is a typical porous biomaterial constructed via polymeric crosslinking generating interconnected protein fibers. It possesses variously sized pores in 3D space which allow fluid to pass. Meanwhile it also hinders fluid free convection and causes the momentum loss. In theory, this momentum loss can be characterized by making momentum source term on right side of Eqn (4.3) as [111]:

$$S_i = -\left(\sum_{j=1}^{3} D_{ij}\mu u_j + \sum_{j=1}^{3} C_{ij}\frac{1}{2}\rho|u|u_j\right) \quad (4.4)$$

where $\left(\sum_{j=1}^{3} D_{ij}\mu u_j\right)$ is viscous loss and $\left(\sum_{j=1}^{3} C_{ij}\frac{1}{2}\rho|u|u_j\right)$ is inertial loss (significant in turbulence), i and j are indices from 1 to 3, D_{ij} and C_{ij} are the *i*-*j*th components of coefficient matrix $\boldsymbol{D}$ and $\boldsymbol{C}$. $|u|$ is velocity magnitude.

When material structure can be simplified into one-dimensional (1D, e.g. a thin membrane), the momentum loss in such 1D homogenous porous medium is presented as:(adapted from [111])

$$S = -\left(\frac{\mu}{K}u + C\frac{1}{2}\rho u^2\right) \quad (4.5)$$

where K is the permeability in Darcy's law, i.e. the ability porous material allows fluid to permeate [112, 113]:

$$K = \mu \cdot \frac{Q}{A} \cdot \frac{\Delta L}{\Delta P} \quad (4.6)$$

where Q is volumetric flow rate, A is cross-sectional area fluid permeates and ratio of Q and A yields the superficial velocity $\bar{u}$, ΔL is the length that fluid diffuses driven by differential pressure ΔP.

4.2.2 O_2 Effective Diffusivity in Porous Material

4.2.2.1 Porous material geometry and permeability

Not only for collagen but in general, porous materials impede the fluid transporting through them and thus hinder the motion of soluble substances in fluid. Therefore the local mass diffusivities in porous material are lowered than in free liquid. The magnitude of momentum loss by such a hindrance is ruled by permeability of material itself, which relies greatly on porous characteristics. Two theories surveyed from literature mathematically answer how the permeability is affected by porous material geometric features: the first is deduced from fiber diameter as key parameter [114], and the other is based upon pore size [115].

Considering collagen in the 4QB cell culture, in "fiber diameter theory", as the flow is assumed to pass through an 3D array of fibers, the scalar collagen permeability K_c is calculated from collagen fiber volume fraction and fiber diameter [114]:

$$K_c = a^2 \cdot \left[\frac{3}{20\phi}(-\ln\phi - 0.931 + O(\ln\phi)^{-1})\right] \quad (4.7)$$

where a is the averaged collagen fiber diameter and ϕ is the collagen fiber volume fraction $(0 < \phi < 1)$, $O(\ln\phi)^{-1}$ is the error margin. For maximizing computational accuracy in our 4QB collagen space, the representative value of fiber diameter a must be determined experimentally, or from literature.

In "pore size theory", the scalar collagen permeability K_c is calculated from collagen fiber volume fraction, collagen geometric factor, and pore size [115-117]:

$$K_c = \frac{\varepsilon b^2}{4k} \quad (4.8)$$

where b is the pore size, ε is porosity given by $\varepsilon = 1 - \phi$, and k is geometric factor defined as [115-117]:

$$k = 2(1-\phi)^3 \left\{ \frac{2}{\phi[2\ln(\phi^{-1}) - 3 + 4\phi - \phi^2]} + \frac{1}{\phi\left[\ln(\phi^{-1}) - \frac{1-\phi^2}{1+\phi^2}\right]} \right\} \quad (4.9)$$

where ϕ is the fiber volume fraction in Eqn. (4.7).

The fiber diameter and pore size are closely coupled in the same material as key identifying properties. Therefore although taking great difference in expressions, these two theories are inherently conjugated. Collagen fiber diameter is at the magnitude of nanometers, requiring advanced technique to measure [118]. Collagen hydration and fixation state also affects its fiber diameter [119, 120]. On the other hand, collagen pore size actually equals to its average fiber spacing at the magnitude of microns. Using microscale pore size for calculation makes measurement easier with less error. Therefore, local O_2 diffusivity in this study will be obtained from the permeability by the "pore size theory".

4.2.2.2 O_2 effective diffusivity in collagen with cells presence

Since most convection outside the 4QB cartridge is dampened and predominant O_2 transport takes in the form of diffusion, and therefore local O_2 diffusivity controls O_2 delivery to cells. The material-dependent permeability K_c influences the effective O_2 diffusivity D_e in porous medium in the way that[†††] [115]:

x. [†††] For other early mathematical equations modeling relation between effective and free diffusivity in porous medium, see 113. Swartz, M.A. and M.E. Fleury, *Interstitial Flow and Its Effects in Soft Tissues.* Annual Review of Biomedical Engineering, 2007. **9**(1): p. 229-256.

$$D_e = D_0 \cdot \frac{\alpha}{1 + \frac{R_h}{\sqrt{K_c}} + \frac{{R_h}^2}{9K_c}} \quad (4.10)$$

where D_0 is the free O_2 diffusivity, α is proportionality constant in porous material (here set as 1), R_h is O_2 hydrodynamic radius[xi]. According to Stokes-Einstein theory, at low Reynolds number the hydrodynamic radius R_h is defined as:

$$R_h = D_0^{-1} \cdot \frac{k_B T}{6\pi\mu} \quad (4.11)$$

where k_B is Boltzmann constant and T is absolute temperature. Further, when seeded cells have a volume density significant enough to affect O_2 effective diffusivity, the modified D_e' is [121]:

$$D_e^{'} = D_e \cdot \left[1 - \left(1 - \frac{D_c}{D_e}\right)\left(0.09075{\phi_c}^3 - 0.8177{\phi_c}^2 + 1.727\phi_c\right)\right] \quad (4.12)$$

where ϕ_c is cell volume fraction in collagen space. In this simulation, assuming RPHs are spheres with uniform diameter at 30 μm, calculation based on current cell density (4-8 million cells per cartridge) showed such an effect is negligible.

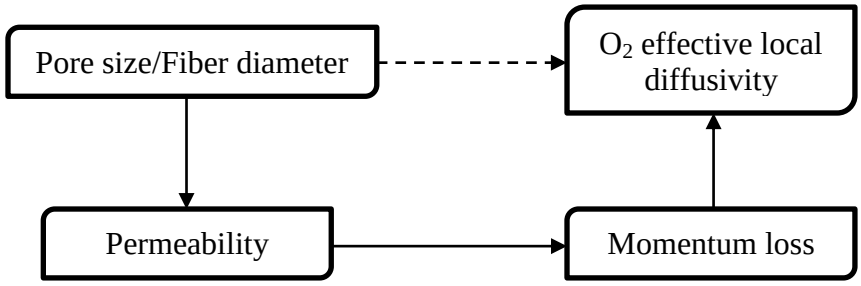

FIGURE 4.1 Chart of relations between each parameter, solid line represents direct deduction; dot line represents indirect deduction.

xi. ‡‡‡ Hydrodynamic radius is the radius of a sphere the hydrodynamic behavior of which is equivalent to interested molecules (e.g. O_2).

Fig. 4.1 recapitulates the intricate theories above that how properties of material and O_2 transport are linked.

4.2.3 Hepatocytes O_2 Uptake Characteristics

Taking RPHs for example, another challenge in 4QB O_2 simulation was how to model their O_2 uptake rate (OUR). Previous studies modeled the OUR of hepatocytes by applying Michaelis-Menten enzymatic kinetics [52, 108, 121, 122]:

$$S_{o_2} = -\rho_{cell} \frac{V_{max}[O_2]}{K_M + [O_2]} \quad (4.13)$$

where S_{o_2} is the volumetric OUR [kg/(s·m^3)], the negative sign indicates a sink source, ρ_{cell} is volumetric cell density (10^6/m^3), V_{max} is the maximum OUR that can be achieved (kg/s), $[O_2]$ is the concentration of substrate O_2 (in unit of kg O_2/kg O_2-dissolved medium), the Michaelis constant K_M is the $[O_2]$ when the magnitude of S_{o_2} is half V_{max}.

4.3 Methods

4.3.1 Computational Details

4.3.1.1 Geometry and mesh

The space where actual flow happens must be discretized ("meshed") before spatially assigning the physical properties and variables for matrices computing. Due to symmetry, only half a quadrant of our 4QB needs to be considered (Fig.4.2). Fig. 4.2 shows a view of half the 4QB single quadrant CAD model (4 cartridges), built using Pro/Engineer Wildfire4 (PTC, Needham, MA) and rendered by Tecplot 360™ (Tecplot, Bellevue, WA). Such CAD model was next meshed in ANSYS Workbench, after assigning proper boundary conditions it was solved using FLUENT 13.0 (ANSYS, Canonsburg, PA). Common geometry-based simplifications include 2D mesh (e.g. by axisymmetry) and partitioned 3D unit (e.g. by periodicity) to reduce computational cost.

However, as discerned from the design, 4QB single quadrant structure lacks further symmetric or periodic feature beyond the one shown in Fig. 4.2. Thus these simplifications do not suit 4QB model. The meshed 4QB quadrant geometry duplicates from its computer aided design (CAD) model. Within a given quadrant of the 4QB, the tissue regions are contained in custom-designed cartridges immersed within medium. The medium's top surface is bound by an air interface and capped by a solid lid above. Naturally the 4QB contains air and medium phases. The computational model therefore would be ideal to include both phases. It would be also more precise to take account of how air affects interface oxygen transport. Each 4QB quadrant has the capacity to maintain 8 cartridges, and was tested with 4 million hepatocytes inoculated per cartridge [106].

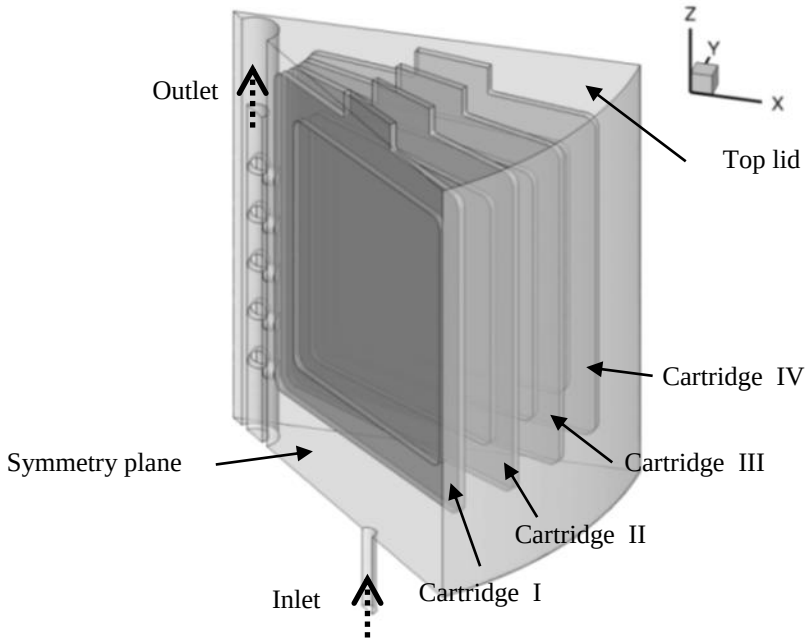

FIGURE 4.2 Half of the 4QB quadrant view in raw Cartesian coordinates for computation, and the positioning of each cartridge: are I, II, III and IV from symmetric plane to periphery, respectively. Dot line arrows indicate flow direction at inlet and outlet

4.3.1.2 Model simplifications and optimizations

Since the 1 mL/s volumetric flow rate in previous 4QB experiments [106] generated low Reynolds number flow throughout the bioreactor, computation was accomplished in laminar flow mode. The volume of fluid (VOF) scheme [123] built in FLUENT ideally should be applied as the key algorithm to distinguish gas-liquid dual regions accurately. Only transient mode which progresses the temporal simulation per time step was compatible with VOF algorithm.

However, such dual-phase transient computation requires demandingly great numerical stability and is very sensitive to the size of time step. For the best interest of CPU-hour, a computation balanced between slim time step around 10^{-5} s and effective simulation progressing must be adapted. Adjustments in FLUENT's explicit transient mode with control of Courant-Friedrichs-Lewy (CFL) condition[§§§] permitted such a strategy. Unfortunately, though global Courant number was throttled down to be 1 (see APPENDIX A), the practical transient mode computation still failed to converge.

Another difficulty in transient dual-phase calculation was that the O_2 diffusivity at air-medium interface is unknown. The air-water O_2 interfacial diffusivity couples with water surface layer thickness l_s, as $D_s/l_s = 1.3 \times 10^{-6}\mathrm{m/s}$ [124]. Obviously the water surface layer thickness l_s is necessarily to be determined for actual interfacial O_2 diffusivity D_s. Measuring this property imposed a tremendous challenge and also was beyond the scope of this study. Both the numerical stability and interfacial O_2 diffusivity issues suggested that current modeling needs a substitution for the dual-phase transient model, perhaps a simplified steady state model with equivalent accuracy. This model

xii. [§§§] Courant-Friedrichs-Lewy condition is a necessary numerical stability gauge for unsteady process, see APPENDIX A.

based on the same geometry should only contain medium (single fluid phase) and also respect O_2 diffusion impact from top air boundary. In this steady state model, boundary condition at the top lid (Fig. 4.2) is set as a constant O_2 diffusive surface acting as if air contacting. The effectiveness of such a simplification had been experimentally verified.[21] Other reasonable simplifications of the re-established steady-state mode included that the isotopic local O_2 diffusivity throughout the collagen space; constant medium flow at inlet neglecting pulsation introduced by peristaltic pump; and constant density of O_2-dissovled medium. The main algorithms in FLUENT used for this steady-state simulation were SIMPLE (acronym of Semi-Implicit Method for Pressure Linked Equations [125]) and second order upwind.

To embed some simplifications in package FLUENT, its user defined function (UDF) had been used and attached into steady state model. It had been used in medium-O_2 mixture density control, as O_2 "dissolved" in medium is treated by FLUENT with O_2 gas density. It also had been used in solubility control for O_2 in medium to avoid unreal O_2 "accumulation" exceeding the real O_2 solubility (see APPENDIX B for source codes).

TABLE 4.1 Major differences between two computational modes: transient mode and steady-state mode in computing practice.

Model Type	Transient	Steady-state (simplified)
Phase	with free gas-liquid interface	without free gas-liquid interface
Boundary	free medium top surface as opened to air	bound medium top surface with O_2 diffusion
Computational cost	~10^5 iterations and failed to achieve convergence	<10^3 iterations before convergence
Hardware requirement	3 octo-core CPUs (24 cores)	single quad-core CPU (4 cores)

In addition, the 4QB flow region had a complicated geometry and optimizing its mesh accelerates the following iteration. For improving mesh quality, meshing functions in ANSYS Workbench and ANSYS FLUENT were both utilized. The cartridge's regular-shaped collagen space was meshed into hexahedrons in ANSYS Workbench. The free medium space was initially discretized as tetrahedrons by Workbench and later converted into polyhedrons in FLUENT for taking its advantage [126, 127]. Tab. 4.1 summarized the major differences between the previous transient model and simplified steady-state model, as comparison.

Calculated results were post-processed via ANSYS CFD-Post (ANSYS, Canonsburg, PA) and Microsoft Excel (Microsoft, Redmond, WA). Contour and other results figures were plotted by OriginPro (OrignLab, Northampton, MA).

4.3.2 Empirical Measurements of Characteristic Parameters

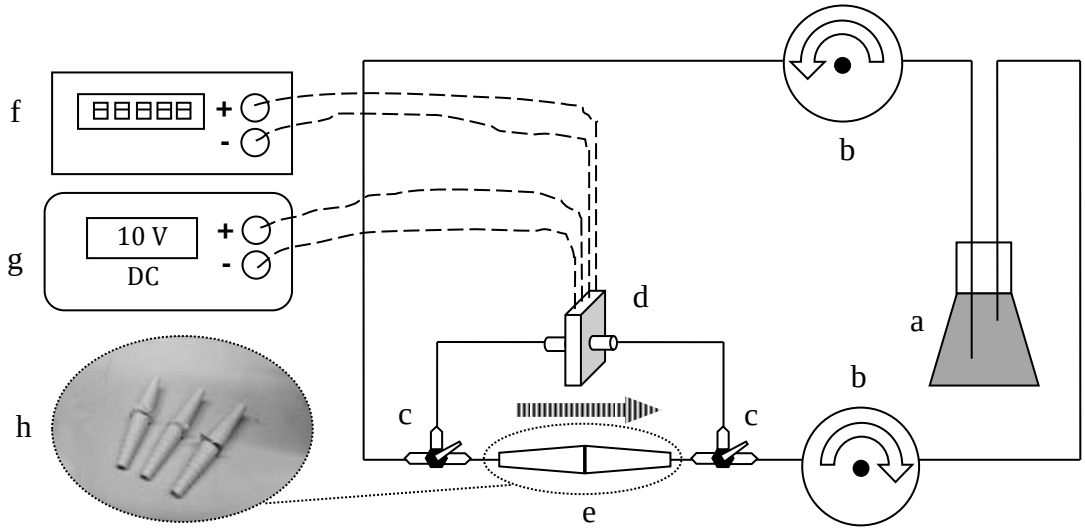

FIGURE 4.3: Flow circuit for measuring pressure drop through Biopore PTFE membrane. (a) open-flask medium reservoir; (b) peristaltic pump; (c) Three-way "T" valve; (d) differential pressure transducer; (e) solid connector with PTFE membrane insertion in the middle; (f) Keithley multi-reader; (g) DC power supply; (h) photo of (e) (3 replicates). Shadowed arrow indicates the direction of medium pumped through the membrane.

There were two types of porous materials in 4QB – PureCol® Type I collagen as ECM purified from bovine source (Advanced BioMatrix, San Diego, CA), and polytetrafluoroethylene (PTFE) porous membrane (Biopore, Millipore, Billerica, MA) to entrap cell-ECM assembly and shield cells from detrimental flow shear stress. Both must be characterized for computation inputs, which required empirical measurement.

4.3.2.1 Key inputs for polymer porous membrane

The 30 μm thick PTFE membrane has the pore size of 0.4 μm [106]. As in theory section Eqn.4.5 described, this thin membrane can be perceived by FLUENT as a homogenous 1D porous film in computation. Thus two key parameters were required – membrane's permeability and momentum-loss coefficient (Eqn. 4.4 & 4.5). According to Darcy's law (Eqn. 4.6), they can be calculated via pressure drop across the membrane and the flow velocity under such pressure drop [114]. Thus experimental apparatus was set up as Fig. 4.3 shows: the pressure drop across the membrane was measured using a differential pressure transducer (PX170-28DV, Omega Engineering, Stamford, CT), and average flow velocity (by the membrane circular cross-sectional area) was determined by volumetric flow rate of pump (Ismatec BVK, Cole-Parmer, Vernon Hills, IL).

4.3.2.2 Approximate collagen gel porosity determination

Being porous and light, collagen gel is also a tender biomaterial composed of nanoscale winded protein fibrils at wet condition [118]. Under normal conditions it cannot be sliced or investigated directly under scanning electron microscope (SEM) for the sake of moisture. Mercury porosimetry is a very accurate porosity measuring method among many [128]. However, this method is hardly applicable to material with great deformability. For instance, fibrils of collagen can only bear very little mechanical load

and will be damaged during mercury pressurized intrusion. A gentler, gas-based method had been developed to measure dry open-pore material's porosity via applying ideal gas law. But not only it requires a unique device with a precise graduation, the error also grows since increasing porosity from 30 - 40% [129]. Since collagen is known to have porosity of 90% or higher, this method will not be used until its accuracy to high-porosity material is confirmed.

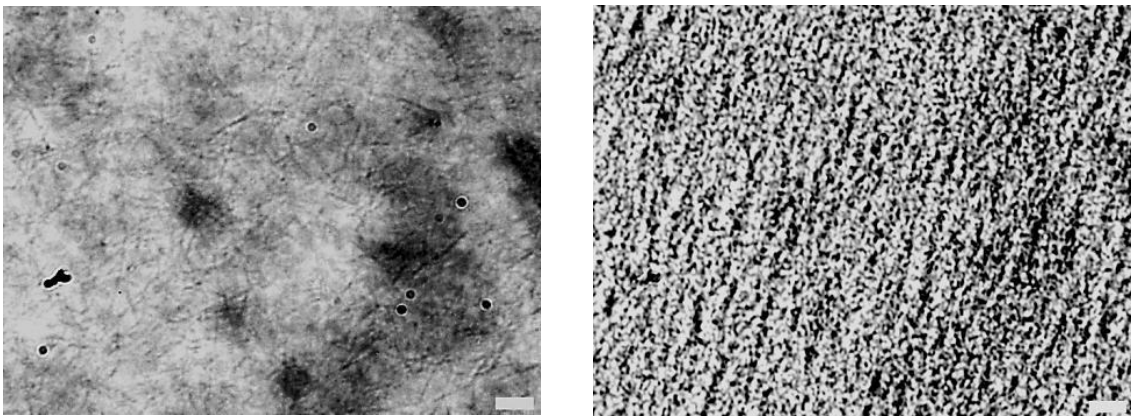

FIGURE.4.4 Two porous materials in 4QB microscope image (60×). LEFT: 1.3 mg/mL polymerized collagen type I fiber spacing and arrangement; RIGHT: PTFE membrane polymer/0.4 μm pore distribution (imaged after wet for its transparency). Calibration bar (down right corner) is 10μm.

An approximate porosity measuring method was thus considered. Note that PureCol®, had been diluted to desired density 1.3 mg/mL from 3 mg/mL 0.01 M HCl-dissolved 97% Type I collagen (and ~3% Type III collagen). Diluting supplements for this were 0.1 M NaOH solution, 10× Dulbecco's Modified Eagle Medium (DMEM) and deionized water. It was these water-based solutions occupying collagen gel's porous space. It is known that the weight of solution's aqueous content can be calculated from weighed difference of wet and dry collagen. If density of this water portion was assumed as that for the solution, the solution's volume can be estimated by water density at 37°C.

Meanwhile, total volume of supplemented collagen solution was already known in pipetting. Since porosity is the ratio of porous volume to total volume, if ignoring total volume change in polymerization, with estimated porous volume the collagen gel approximate porosity (at given conditions 37°C and 1 atm) will be obtained.

To implement, the weight difference of fresh 1 mL 1.3 mg/mL collagen gel with above supplements in P35 before and after vacuum desiccation was measured using lab balance (Mettler-Toledo, Columbus, OH). Because collagen gel's non-protein (solution) content was also available from the density (1.3 mg/mL), solution's rough weight can also be calculated to compare with empirical measurements. The calculation showed small difference (< 3%). With Eqn. 4.8 & 4.9 given known collagen permeability value, the fiber diameter can be deduced from the porosity. Collagen fiber diameter obtained by estimated porosity from "differential weights" method agrees with others values [120, 130], extrapolated or directly match, demonstrated the accuracy of the porosity estimation.

4.3.2.3 Approximate collagen gel pore size determination

Fiber spacing is a good estimation for pore size of unfixed collagen gel. To image fiber distribution, 500 µL 1.3 mg/mL collagen was placed into a Costar® Snapwell™ 12 mm insert (Corning, Lowell, MA) and incubated at 37°C for 4 hours to achieve full gelation and thickness resembling culture in 4QB cartridge. Such insert was imaged under an Olympus IX70 microscope with Olympus 60× oil immersed objective (Olympus America, Center Valley, PA) and Hamamatsu C4742-95 digital camera (Hamamatsu, Bridgewater, NJ). MetaMorph® (Molecular Devices, Sunnyvale, CA) was used as the image capturing and processing software.

4.3.2.4 Approximate gelatin sponge porosity determination

When the simulation indicated that only limited O_2 local diffusion with 8 million cells per cartridge had been permitted, it was imperative to identify the reason. The test simulation showed increasing flow rate or membrane removal yielded the same low cellular O_2 content. Rather, only when collagen gel as original ECM had been replaced by Gelfoam® gelatin sponge, cellular O_2 content was significantly improved.Characterization for this ECM was similar to collagen gel. Its porosity was estimated via "differential weights" method by wetting a circular sample piece. Specifically, since gelatin sponge is hydrophobic, to saturate it with water, the precisely cut sample was placed in a glass jarcontaining deionized water in a 37°C vacuum oven (Isotemp® 280A, Fisher Scientific, Pittsburg, PA) for fully degassing. Then wet diameter and height of the sample were measured for volume calculation. Its net wet weight was also measured by same lab balance. Later such a sample was dried using lab vacuum and weighed again. The weight difference of gelatin sponge was obtained and its porosity was estimated. By this material change, momentum transfer in porous space was altered, and consequently so is the effective O_2 local diffusivity. Re-simulated results were shown in results to compare with the collagen-based results.

All key parameters used in this simulation are tabulated in APPENDIX A, Tab. 1, with descriptions and units.

4.3.3 Summary of O_2 Balance in 4QB

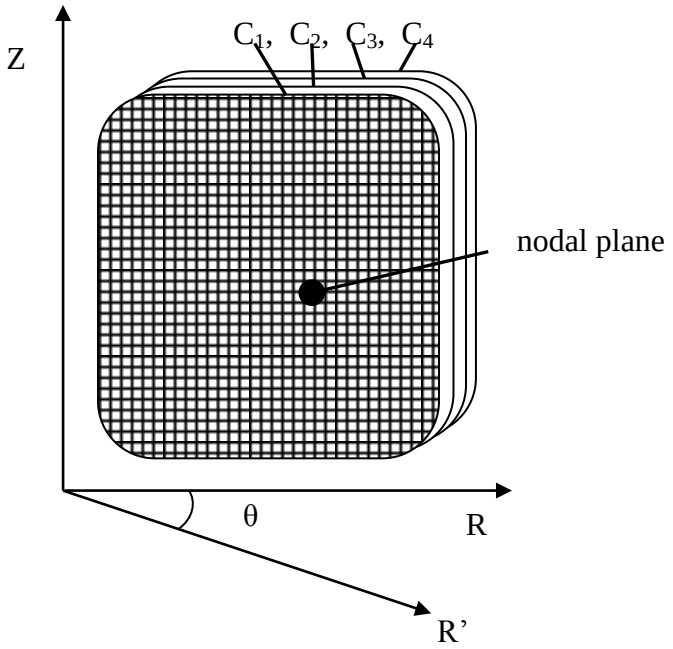

FIGURE 4.5 Illustration of collagen space in a single cartridge that is discretized into 3 computational grid layers, where computing nodes spread on 4 planes parallel to each other. Coordinate system is set cylindrical. C_1, C_2, C_3 and C_4 denote O_2 concentration (in terms of mass fraction) for each nodal plane. Averaged values of paired C_2 and C_3 with (r, θ, z) coordinates, where only θ differs, are used to represent O_2 distribution in each cartridge. Data are presented in cylindrical (Z-R) coordinates: $R = \sqrt{x^2 + y^2}$

O_2 at inlet in medium was saturated as a result of sufficient oxygenation. The air oxygenating effect at air-medium interface was also considered as previously described. The Michaelis-Menten kinetics implemented in model was programmed in UDF.which set RPHs as the O_2-consumping component in cartridge that performs liver function.

4.3.4 Data Representation for Contour Plots

Because only O_2 values in cartridge interior space were of concern, their data for contour plots were selected as shown in Fig. 4.5. Each collagen space entrapped by cartridge-membrane assembly has totally 3 layers of hexahedron-structured grids, which

yields 4 node layers (Fig. 4.5). O_2 concentration at the first (C_1) and last nodal layer (C_4) are boundary conditions for one interested collagen space. The middle two nodal layers (C_2, C_3) represent numerical O_2 profile of inside the collagen. In the global cylindrical coordinates, the paired values of C_2 and C_3 that have the same (r, z) coordinates (but different θ) are averaged into $\overline{C}$ (i.e., $\overline{C^n} = \frac{C_2^n + C_3^n}{2}, n = 0,1,2 \dots, Max$). Such averaged $\overline{C}$ values delineate the internal O_2 distribution of a single cartridge that cells are sensitive to, and thus are plotted as essential O_2 results.

4.4 Results

The estimated collagen gel porosities acquired by "differential weight" method was 92.9 ± 1.3% (n=4, Mean ± SE). While calculation based on collagen solution protein density gave 96.0 ± 0.3% (n=4, Mean ± SE), it indicated negligible discrepancy (3%) between the two.

According to Eqn.4.8 & 4.10, the local effective O_2 diffusivity for a porous material is modulated by its pore size. The ratio of effective O_2 diffusivity to free O_2 diffusivity (D_e/D_0) is plotted against material pore size in Fig.4.6. It demonstrates that effective O_2 diffusivity increases along with pore size enlargement. Such relation is non-linear: when pore size is comparable to 1 μm, the effective O_2 diffusivity is one tenth of that in free medium; when pore size is larger than 100 μm the effect of increasing pore size to increase O_2 diffusivity diminishes (Fig.4.6). This relation implies that an ECM with larger pore size will enable higher local effective O_2 diffusivity. Applying such ECM for higher hepatocytes population can possibly eliminate hypoxia region.

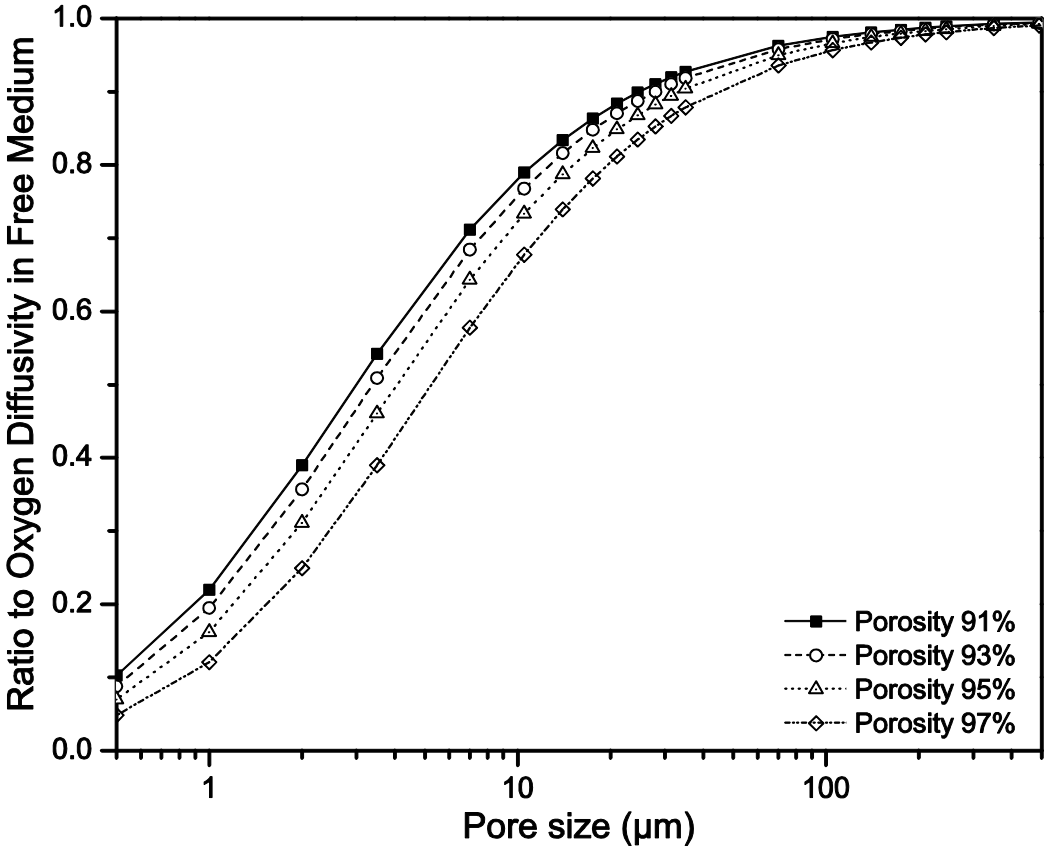

FIGURE 4.6. Theoretical relation between ratio of O_2 diffusivities (in porous region: in free medium) and material pore size ($\log_{10}$ scale), under different porosities (91-97%). For all calculated porosities, trends are that when pore sizes are larger, oxygen diffusion has less hindrance in porous material.

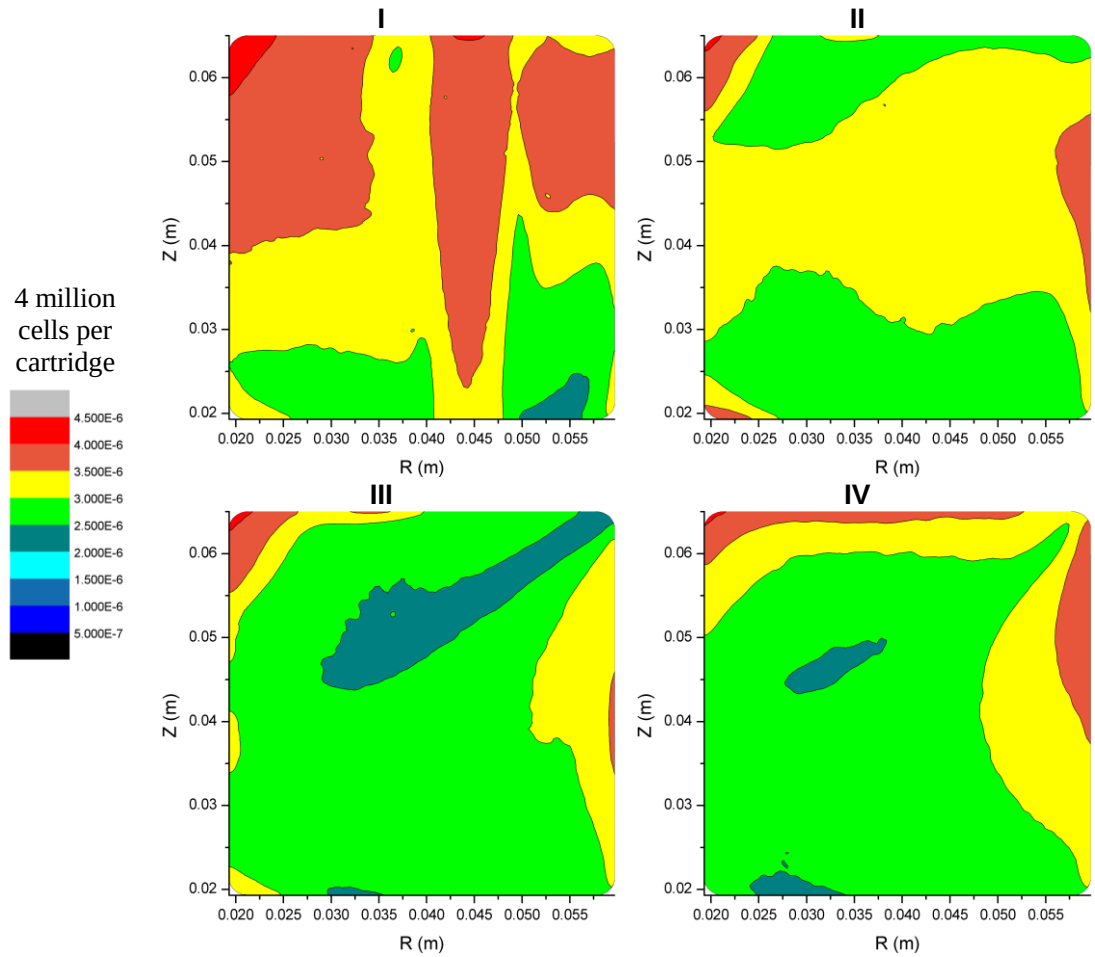

FIGURE 4.7-a: Calculated O_2 profiles of cartridge I, II, III and IV, 4 million cells per cartridge, collagen gel, in a cylindrical Z-R coordinate.

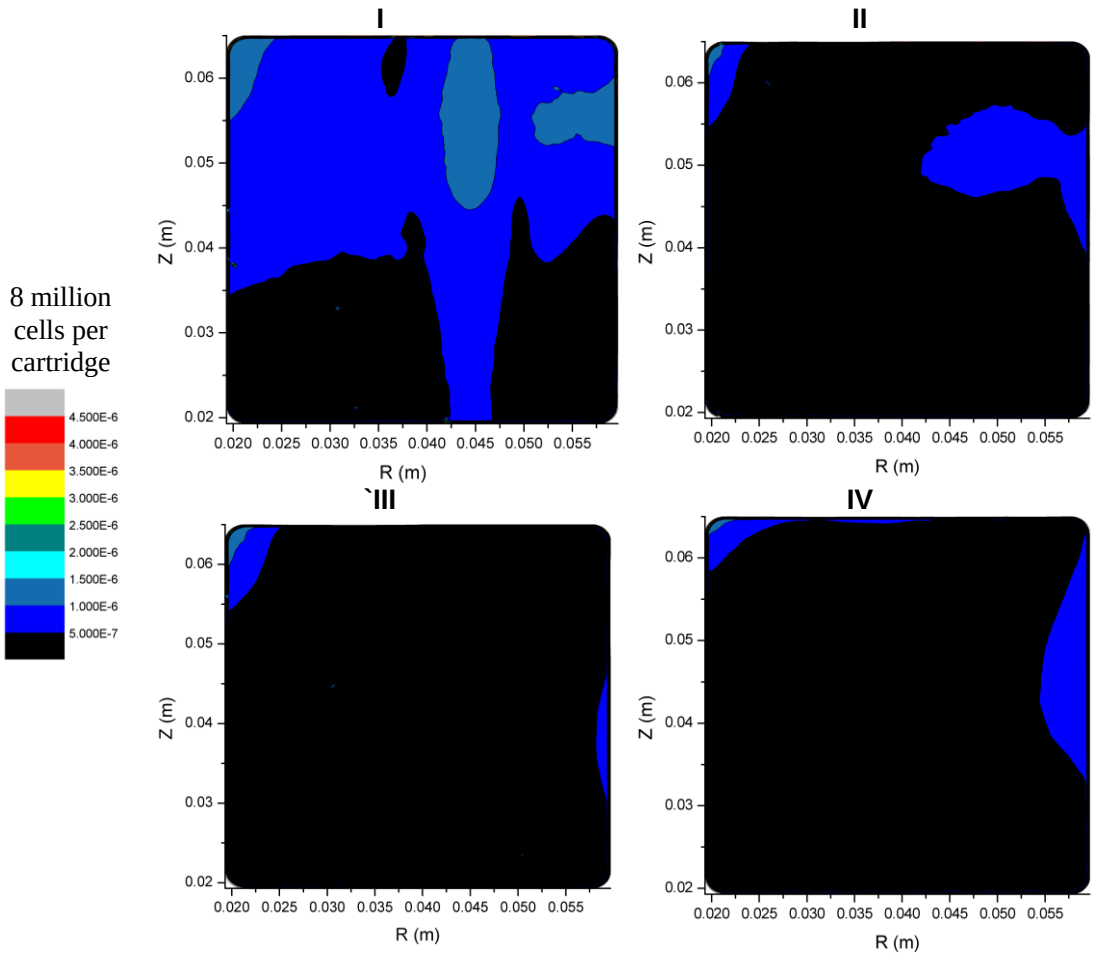

FIGURE 4.7-b: Calculated O_2 profiles of cartridge I, II, III and IV, 8 million cells per cartridge, collagen gel, in a cylindrical Z-R coordinate.

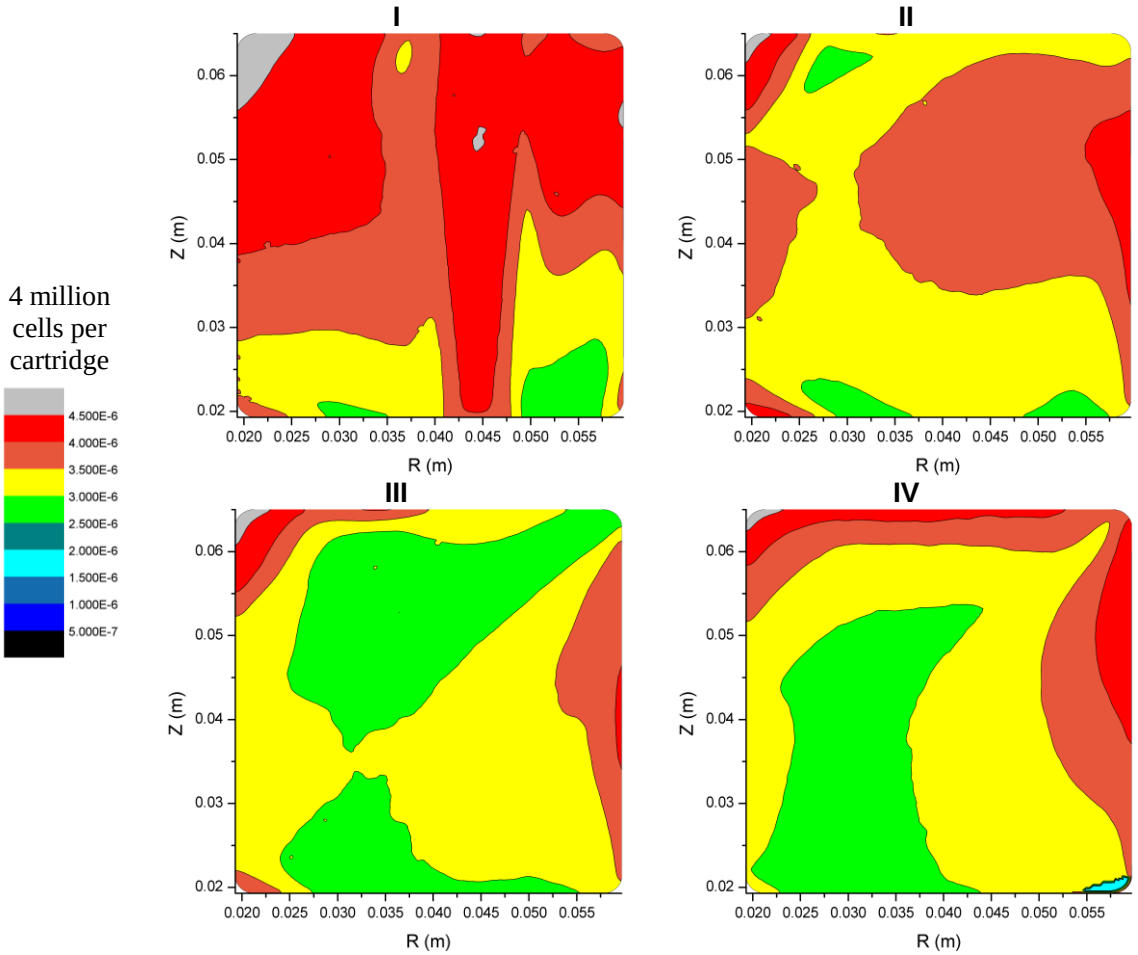

FIGURE 4.8-a: Calculated O_2 profiles of cartridge I, II, III and IV, 4 million cells per cartridge, gelatin sponge, in a cylindrical Z-R coordinate.

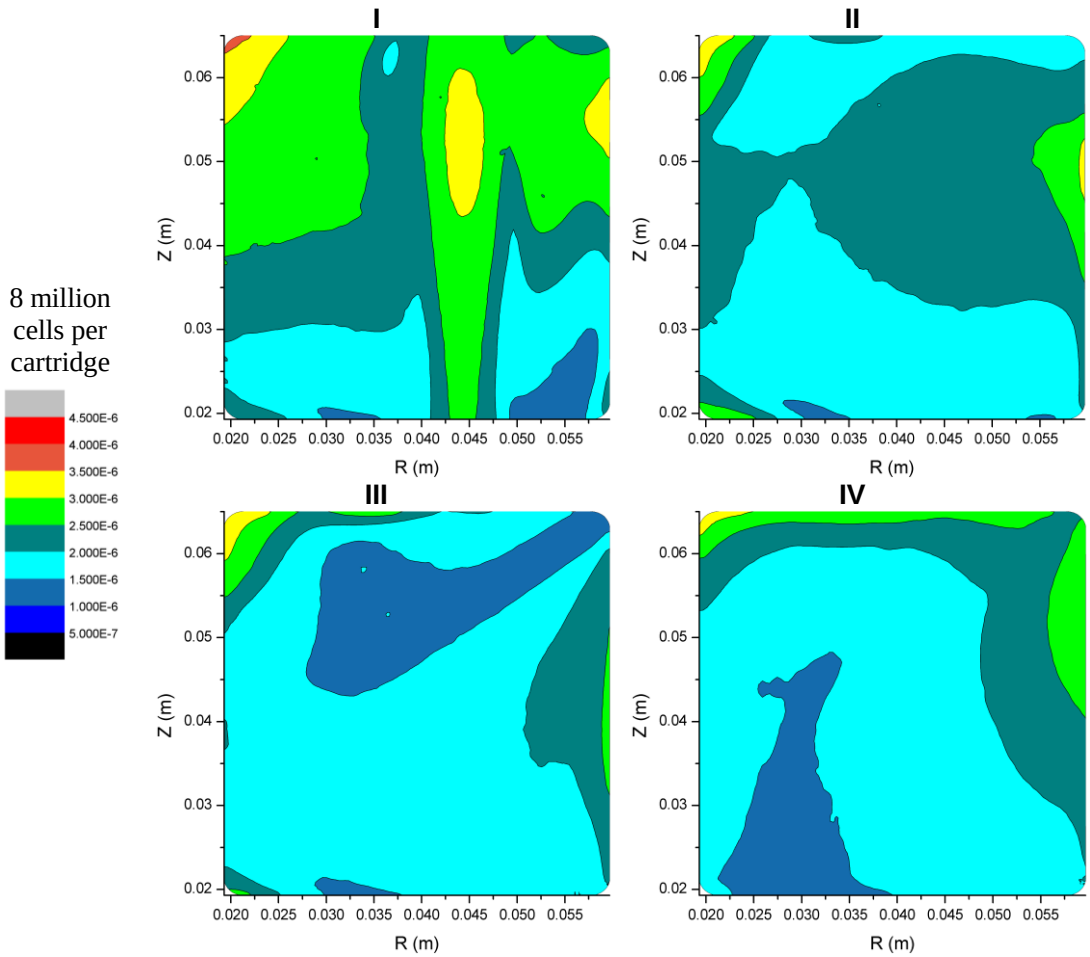

FIGURE 4.8-b: Calculated O_2 profiles of cartridge I, II, III and IV, 8 million cells per cartridge, gelatin sponge, in a cylindrical Z-R coordinate.

The results of a fully loaded, 8-cartridge quadrant (maximally designed capacity) are plotted in panel view (Fig. 4.7 & 4.8-a,b). It can be discerned rom the figures that at full designed capacity (64 million rat hepatocytes per quadrant), gelatin sponge as an ECM with larger pore size (characterized at 350 μm) effectively permits more O_2 transporting into the extracellular space when the overall population is doubled.

Once ECM switched to gelatin sponge, the O_2 supply has been considerably improved and the optimized O_2 distribution has been increased 12-fold in each cartridge on average (Fig.4.9, condition D versus condition B).

Beside the primary focus on characterizing gelatin sponge as an ECM for elaborating its advantage in O_2 enhancement, there are still other questions not answered: since collagen gel in 4QB is cased in membrane-cartridge structure and protected from shear stress, there will be no concern to increase the medium flow rate – will this necessarily increase the final O_2 level in cartridge? Under normal flow rate (60 mL/min), although the PTFE membrane has a substantially larger pore size (0.4 μm = 4000 Å) than O_2 molecule diameter and is very thin (30 μm), is it also impeding O_2 traveling through? To investigate cartridge space O_2 level under these two conditions, the doubled flow rate (120 mL/min) and membrane-free cases were also computed. As shown in Fig. 4.9 (condition E), double flow rate (120 mL/min) indeed improve the O_2 condition even slightly more than engineering the ECM material at original flow rate (60 mL/min), while removing the membrane (though not feasible in experiment) does not help to raise significant O_2 in cell-residing cartridge space (condition F).

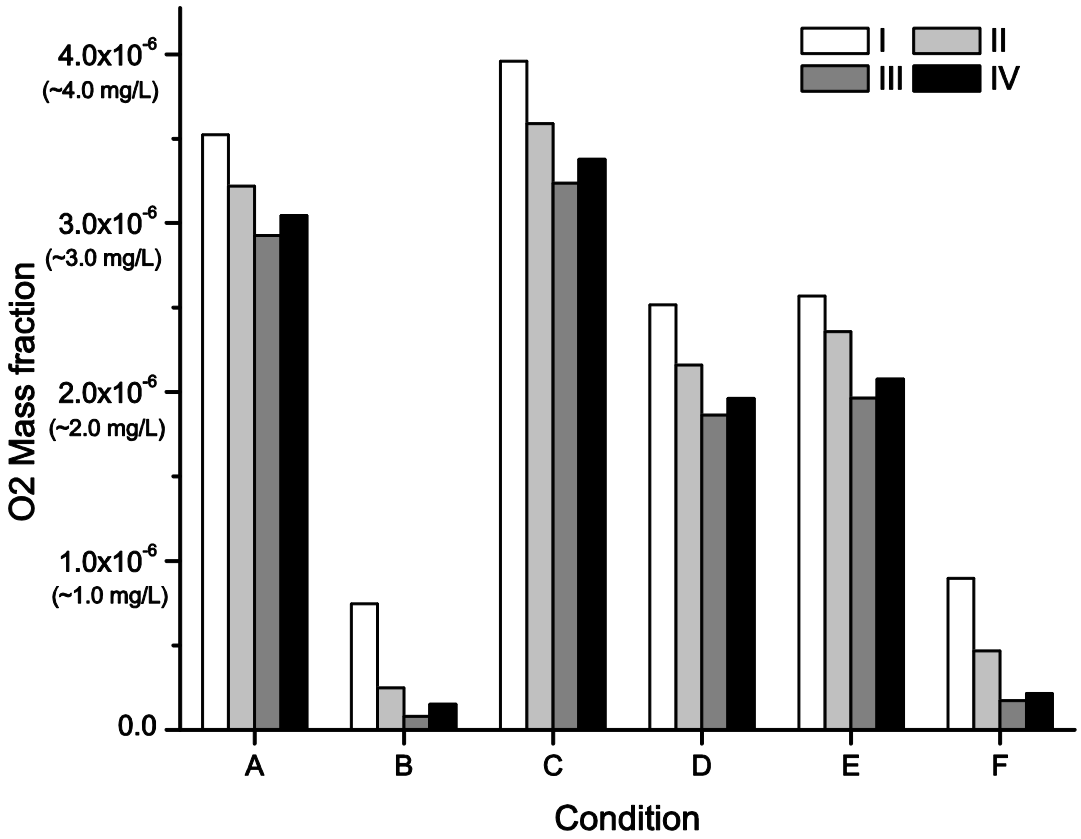

FIGURE 4.9 Average O_2 mass fractions in each cartridge (I, II, III and IV). A, B, C, D, E, F indicate conditions as:
A: collagen gel ECM, 4×10^6/cartridge, original flow rate (60 mL/min);
B: collagen gel ECM, 8×10^6/cartridge, original flow rate (60 mL/min);
C: gelatin sponge ECM, 4×10^6/cartridge, original flow rate (60 mL/min);
D: gelatin sponge ECM, 8×10^6/cartridge, original flow rate (60 mL/min);
E: collagen gel ECM, 8×10^6/cartridge, double flow rate (120 mL/min);
F: collagen gel ECM, 8×10^6/cartridge, original flow rate (60 mL/min), no PTFE membrane.
A, B, C, and D have the same original flow rate and PTFE membrane, while E has double flow rate and PTFE membrane, and F has original flow rate but PTFE membrane was removed (in computation).
To convert the unit here, 10^{-6} = 1 mg O_2 / 1 kg mixture ≈ 1 mg O_2 /L mixture considering O_2-contained aqueous medium density is 1.00967 kg/L.[121])

4.5 Discussion

As a liver-mimicking medical bioreactor, BAL must have the efficiency competitive to natural liver for accomplishing the functions. As hepatocytes in BAL are inherently aerobic, it is necessary to supply abundant O_2 supply into cellular space (i.e., ECM's interstitial space), not just superficially to have O_2-enriched medium flow in BAL. To improve this O_2 condition, the reason casting such a limit must be identified. As in ECM porous region where convection is very limited, O_2 transport mainly relies on diffusion. Therefore, the local effective O_2 diffusivity that a particular ECM permits is crucial to determine the extracellular O_2 content level.

Previous studies have successfully increased O_2 diffusion distance using microbeads-embedded collagen ECM [30, 98] and achieved 6-fold viable hepatocytes population than normal collagen gel [30, 98]. This agrees with prediction in this chapter that the intrinsically low local O_2 diffusivity of collagen (causing the short distance O_2 can diffuse in limited time) is the main reason for insufficient O_2. At large cell population, this issue is aggravated. As Fig. 4.9 summarized, when local O_2 diffusivity is increased, significant change of O_2 profile is achieved as equivalent as double flow rate. This implies the low local O_2 diffusivity mainly by hindrance of collagen ECM is an important cause to mediocre cellular O_2 condition in 4QB. Using an alternative ECM having higher effective O_2 diffusivity could attenuate the O_2 issue and remove the barrier for higher performance. This has been corroborated in functional results of previous CHAPTER 3 (Fig. 4.10, treated by normal medium only): it is demonstrated that using gelatin sponge as ECM alone enables C3A cells to have better long-term albumin secretion and EROD activity results.

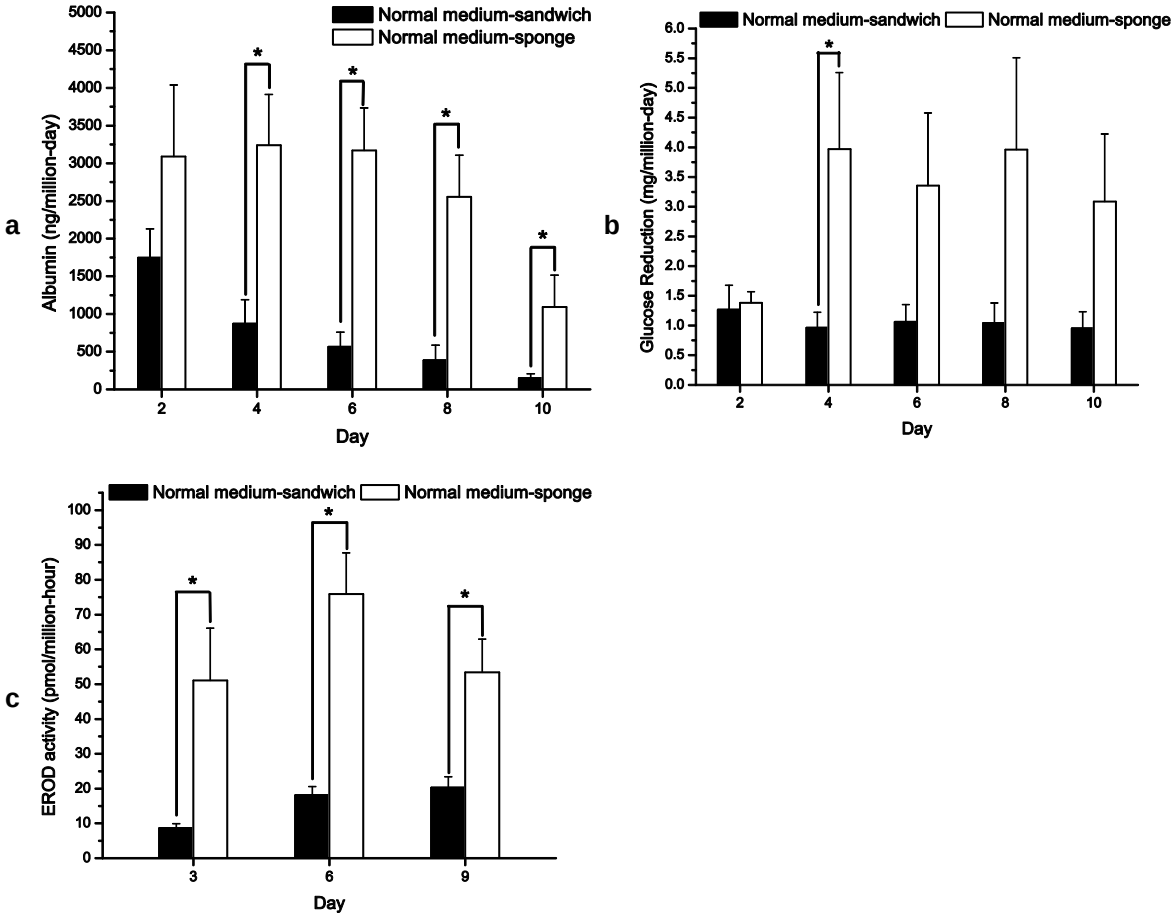

FIGURE 4.10 (Rearranged CHAPTER 3 results) Results of Albumin secretion (a), glucose reduction (b) and EROD activity (c) in static plate culture, collagen gel ECM compared to gelatin sponge ECM. n=9, Mean ± SE, *:$p<0.05$ (adapted from Fig. 3.4 I & II).

As simulated results indicate, gelatin sponge with larger pore size is a promising candidate to solve O_2 issue in 4QB cartridge. When simulated again setting gelatin sponge as ECM, the results showed that on average 12-fold O_2 content has been achieved at 8 million cells per cartridge than previous predicted O_2 distribution (Fig. 4.9). By its success, the model has allowed us to avoid high "trial-error" costs associated with real experiments.

In addition, to prove accuracy and effectiveness of the model, it would be ideal to introduce O_2 sensor into our cell-seeded 4QB and compare the acquired O_2 concentration data with numerically predicted results. An ideal sensor would feature such properties as: easy to handle and mount; small but with high sensitivity, for O_2 varies spatially in 4QB and usually its concentration is low; and preferably with low maintenance. The size of traditional O_2 probe (polarographic, Clark-type or Galvanic) would trouble its fitting into the small celluar space (such as that in 4QB cartridge) and have a high spatial definition. An alternative method is to use the O_2 optode incorporating optic fiber and measures O_2 based on luminescence which does not consume O_2 [20, 21]. The clear advantages of such optode are tiny size that allows insertion of small space, and zero O_2 consumption which leaves original O_2 state undisturbed. Though this measurement is beyond the scope of this study due to the cost and experimental limitations, its effects in impending research publications are highly expected.

CHAPTER 5: PERFORMANCE OF RAT HEPATOCYTES DRUG METABOLISM IN 3D CULTURE AND DYNAMIC FLOW DEVICES

5.1 Introduction

Drug detoxification is one of the most important functions of hepatocytes. Drug, mostly lipophilic, is apt to affix cell membrane and thus retain in human body to form unwanted toxins. To clean the unnecessary drugs that dwell in human body, the cleansing mechanism in human liver plays a crucial role. Drug metabolism by hepatocytes biochemically transforms such foreign chemicals into hydrophilic compounds (via hydroxylation) which are more soluble in water (and blood stream). General formula of such biotransformation for drug is as below [22, 26]:

$$RH + NADPH + H^+ + O_2 \xrightarrow{CYP450} ROH + NADP^+ + H_2O \qquad (5.1)$$

where RH is the drug to be transformed, NADPH is the co-factor nicotinamide adenine dinucleotide phosphate. In this type of reaction, molecular O_2 also serves as electron acceptor as it is in energy metabolism. Specifically, one oxygen atom is used in hydroxylating RH into ROH, the other atom accepts hydrogen atom and forms water H_2O (Eqn. 5.1). As a result, drug is biotransformed into more hydrophilic compounds and its excretion is facilitated (via urination, perspiration etc.). In hepatocytes, such biotransformations are catalyzed via a superfamily of enzymes – cytochrome P 450 (CYP450). Each specific type of CYP 450 hydroxylates a certain category of substrates.

In this chapter, the drug metabolism function of rat hepatocytes (RPHs) were evaluated in different extracellular matrices (ECM) under static and dynamic flow

conditions, to investigate how different oxygenation conditions particularly impact the catalyzing efficiency of CYP450 (i.e., CYP450 activity). Such functions were tested under different cell seeding populations, as a specific aim of future's BAL is to achieve higher capacity for which the BAL demands more densely packed cells as researchers striving to attain [15]. Specifically, to activate such enzymes, two polycyclic aromatic hydrocarbons (or polynuclear aryl hydrocarbons, PAHs): 2,3,7,8-tetrachlorodibenzo-p-dioxin (TCDD), the most potent dioxin, and 3-methylcholanthrene (3-MC), also a strong carcinogen, were supplemented in medium as inducers to stimulate CYP450 enzyme activities. These enzyme activities were measured by ethoxycoumarin (EC) and ehtoxyresorufin (ER) which are substrates for ethoxycoumarin-O-deethylase (ECOD) and ethxyresorufin-O-deethylase (EROD) assays, respectively. The hydroxylation rate of substrates in each assay was regarded as the indication of ECOD/EROD activity. Advantages of gelatin sponge as ECM and dynamic flow conditions were demonstrated in results having notably higher RPH CYP 450 activity as contrast to the control. Also, the encountered issues were analyzed and possible causes to them are discussed.

5.2 Materials and Method

Following previously established procedures, hepatocytes were isolated from Sprague-Dawley male rats weighing 150-280 g that were fasted 24 hours prior to isolation [131]. The viability of received hepatocytes was accessed immediately using Trypan Blue exclusion assay (Sigma-Aldrich, St. Louis, MO). For each experiment, hepatocytes with viability higher than 90% are used, otherwise the cells were Percoll®-centrifuged (GE healthcare, Waukesha, WI) to screen out dead cells until viability reaches higher than 90%.

The regular cell culture medium bases on Gibco® William's E medium (Life Technologies, Grand Island, NY) was supplemented by 10% (v/v) standard fetal bovine serum (HyClone, Thermo Scientific, Waltham, MA) and 1% (v/v) antibiotic/antimycotic solution (JR Scientific, Woodland, CA).Separate inducers (TCDD or 3-MC) were added to this regular culture medium to initiate different function assays (EROD or ECOD, details elaborated in assay section).

5.2.1 Cell Culture 3D Configuration

5.2.1.1 Collagen dispersion configuration

PureCol® collagen (containing 98% Type I collagen) at the concentration 3.1 mg/mL was diluted down to 1.8 mg/mL using 1/8 final volume of 10× Dulbecco's Modified Eagle Medium (DMEM). To prepare the collagen for entrapping RPHs in 3D space, 1.8 mg/mL collagen was pre-warmed in 37°C water bath for 2-10 minutes (depending the volume) till a significant higher viscosity was achieved yet no gelation started. Meanwhile, quantified cell solution was pelleted and evenly mixed with proportional pre-warmed viscous collagen, forming desired uniform cell density (2 million/mL or 4 million/mL). Subsequently, 1 mL of such homogenous cell-collagen mixture was pipetted into each well of a standard 12-well plate to obtain 2 or 4 million cells per well density, and incubated at least 3 hours for full gelation. After firmly gelled, each cell-collagen sample was added 2 mL regular culture medium and incubated for another 24 hours after when 2 mL inducer-medium (TCDD or 3-MC) replaced the regular medium in each well and cultures were returned to incubation for one more day (day 2). Drug metabolism assays (ECOD, EROD) were performed on day 2.

5.2.1.2 Gelatin sponge configuration

Gelfoam® (Pharmacia & Upjohn, New York, NY) gelatin sponge dry sheet (the same scaffold applied in CHAPTER 3) was cut into discs with radius of 16 mm (same as inner diameter of standard 15 mL conical tube) and sterilely hydrated using same method in CHAPTER 3, for culture in standard 12 well plate. The same cell population (2 or 4 million per disc) was also implemented to this type of ECM culture.

5.2.2 Drug Metabolism Assays

5.2.2.1 Ethoxycoumarin O-Deethylase (ECOD) assay

For static plate culture, previously induced 3D cell collagen-suspension or cell-loaded sponge discs were placed in 12-well plate cell culture units. Each unit was induced by 2 mL of 10 nM TCDD conditioned culture medium since day 1 and last for 24 hours. Then supernatant of each well was aspirated and each sample was added 3 mL Hank's Balanced Salt Solution (HBSS) and incubated 20 minutes for rinsing. After 1.5 mL 100 μM 7-ethoxycoumarin (7-EC) in serum-free William's E medium was added as substrate, and all samples were incubated for 1 hour. Each sample was pressed in culture well using a syringe plunger until all free 7-EC solution has been collected into a 2 mL Eppendorf vial (Fisher Scientific, Pittsburgh, PA). Collected original sample solutions were stored at -20°C till use.

As the start, the first step is to directly extract the net 7-hydroxycoumarin (7-HC) in solution. Each 0.5 mL original sample solution was added 1 mL chloroform (Sigma-Aldrich, St. Louis, MI) and vortexed for 30 seconds, then centrifuged at 2000 *g* for 7 minutes. Then 0.5 mL of 7-HC dissolved chloroform was transferred to a clean 2 mL eppendorf vial and added 1.25 mL 0.01 M NaOH/1 M NaCl, vortexed and centrifuged

again (3 minutes instead of 7 minutes). At the end, 1 mL of the 0.01 M NaOH/1 M NaCl solution in each vial (final 7-HC solution) was pipetted in plastic cuvette (Fisher Scientific, Pittsburgh, PA) and read by a F-2500 fluorescence spectrophotometer (HITACHI, Tarrytown, NY) with excitation/emission at 360/450 nm. Concentrations of the 7-HC were determined via comparing the readings of known 7-EC standard curve such that final 7-HC amount of each sample was calculated using dilution ratio in extraction.

In order to measure all 7-EC including that also has been biotransformed phase II drug metabolism, 0.5 mL 100 units/mL β-glucuronidase (Sigma-Aldrich, St. Louis, MO) solution[xiii] was mixed with 0.5 mL original sample solution in the same 2 mL eppendorf vial. Each vial with such mixture was shaken in water bath for 3 hours, and the same extraction and reading steps were performed. Data from both forward (drug metabolism phase I) and reverse reaction (phase II) were summed to evaluate the total 7-EC generated via hydroxylation (i.e., the ECOD activity). For dynamic culture (plate & tube devices) and the static tube culture (as control for tube device), except that the induction part was completed in flow-perfused device, the rest of the assay was identical to that in static plate culture described above.

5.2.2.2 Ethoxyresorufin O-Deethylase (EROD) assay

Similar to ECOD assay, for static culture, after 48 hours of sample units cultured in 2 μM 3-MC medium (refreshed once at 24-hour time point), each sample was rinsed in 3 mL HBSS for 20 minutes. Then 1.5 mL 10 μM ethoxyresorufin (ER) and 10 μM dicumarol in 50 mM HEPES buffer was added following 1 hour incubation. At the end,

xiii. [****] This concentration is diluted from 840 units/mL (1.4 mg/mL) β-glucuronidase stock using 60 mM sodium acetate (Sigma-Aldrich, St. Louis, MO) solution.

as in ECOD assay, maximum volume of free ER solution was collected (for sponge culture the disc was pressed), and was stored at -20°C until use. The reading was taken at excitation/emission of 530/590 nm using the same HITACHI spectrophotometer. Similar to ECOD assay, for dynamic culture and the static tube culture, except that the induction part the rest of the assay was also kept identical as that above.

For both ECOD and EROD assays, the inducer-free regular medium cultured groups were used as negative control (supposed to be blank), and their readings were subtracted from the readings of sample group (i.e., the inducer supplemented medium).Therefore, all results recorded had considered normal medium effect to CYP450 activity.

5.2.3 Flow Devices used in Dynamic Cell Culture

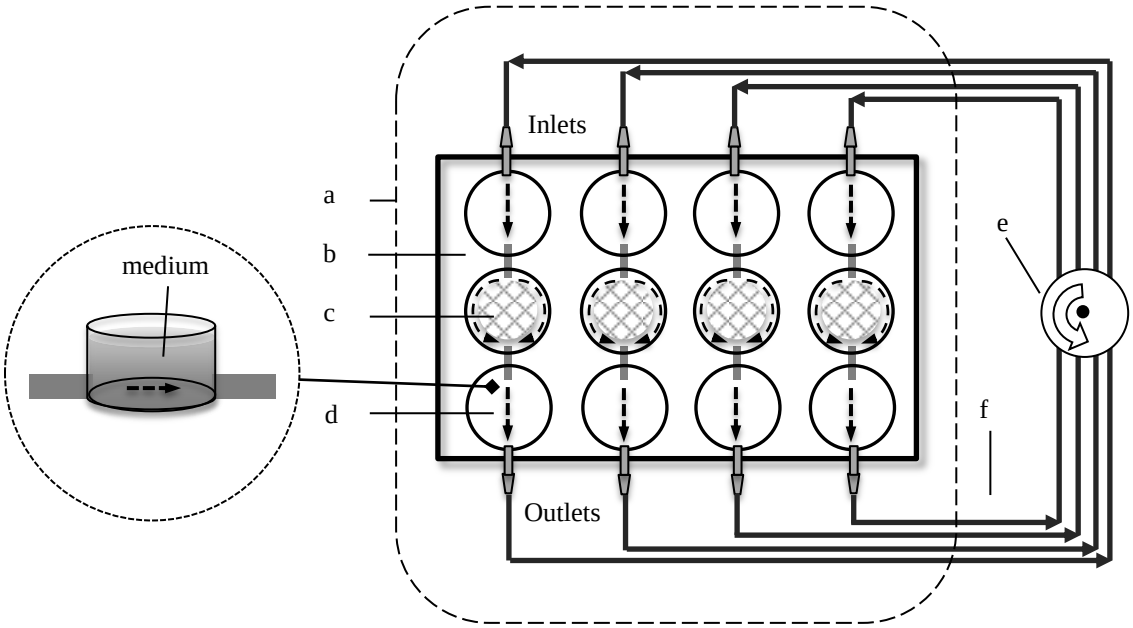

FIGURE.5.1 Schematic of the flow device based on regular 12-well tissue culture plate (plate device). (a): incubator; (b) standard 12-well plate with each well serially connected at bottom; (c) cell-loaded gelatin sponge disc; (d) flow direction maked as arrowed dash line; (e): peristaltic pump; (f) silicone tubing (except for pump-pressed portion).

To investigate the effects of flow condition to RPHs' drug metabolism, two distinct flow devices were designed and used for this study: flow device No.1 is based on a 12-well cell culture plate ("plate device"), and device No.2 is based on a 15 mL conical tube ("tube device"). Medium flow of both designs was driven by the same peristaltic pump (Cole-Parmer, Vernon Hills, IL) at certain rates.

5.2.3.1 The plate device

The plate device relies on the same passive oxygenating mechanisms that regular multi-well plates does. Modified from a regular 12-well cell culture plate, such plate device can house 4 separate samples at one time. Having its wells of each column punched through at the bottom and was connected serially by tubing segment (Fig. 5.1), it enables medium flows from the 1st well to the 3rd well in the same column and culture the cell-loaded sponge disc was placed in the 2nd well (Fig. 5.1, middle well), in a "circumventing" manner.

At the 1st and 3rd well, fittings were used to connect the medium-supplying tubing and interior well space as inlets and outlets. Sealing of all junctions is done via silicone sealant (IS 808, Momentive Performance Materials, Waterford, NY). The medium-supply tubings are made of silicone to permit sterile O_2 diffusion from air aside that through top cover. After drilling, accessories attaching and sealing of the plate had been finished, the whole plate device was soaked in 70% ethanol for 1 hour then dried in laminar flow hood under ultraviolet (UV) light. Prior to culture, 12 mL of medium was slowly added to each column, ensuring the whole cell-loaded gelatin sponge disc in the 2nd well (middle well) would be fully immersed at flow running (Fig. 5.1). The main advantage of this device is that since most of the flow circumvents around the disc, the shear stress generated within

the disc structure is minimized, while the culture-surrounding medium was always agitated to optimize O_2 and nutrient condition. As the O_2 delivery in such a device derives from the passive diffusion static plate culture relies on, plus O_2 also diffuses from circuit's silicone tubing, at given cell population O_2 supply in plate device is not a concern.

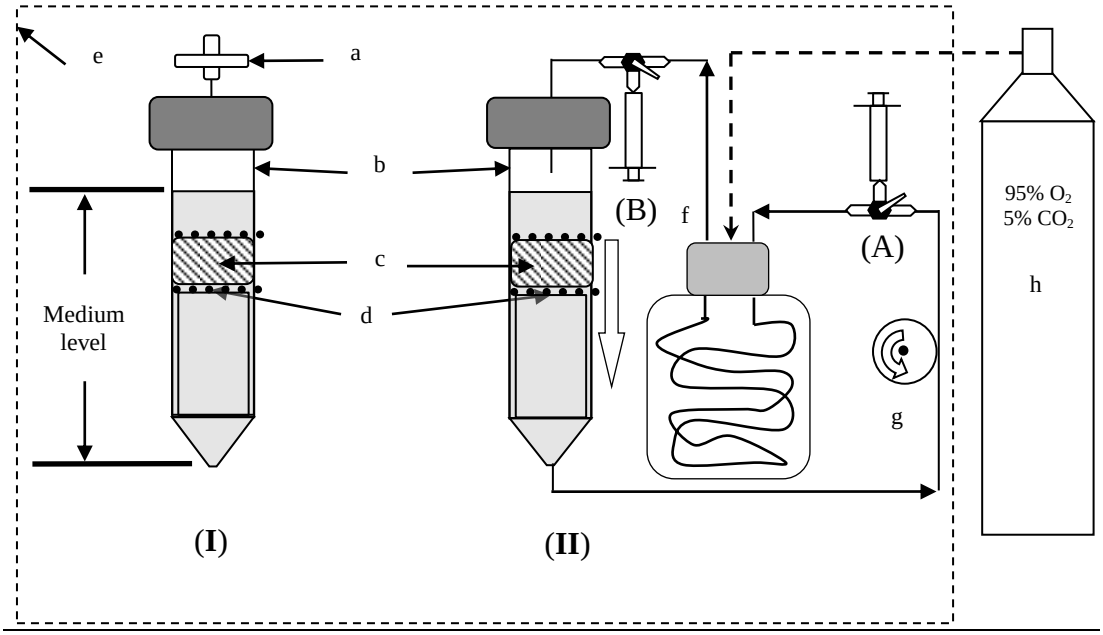

FIGURE.5.2: Schematic of the flow device based on regular 15 mL conical tube (tube device). (a)syringe filter; (b)15 mL conical tube; (c)cell-loaded gelatin sponge disc; (d)stainless steel mesh; (e)incubator; (f) gas exchanger; (g) peristaltic pump; (h) gas tank. (A)&(B): syringe sampling ports for measuring O_2 at outlet & inlet of tube flow device

5.2.3.2 The tube device

In the plate device, the sponge disc-circumventing medium lacked the momentum to force fluid through cellular region and a poor perfusion was foreseen. To regulate the flow going thoroughly into the sponge disc interstitial space, previous conical tube-based flow device in CHAPTER 3 is redesigned to apply to current flow study. Sharing a large portion of design features as the flow device in CHAPTER 3, this 15 mL conical tube-

based device has smaller diameter (16 mm) to house the 3D cell-loaded sponge disc with the same size of discs in 12 well-plate static culture and plate device culture, meanwhile allowing vertical medium perfusion. This size shrinkage offers more calibrated parameters and costs less expensive gelatin ECM material than previous device design in CHAPTER 3. Since *in vitro* RPHs do not proliferate, quantitating their number becomes more convenient. Cells were seeded at the same density (2 or 4 million per disc) as in static plate culture. This is a considerably higher density than that implemented in CHAPTER 3, in which replicating C3A cell line having a smaller OUR [103] was used.

5.2.4 O_2 Measurements for Tube Flow Device

As previously mentioned, the prototype of tube flow device shown in Fig. 5.2 was firstly tested in CHAPTER 3 for PFC study. Here it is modified into a smaller version with reduced size of 3D culture. The actual O_2 situation of either case, however, was not measured. As RPHs consumes O_2 considerably faster than HepG2 cell line especially in dynamic flow condition [103] and this smaller tube flow device was going to accommodate a lot more cells (up to 4 million per device), it is imperative to validate the O_2 condition in flow device with cell presence. A straightforward method to attain this is to measure the O_2 concentration in medium outflow (spent medium).

5.2.4.1 Relation between O_2 concentration and partial pressure (pO_2)

Henry's law states that with temperature held constant, molar concentration of a gas as solute in dilute liquid solution (i.e., far from saturated) is proportional to the gas's partial pressure equilibrated to this liquid, and the proportionality is the Henry's constant [132] (also named "gas solubility" in literature). Henry's constant varies when temperature changes in the way the van't Hoff equation (Eqn. 5.2) describes [133]:

$$K_T = K_{T_0} \cdot exp\left[C\left(\frac{1}{T} - \frac{1}{T_0}\right)\right] \quad (5.2)$$

where K_T is Henry's constant at temperature T, and K_{T_0} is that at standard temperature T_0 (e.g. 25ºC or 298K), C is constant depending on gas species, and for O_2 it is 1700. Acocrding to standar Henry's constant at 298K is 1.3×10^{-3} mol/(L·atm) and Eqn. 5.3, for O_2 in aqueous solution at 37ºC Henry's constant is 1.042×10^{-3} mol/(L·atm) [1.371×10^{-9} mol/(mL·mmHg)]. This value closely agrees with that has been used in literature [1.29×10^{-9} mol/(mL·mmHg)].[103] To comprehend the DO probe-measured O_2 concentrations in unit of mg/L in a sense of the *in vivo* physilogical pO_2 data with unit mmHg (Torr), Henry's law must be applied.

5.2.4.2 OUR determination

Meanwhile, the O_2 uptake rate (OUR) in this particular device was also of interest. Together with flow rate, this value could also be acquired via the difference between O_2 concentrations at inlet and outlet, as in Eqn. 5.3:

$$OUR = \frac{Q(DO_{in} - DO_{out})}{N} \quad (5.3)$$

where Q is perfusion flow rate (mL/minute), DO_{in} is the O_2 concentration at tube device inlet (mg/L) and DO_{out} is that at outlet (mg/L), N is cell population in device (10^6).

For measuring, two T- connectors were mounted at illustrated positions in Fig. 5.2: "A" before gas exchanger and the other "B" after gas exchanger. Each connector was connected to a 3 mL syringe as sample receiver. The tube flow system was allowed to run as the same assay inducing period (1 day of TCDD-medium and 2 days of 3-MC medium). At the end of such dynamic culture, medium flow toward gas exchanger was redirected to syringe at "A", and 3 mL sample solution was collected, volume as

minimally required by our dissolved oxygen (DO) meter (AccumetXL60, Thermo Fisher Scientific, Waltham, MA) to measure its O_2 concentration in the same way as CHAPTER 2 describes.

The measured 3 mL medium did not return to the device. Instead, equal volume fresh inducing medium were injected back to flow device via the sampled syringe as compensation. During measuring time, the pump was stopped till medium compensation was done, then resumed running to allow re-equilibrium for 20 minutes. The same sampling steps were performed again at "B" to evaluate freshly re-oxygenated medium. Readings were taken once stabilized, as previously described in CHAPTER 2. Immediately after completion of O_2 measurements, cell-loaded sponge discs were retrieved from each flow device and controls (static tubes) into 12-well plates, and ECOD/EROD assays were then performed.

5.2.5 Flow Rates Setup

The flow rate of circulating medium was 0.82 mL/min in the plate device experiments. This rate seems arbitrary but in fact it is easily scaled up or down as it is set by peristaltic pump at 10 rpm[††††]. The flow rate of the tube-device was set as 0.41 mL/min (5 rpm), to avoid unexpected shear stress condition, as well as to accommodate single sponge disc's hydraulic permeability.

5.2.6 Plotting and Statistical Analysis

The O_2 measurement of the device was repeated 3 different times. Each ECOD and EROD assay experiment consisted of at least 4 samples (static plate, collagen dispersion and gelatin sponge) or 3 samples (dynamic plate- and tube-devices). Each type of experiment was independently performed 3 times. Results are presented as Mean ±

xiv. [††††] This peristaltic pump has the rpm range 0-999 rpm.

Standard Error (SE). One-way analysis of variance (ANOVA) was performed and $p < 0.05$ is regarded as judge criterion for statistical difference. OriginPro (OriginLab, Northampton, MA) was used to plot the data as well as to perform the statistical analysis.

5.3 Results

5.3.1 O_2 Measurement for Tube Flow Device

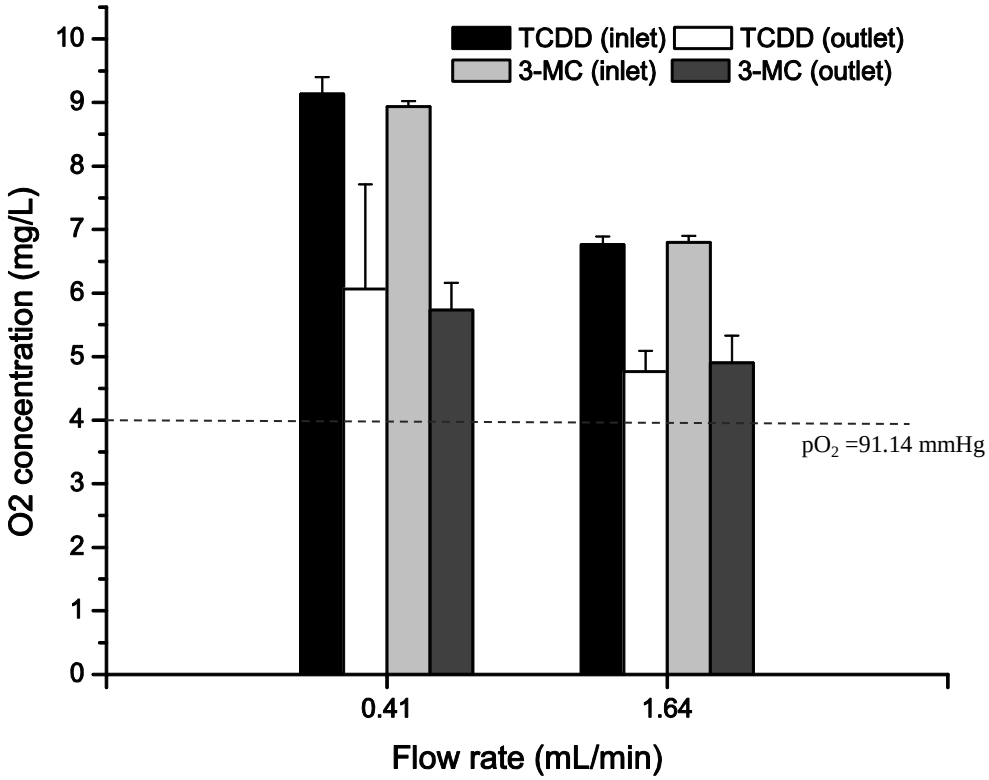

FIGURE 5.3 O_2 concentrations at inlet and outlet at two different inducer conditions and two perfusion flow rates (0.41 and 1.64 mL/min), in tube flow device as shown by Fig. 5.2. n ≥3, Mean ± SE.

Fig. 5.3 illustrates measured different O_2 concentration levels at tube flow device inlet and outlet, at different . Since the main purpose to examne this O_2 condition is to make sure no obvious O_2-defficient flow occurs during the inducing period, only the minimum O_2 concentration should be examined. As Fig. 5.3 shows, the minimum O_2

concentration (TCDD medium treated , outlet) is higher than 4 mg/L. Using Henry's law to convert 4 mg/L and obtain the equilibrated pO_2 level at 91.14 mmHg (Torr), it can be concluded that the average supply and spent media pO_2 levels were all above this value.

Tab. 5.1 shows the OUR results calculated from Eqn. 5.3 for different inducer conditioned media. Among all results in Tab. 5.1, no statistical significance was found.

TABLE. 5.1 O_2 uptake rates (OUR) of RPHs in custom designed flow device compared with value from literature. The measured original O_2 concentration unit was mg/L. In order to compare with results in [103] data unit were converted in to μmol/L. 4-MU stands for 4- methylumbelliferone.

Device type	Total RPHs population	Flow rate (mL/min)	Inducer in medium	OUR (μmol/10^6-hour) (Mean ± SE)
Flow device in Fig. 5.2	1×10^6	0.41	10 nM TCDD	2.36 ± 1.28
			2 μM 3-MC	2.46 ± 0.29
		1.64	10 nM TCDD	6.15 ± 0.81
			2 μM 3-MC	5.84 ± 1.27
Hollow fiber bioreactor in [103]	1×10^8	0.15	5 μg/mL Lidocaine and 60 pM 4-MU	0.173±0.021

5.3.2 CYP450 Functions

For static plate culture, the 2 million cells in both collagen gel and gelatin sponge ECMs had ECOD activity on the same level (Fig. 5.4-Ia). Yet when population increased to 4 million, it was the gelatin sponge-cultured hepatocytes that had a higher rate of catalyzing the EC-HC transformation. Such a phenomenon also exist in static plate culture EROD assay (Fig. 5.4-IIa), where hepatocytes in gelation sponge matrix has higher EROD activity.

However, for the above populations under flow condition, neither enzyme (ECOD or EROD) of hepatcoytes cultured in plate device showed higher activity than static culture. Rather, though both cultured in the same gelatin sponge ECM, the EROD activity

of cells embedded in dynamic flow-surrounded sponge disc of plate device even fell below the level that static plate cultured hepatocytes had (Fig. 5.4-IIb).

For tube device, activities of these two CYP 450 enzymes were contrasted to the hepatocyte sponge culture in a tube having no flow (static tube). The ECOD result of population at 4 million per disc demonstrated that at such a higher cell density, hepatocytes in flow device had a higher EC-HC catalyzing speed than the static control.

Fig. 5.4-IIc shows the EROD assay results for both dynamic tube device and its static tube control. Nonetheless, similar to the phenomenon in Fig. 5.4-IIb, for both 2 million and 4 million cells per sponge disc, static tube allowed hepatocytes to perform EROD function better, and this was even more obvious in the case of 4 million cells per disc.

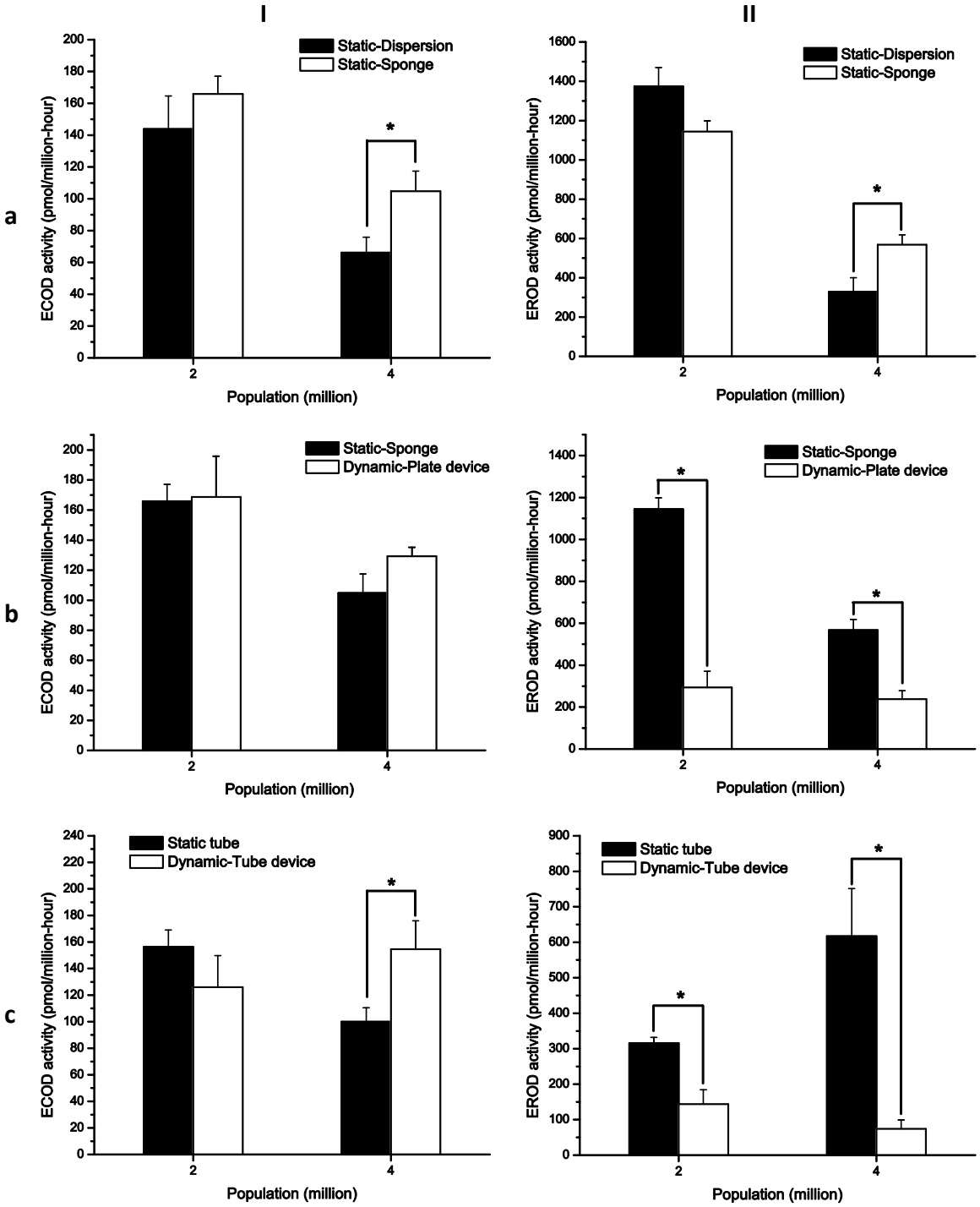

FIGURE 5.4: ECOD (column I) and EROD (column II) activities of rat hepatocytes. Row a: comparison of static cultures in collagen dispersion and gelatin sponge (n = 12); Row b: comparison of static culture in gelatin sponge (n=12) and plate device dynamic culture (n=4); Row c: comparison of cultures in static tube and dynamic tube device (n=4). Mean ± SE *: $p<0.05$.

5.4 Discussion

In this study, the O_2 concentrations at the inlet and outlet of a conical tube based device were measured, from which the OUR per million of RPH in such a device was determined. More importantly, the activities of two specific CYP 450 enzymes – ECOD and EROD – were evaluated under 3D gelatin sponge ECM and dynamic flow conditions with two different seeding densities assigned to each assay.

Firstly the O_2 concentration levels at inlet and outlet of the tube device to be used for CYP450 fucntion study were measured, to guarantee that the gas exchanger was effecitvely re-oxygnating the circulating medium. Considering the pO_2 in average liver periportal blood ranges 60-65 mmHg and in perivenous blood it is 30-35 mmHg [134], the minimum pO_2 value derived from Fig. 5.3 (91.14 mmHg) ensured that the O_2 supply in the flow device will be fairly abundant through the perfusion period at inducer presence.

When the same data were used to characterize OUR between two distinct flow rates tested (0.41 and 1.64 mL/min) for the same inducer type in Tab. 5.1, there was actually no statistical significance found. However, the climbing average OUR values along increasing flow rate suggest that with in a moderate range, higher flow rate (i.e., higher O_2 availability) may encourage cells to consume more O_2. This trend agrees with Michaelis-Menten enzyme kinetics theory (see CHAPTER 4), previous OUR studies perfusing *ex vivo* rat liver [135] and isolated hepatocytes [136, 137].

ECOD and EROD results in static culture suggested that for both assays, when hepatocytes were cultured at higher density, gelatin sponge-seeded cells demonstrated higher CYP 450 activities than cells dispersed in collagen gel. This may attribute to the

different ECMs been used and the different configurations such ECMs necessarily introduced. For example, in collagen dispersion, though cells were also suspend in 3D gel trap (Fig. 5.5, left), as 1 mL cell-collagen mixture was plated in culturing well, forming a gel layer with height of ~2.5 mm from bottom, O_2 supply to all cells through this layer has to be through the top layer of medium and then reaches the collagen region. As a contrast, the gelatin sponge having a larger volume holds the same number of cells. Therefore its actual cell volume density is less than the dispersion (Fig. 5.5, right).

A more important positive aspect of the gelatin sponge material is that due to a higher O_2 local diffusivity it permits (as analyzed in CHAPTER 4), cells have the opportunity to consume more O_2 transported into their neighborhood. As a result, their CYP 450 activities were enhanced. Thus the advantage of gelatin sponge for cell 3D cultivation ECM has been proved again in static drug metabolism related experiments (for more comparison, see CHAPTER 3).

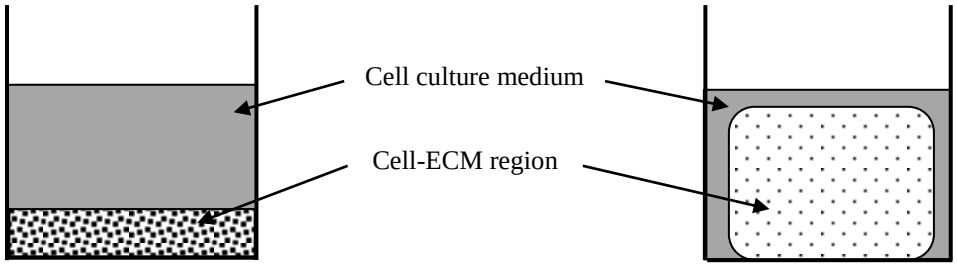

FIGURE 5.5. Schematic of two static culture configurations in 12-well standard plate (not to scale). LEFT: cells in collagen gel dispersion; RIGHT: cells in gelatin sponge.

When comparing both static and dynamic plate culture using the same gelatin sponge as ECM, the results were seemingly confounding: in ECOD assay as no statistical difference was found between the static and dynamic plate culture (Fig. 5.4-Ib). If this is because flow did not sufficiently perfuse through the sponge disc central region in plate

device, same justification cannot explicate that the EROD counterpart had weaker CYP 450 activity in dynamic plate culture than static plate culture, for both populations (Fig. 5.4-IIb).

Similar phenomenon continued: when EROD results are revisited, it is shown that neither population at dynamic condition yielded higher resorufin production rate per million cells than those in static tubes. Initially it was assumed that the shear stress in dynamic tube may have reached the deleterious level, as RPHs have a low threshold to bear shear stress above which their function performance will be weakened (0.5 Pa in normal hepatic sinusoids) [138] (more shear stress discussion in APPENDIX C). However, the shear stress in plate device that has non-perfusive flow should not impose sensible shear stress to cells, particularly when most of them were seeded in the disc central region where motionless flow can be expected.

TABLE. 5.2 Levels of drug inducer (TCDD and 3-MC) as toxin and flow rates in each type of RPH cultures.

Culture configuration	Medium volume per culture (mL/unit)	10 nM TCDD amount (nmol/10^6)		2 μM 3-MC amount (nmol/10^6)		Flow rate (mL/min)	Estimated extracellular shear stress level
		2×10^6 cells	4×10^6 cells	2×10^6 cells	4×10^6 cells		
Static plate	2	0.01	0.005	2	1	-	zero
Dynamic plate	12	0.06	0.03	12	6	0.82	minimum
Static tube	8	0.04	0.02	8	4	-	zero
Dynamic tube	24	0.12	0.06	24	12	0.41	moderate to high
4QB [106]	40 (per cartridge)	-		20 (32×10^6 cells)		60	zero/ minimum

One possible cause to the deteriorated EROD activities in both devices is likely to be the excessive 3-MC amount per cell was added, which was not effectively metabolized

and exerted remarkable toxicity. Placing quantities of both TCDD and 3-MC inducers under review, for ECOD assay it was10 nM TCDD medium while in EROD assay the concentration of 3-MC was 2 μM. Both concentrations were consistently used in all types of static culture and dynamic culture. However, in the two flow devices, a greater volume (plate device: 12 mL; tube device: 24 mL) was required, such that total toxin levels were significantly increased (Tab. 5.2). For example, in plate device, TCDD and 3-MC quantities per million cells are 6 times of those in static plate (Tab. 5.2). Among all types of cultures, normalized TCDD amount was sustained below 1 nmol per million cells, while 3-MC dramatically increased from 1 up to 24 nmol per million cells. This 3-MC quantity may contribute to the fact that cultured hepatocytes were not only induced, but also overwhelmed by its toxicity and had suppressed metabolic activity or even lower viability.

But such level of 3-MC was already used in previous study , resulting up to 20 nmol per million cells for cartridge-entrapped RPHs [106] (Tab. 5.2), the question thus now becomes why previous dynamic 4QB cultured cells had a higher EROD activity than its control: the 24-well plate cultured cells (Fig. 5.6).

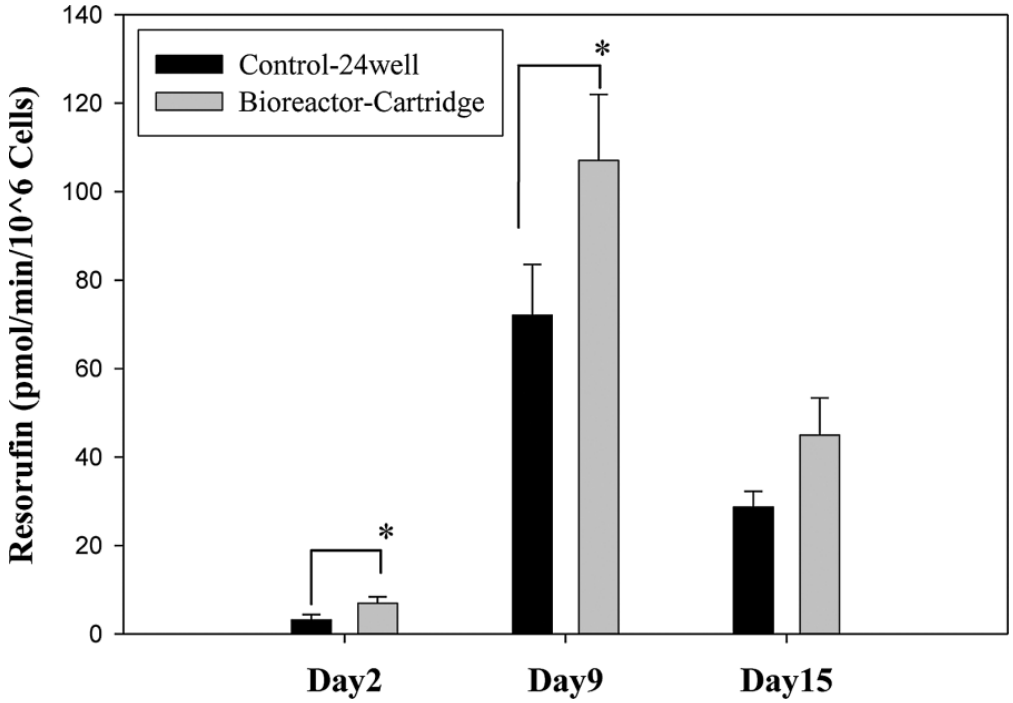

Figure 5.6 Ethoxyresorufin O-deethylase activity of hepatocytes before placement in the bioreactor (day 2 after isolation) and after (days 9 and 15). The values are the mean±SD, n=3.Statistically significant difference: *p<0.05.Reproduced from [106].

It is believed that the answer also lies in the diffusion hindrance theory. In 4QB the cell-embedded collagen may have hampered not only the diffusion of O_2 molecules, but also the loading rate of 3-MCmolecules as well. Though there was convective flow in chamber for long term, according to the universal diffusion hindrance elaborated by Stokes-Einstein theory in CHAPTER 4 (Eqn.4.10), the 3-MC diffusion rate into cellular space was actually also throttled. In this case, the cellular CYP450 enzyme had been catalyzing the reactant 3-MC with an appropriate supply rate. As there was no 3-MC accumulation, its toxicity also diminished. On the contrary, the gelatin sponge has characteristic pore size more than 30 μm [80] and permits a high mass transport rate for general substances including both O_2 and 3-MC. With such enhanced diffusivity enabled, both 3-MC and O_2 delivery into the interstitial space of gelatin sponge were facilitated.

More 3-MC, as far as available, entered cytoplasm directly and stressed the entire hepatocellular metabolism. To confirm this adverse "overdosing effect", one method is using relevant cytotoxicity assays [such as almarBlue® (resazurin)] to check cell metabolic responses under different 3-MC concentrations, which starts to be reduced from 2 μM.

Since design and design-determined circulating volume varies from device to device it is difficult to immediately select an optimal inducer concentration for function study. Therefore, in the future bioreactor CYP450 study, it would be always prudent to use a diluted inducer concentration from culture condition that has lower volume (e.g., petri dish culture), and adjust dynamically according to the feedback.

CHAPTER 6: CONCLUSION AND REMARKS FOR FUTURE WORK

Initiated with the intention to bridge FHF patients, over the past 40 years BAL has yet to be approved by regulatory agencies [8]. As a future medical device, a myriad of challenges regarding BAL applicability to clinical therapy or pharmaceutical test need to be overcome, including establishing design standardization and manufacturability, efficacy of distinct cell sources, and availability of any chosen cell source. However, because the throughput level of BAL determines radically how well it performs function, the most critical factor barring its clinical and industrial applications is the efficiency that protrudes as a fundamental problem awaiting solutions. Hepatocytes, primary or genetically derived, have a high demand of O_2 despite that the levels may vary. This trait suggests that one possible solution to BAL's efficiency issue is to supply more O_2 into the BAL kernel reacting region and evaluate how much efficiency melioration has been received under such condition. Advancing to this answer is the ultimate aim that this dissertation strives to serve.

The study in CHAPTER 2 characterized the O_2 absorption profile a commercially prepared Oxycyte® (effective compound: PTBCH) for the first time. Main purpose of this is to take advantage of the high O_2 affinity of this new PFC product for O_2 supplementation in a 3D thick hepatic culture. The fact that under the same pressurizing system, 5% PFC-medium (MEM based) may carry significant higher O_2 content than its 10% competitor was a surprise, as on the contrary it was conventionally believed that more PFC fraction in aqueous emulsion assist to carry more O_2. This specific

phenomenon coming from measured results was discussed in CHAPTER 2, and possible default DO probe device setting that only applies to pure aqueous solution was deemed contributing to this deviation.

In CHAPTER 3 the commercially prepared Oxycyte® was applied to both static and dynamic hepatic culture, for assessing its efficacy on cell metabolism and functions. C3A human hepatoblastoma cell line was selected as the subject for this PFC efficacy test and gelatin sponge product Gelfoam® was used as the 3D scaffold. This 3D ECM supports cells anchorage and suspends them spatially to experience incoming PFC fluid perfusion. A great advantage is demonstrated by such *in vitro* organoid system: it can examine the PFC's separate effects to hepatic cells by moderate simplification with other unwanted intriguing physiological restrictions excluded. Although CO_2 highly dissolved in Oxycyte® [139], some PFCs are reported having low CO_2 solubility and if tested during *in vivo* perfusion may cause hypercapnia [140]. Other side effects when PFC is instilled to animal or human subject for administration also include thrombocytopenia [141].

In this *in vitro* organoid system the 3D gelatin scaffold that is necessary to the flow system and controls, however, somewhat perplexed the analysis to PFC independent effects to cells. As Fig. 4.10 illustrates, the 3D gelatin sponge scaffold alone had already promoted albumin synthesis of C3A cells and further addition of PFC (Oxycyte®) into static culture and dynamic culture did not extend this promotion (Fig. 3.4-IIa & Fig. 3.6-a). Considering the genetic alteration of C3A inherited from HepG2, it is likely that improvement in Fig. 4.10 had approached the paramount of C3A albumin expression in static culture that can be affected by O_2 alone. To C3A cells, the benefit of more O_2 to its

functionalities was manifested more on their activity of EROD, a representative CYP 450 enzyme, and meanwhile flow condition must be accompanied. External comments used to be received questioned if this CYP450 function improvement could be resulted from unidentified Oxycyte® cytotoxicity. Yet since in general PFCs are nonpolar (lipophobic) compounds that are and do not dissolve in cell membrane, either it is difficult to believe or to date there is no documented evidence indicating that PFC can participate in metabolism within cellular compartments. A separate and complete Oxycyte® cytotoxicity investigation may finally answer whether it can be totally trusted as safe for BAL systems.

Due to the versatile capabilities, the simulation work in CHAPTER 4 did not only aim to find a solution for previous bioreactor O_2 delivery issue, but also to characterize why the gelatin sponge scaffold let cells generate different function results than collagen gel, e.g. albumin secretion (Fig. 4.10). Simulated results entails that RPHs in gelatin sponge receive O_2 as if they are in free O_2-saturated aqueous medium (according to the high local O_2 diffusivity) or as if the flow rate was doubled to offer more agitated convection and amplified O_2 conditions (Fig. 4.9).

Advantage of the gelatin sponge shown in CHAPTER 3 and 4 was again applied in CHAPTER 5, specifically focusing on experimentally how this ECM and its accompanied flow device (modified version) could support more cells and enhance their drug metabolism performances. CHAPTER 5 utilized RPHs not only because they are non-proliferative primary cells, but also they are known to be far more superior in drug biotransformation function than HepG2 cell line (same presumably applied to C3A cell line too) [103]. Of the two enzymes tested, the effect of gelatin sponge and flow

perfusion for ECOD enzyme was clear: more O_2 entering cellular space enabled by such biomaterial which is believed help cells to achieve higher ECOD enzyme activity. For the other enzyme – EROD – the effect of improvement was clear in static culture. While the adverse effect in tube flow device appeared, it is believed that this function suppression was caused by the 3-MC increment per unit cell population during circulating medium scale-up. A fact that supports this hypothesis is that when 12-well plate sandwich C3A cell culture (initially 10^5 cells/well) used the original 3-MC concentration (5 μM) in original EROD assay protocol (initially 15×10^5 cells per well in 96-well plate) [71], very poor cell viability under confocal microscope, poor resazurin assayed metabolic activity as well as very weak EROD's resorufin signal reading were found. It was found also that cell viability rose back to normal level when the 3-MC concentration for 12-well plate culture was adjusted down to 2 μM. This protocol adjustment suggests that the absolute 3-MC amount per cell, instead of a fix concentration, should be consistent during medium volume scaling for minimizing cytotoxicity and resultant cell death. It is speculated further diluted 3-MC concentration will allow the flow device to demonstrate its effect to EROD activity as it did in ECOD.

Overall, this dissertation explored several innovative engineering approaches to further enhance O_2 delivery in hepatic devices fundamentally, including both experimental and numerical methods. These efforts, very important as the author considers, would directly contribute to better BAL design and functioning, and have profound impacts to the future development of this medical device.

6.1 Remarks for Future Work

For the future of medical device BAL, the fundamental O_2 enhancement studies contribute to BAL under trial progressing to ultimate FDA approval and market entry. Although there were decades of BAL development, today its medical application status still staggers in clinical trial. It appears that the route toward maturity of BAL is a long march. For example, one outstanding problem comes from selecting an optimal BAL cell source, and as of date there is no definitive answer yet: human primary hepatocytes are very limited for mass production; animal primary hepatocytes give concern of transferring zoonosis (e.g., Porcine Endogenous Retrovirus transmission), while hepatoma-derived cell lines (e.g. C3A cells) have efficiency issues and potential risk of tumorigenicity, and differentiating stem cells into hepatocytes is still extremely difficult so far [4, 8, 68, 142, 143].

There are other noticeable stem cells research updates, applicability of which BAL researchers would like to review: On June 8th, 2012, in Japan "a team at Yokohama City University, led by Professor Hideki Taniguchi, successfully transplanted induced pluripotent stem (iPS) cells into the body of a mouse, and then they began to grow into a human liver" [144, 145]. With a final scientific publication pending to formalize this report, options for BAL cell sources had already been recognized open to stem cells though cost is high and other *in vitro* differentiation restrictions apply [146]. Using autologous iPS cells can avoid the bioethical issue that using the allogeneic embryonic stem cells has. Either growing into a real human liver replacement for transplant patients, or serves as BAL's cell source for solving availability issue, stem cells from appropriate sources might be the key to the solution for final organ replacement.

The initial work that is deemed for characterizing BAL feasibility for liver drug metabolism occurred in the 1980s [147] and this development is still undergoing [14, 148-150]. Regarding such a particular category of function re-establishment *in vitro*, similar questions of cell source choice as testing model has been discussed [104, 151-155], and a very informative broad comparison between human hepatic cell line and primary hepatocytes has been reported [156]. Just as the clinical application for BAL, many questions from this aspect of BAL usage remain to be answered by extensive studies, which will necessarily take significant labor, funds and time.

To conclude this dissertation, regarding all aforementioned BAL imperfections, it is speculated that there will be still years before applying this therapeutic apparatus into reality and commercialization. Length of this duration is determined by the entire liver tissue engineering community and fundable resources. Before that day comes, the combining e engineering effort for BAL development should not be given up.

REFERENCES

1. Lamb, C.A., *Rupture of the Liver.* New England Journal of Medicine, 1939. **221**(22): p. 855-859.

2. Mann, F.C. and F.D. Mann, *Liver.* Annual Review of Physiology, 1953. **15**: p. 473-492.

3. Berne, R.M., *Physiology*. 2004: Mosby.

4. Tsiaoussis, J., et al., *Which hepatocyte will it be? Hepatocyte choice for bioartificial liver support systems.* Liver Transplantation, 2001. **7**(1): p. 2-10.

5. Atillasoy, E. and P.D. Berk, *Fulminant hepatic failure: pathophysiology, treatment, and survival.* Annu Rev Med, 1995. **46**: p. 181-91.

6. Kurtovic, J., S. Riordan, and R. Williams, *Fulminant hepatic failure.* Current Treatment Options in Gastroenterology, 2005. **8**(6): p. 503-518.

7. Onodera, K., et al., *Artificial liver support at present and in the future.* Journal of Artificial Organs, 2006. **9**(1): p. 17-28.

8. Sussman, N.L., B.M. McGuire, and J.H. Kelly, *Hepatic assist devices: will they ever be successful?* Curr Gastroenterol Rep, 2009. **11**(1): p. 64-8.

9. Berthiaume, F., C. Chan, and M.L. Yarmush, *Liver, Bio-artificial*, in *Encyclopedia of Biomaterials and Biomedical Engineering*. p. 1649-1660.

10. Pless, G., *Artificial and bioartificial liver support.* Organogenesis, 2007. **3**(1): p. 20-4.

11. McKenzie, T.J., J.B. Lillegard, and S.L. Nyberg, *Artificial and Bioartificial Liver Support.* Semin Liver Dis, 2008. **28**(02): p. 210,217.

12. Chamuleau, R.A., *Future of bioartificial liver support.* World J Gastrointest Surg, 2009. **1**(1): p. 21-5.

13. Park, Y., et al., *Method for evaluating metabolic functions of drugs in bioartificial liver.* Biotechnology and Bioprocess Engineering, 2003. **8**(5): p. 279-285.

14. Iwahori, T., et al., *CYP3A4 inducible model for in vitro analysis of human drug metabolism using a bioartificial liver.* Hepatology, 2003. **37**(3): p. 665-673.

15. Hongo, T., et al., *Three-dimensional high-density culture of HepG2 cells in a 5-ml radial-flow bioreactor for construction of artificial liver.* J Biosci Bioeng, 2005. **99**(3): p. 237-44.

16. Dash, A., et al., *Liver tissue engineering in the evaluation of drug safety.* Expert Opinion on Drug Metabolism & Toxicology, 2009. **5**(10): p. 1159-1174.

17. Elkayam, T., et al., *Enhancing the drug metabolism activities of C3A--a human hepatocyte cell line--by tissue engineering within alginate scaffolds.* Tissue Eng, 2006. **12**(5): p. 1357-68.

18. Shvartsman, I., et al., *Perfusion cell seeding and cultivation induce the assembly of thick and functional hepatocellular tissue-like construct.* Tissue Eng Part A, 2009. **15**(4): p. 751-60.

19. Zinchenko, Y.S., et al., *Hepatocyte and Kupffer Cells Co-cultured on Micropatterned Surfaces to Optimize Hepatocyte Function.* Tissue Engineering, 2006. **12**(4): p. 751-761.

20. Cho, C.H., et al., *Oxygen uptake rates and liver-specific functions of hepatocyte and 3T3 fibroblast co-cultures.* Biotechnol Bioeng, 2007. **97**(1): p. 188-99.

21. Domansky, K., et al., *Perfused multiwell plate for 3D liver tissue engineering.* Lab on a Chip, 2010. **10**(1): p. 51-58.

22. Becker, W.M., L.J. Kleinsmith, and J. Hardin, *Beyond the Cell: Extracellular Structures, Cell Adhesion, and Cell Junctions*, in *The World of The Cell*. 2005, Benjamin Cummings. p. 944.

23. Tilles, A.W., et al., *Critical issues in bioartificial liver development.* Technology and Health Care, 2002. **10**(3): p. 177-186.

24. Kidambi, S., et al., *Oxygen-mediated enhancement of primary hepatocyte metabolism, functional polarization, gene expression, and drug clearance.* Proceedings of the National Academy of Sciences, 2009. **106**(37): p. 15714-15719.

25. Becker, W.M., *The World of the Cell*. 2009: Pearson/Benjamin Cummings.

26. Bernhardt, R., *Cytochrome P450: Structure, function, and generation of reactive oxygen species*, in *Reviews of Physiology, Biochemistry and Pharmacology*. 1996, Springer Berlin Heidelberg. p. 137-221.

27. Rotem, A., et al., *Oxygen is a factor determining in vitro tissue assembly: Effects on attachment and spreading of hepatocytes.* Biotechnology and Bioengineering, 1994. **43**(7): p. 654-660.

28. Maguire, T.J., et al., *Design and application of microfluidic systems for in vitro pharmacokinetic evaluation of drug candidates.* Curr Drug Metab, 2009. **10**(10): p. 1192-9.

29. McClelland, R.E., J.M. MacDonald, and R.N. Coger, *Modeling O2 transport within engineered hepatic devices.* Biotechnology and Bioengineering, 2003. **82**(1): p. 12-27.

30. McClelland, R.E. and R.N. Coger, *Use of Micropathways to Improve Oxygen Transport in a Hepatic System.* Journal of Biomechanical Engineering, 2000. **122**(3): p. 268-273.

31. Lovett, M., et al., *Vascularization strategies for tissue engineering.* Tissue Eng Part B Rev, 2009. **15**(3): p. 353-70.

32. Allen, J.W., T. Hassanein, and S.N. Bhatia, *Advances in bioartificial liver devices.* Hepatology, 2001. **34**(3): p. 447-455.

33. Amaral, P.F., et al., *Optimization of oxygen mass transfer in a multiphase bioreactor with perfluorodecalin as a second liquid phase.* Biotechnol Bioeng, 2008. **99**(3): p. 588-98.

34. Nahmias, Y., et al., *A novel formulation of oxygen-carrying matrix enhances liver-specific function of cultured hepatocytes.* FASEB J., 2006. **20**(14): p. 2531-2533.

35. Kinasiewicz, A., et al., *Impact of Oxygenation of Bioartificial Liver Using Perfluorocarbon Emulsion Perftoran on Metabolism of Human Hepatoma C3A Cells.* Artificial Cells, Blood Substitutes and Biotechnology, 2008. **36**(6): p. 525-534.

36. Khattak, S.F., et al., *Enhancing oxygen tension and cellular function in alginate cell encapsulation devices through the use of perfluorocarbons.* Biotechnology and Bioengineering, 2007. **96**(1): p. 156-166.

37. Riess, J.G., *Perfluorocarbon-based Oxygen Delivery.* Artificial Cells, Blood Substitutes and Biotechnology, 2006. **34**(6): p. 567-580.

38. Kurosawa, H., et al., *Morphology and albumin secretion of adult rat hepatocytes cultured on a hydrophobic porous expanded polytetrafluoroethylene membrane.* Journal of Bioscience and Bioengineering, 2003. **95**(1): p. 59-64.

39. Kiepert, P., *Perfluorochemical emulsions: future alternatives to transfusions.* Blood Subst Princ Meth Prod Clin Trials, 1998(2): p. 127-156.

40. Spahn, D.R., *Blood substitutes Artificial oxygen carriers: perfluorocarbon emulsions.* Critical Care, 1999. **3**(5): p. R93 - R97.

41. Haeberle, H.A., et al., *Perflubron Reduces Lung Inflammation in Respiratory Syncytial Virus Infection by Inhibiting Chemokine Expression and Nuclear Factor-{kappa}B Activation.* Am. J. Respir. Crit. Care Med., 2002. **165**(10): p. 1433-1438.

42. Mattrey, R.F., *The Potential Role of Perfluorochemicals (PFCS) in Diagnostic Imaging.* Artificial Cells, Blood Substitutes and Biotechnology, 1994. **22**(2): p. 295-313.

43. Centis, V., C.J. Doillon, and P. Vermette, *Perfluorocarbon Emulsions Cytotoxic Effects on Human Fibroblasts and Effect of Aging on Particle Size Distribution.* Artificial Organs, 2007. **31**(8): p. 649-653.

44. Rotta, A.T., et al., *Perfluorooctyl bromide (perflubron) attenuates oxidative injury to biological and nonbiological systems.* Pediatric Critical Care Medicine, 2003. **4**(2): p. 233-238.

45. McGregor, D.F.S.S.J., *Novel oxygenation system supports multilayer growth of HeLa cells.* BioTechniques, 1996(21): p. 672-677.

46. Nieuwoudt, M., et al., *Imaging glucose metabolism in perfluorocarbon-perfused hepatocyte bioreactors using positron emission tomography.* Journal of Artificial Organs, 2009. **12**(4): p. 247-257.

47. Chin, K., et al., *Hydrogel-Perfluorocarbon Composite Scaffold Promotes Oxygen Transport to Immobilized Cells.* Biotechnology Progress, 2008. **24**(2): p. 358-366.

48. Zhou, Z., et al., *Perfluorocarbon Emulsions Improve Cognitive Recovery After Lateral Fluid Percussion Brain Injury in Rats.* Neurosurgery, 2008. **63**(4): p. 799-807.

49. de Lange, F., et al., *Perfluorocarbon Administration During Cardiopulmonary Bypass in Rats: An Inflammatory Link to Adverse Outcome?* Anesthesia & Analgesia, 2008. **106**(1): p. 24-31.

50. Rosoff, J.S., LO; Vocelka, CR; Schmer, G; Chandler, WL; Cochran, RP; Kunzelman, KS and Spiess, BP, *Second generation perfluorocarbon (perfluorodichloro-octane) does not increase complement activation in ex vivo extracorporeal bypass experiments.* Anesth Analg, 1996. **82**(SCA).

51. Yang, Z.-j., et al., *The Effect of Isovolemic Hemodilution with Oxycyte®, a Perfluorocarbon Emulsion, on Cerebral Blood Flow in Rats.* PLoS One, 2008. **3**(4): p. e2010.

52. Radisic, M., et al., *Mathematical model of oxygen distribution in engineered cardiac tissue with parallel channel array perfused with culture medium containing oxygen carriers.* Am J Physiol Heart Circ Physiol, 2005. **288**(3): p. H1278-1289.

53. Chen, G. and A.F. Palmer, *Perfluorocarbon facilitated O2 transport in a hepatic hollow fiber bioreactor.* Biotechnology Progress, 2009. **25**(5): p. 1317-1321.

54. Hatschek, E., *The general theory of viscosity of two-phase systems.* Transactions of the Faraday Society, 1913. **9**: p. 80-92.

55. Sibree, J.O., *The viscosity of emulsions.-Part I.* Transactions of the Faraday Society, 1930. **26**: p. 26-36.

56. Bird, R.B., W.E. Stewart, and E.N. Lightfoot, *Transport Phenomena*. 2007: J. Wiley.

57. Ju, L.-K., J.F. Lee, and W.B. Armiger, *Enhancing Oxygen Transfer in Bioreactors by Perfluorocarbon Emulsions.* Biotechnology Progress, 1991. **7**(4): p. 323-329.

58. Deindoerfer, F.H. and E.L. Gaden, Jr., *Effects of Liquid Physical Properties on Oxygen Transfer in Penicillin Fermentation.* Appl. Environ. Microbiol., 1955. **3**(5): p. 253-257.

59. Ryu, D.Y.H.A., *A Reassessment of Oxygen Transfer Rates in Antibiotic Fermentations.* Journal of Fermentation Technology, 1972: p. 423-431.

60. Feng, Z.-G. and E.E. Michaelides, *Heat and mass transfer coefficients of viscous spheres.* International Journal of Heat and Mass Transfer, 2001. **44**(23): p. 4445-4454.

61. Fraker, C.A., A.J. Mendez, and C.L. Stabler, *Complementary methods for the determination of dissolved oxygen content in perfluorocarbon emulsions and other solutions.* J Phys Chem B, 2011. **115**(35): p. 10547-52.

62. Haynes, W.M. and D.R. Lide, *CRC Handbook of Chemistry and Physics: A Ready-Reference Book of Chemical and Physical Data*. 2010: Taylor & Francis Group.

63. Remy, B., G. Deby-Dupont, and M. Lamy, *Red blood cell substitutes: fluorocarbon emulsions and haemoglobin solutions.* British Medical Bulletin, 1999. **55**(1): p. 277-298.

64. Mathy-Hartert, M., et al., *Effects of perfluorocarbon emulsions on cultured human endothelial cells.* Artif Cells Blood Substit Immobil Biotechnol, 1997. **25**(6): p. 563-75.

65. Bucala, R., M. Kawakami, and A. Cerami, *Cytotoxicity of a perfluorocarbon blood substitute to macrophages in vitro.* Science, 1983. **220**(4600): p. 965-7.

66. Estacia, P., et al., *The cytotoxicity in vero cells of a perfluorocarbon used in vitreoretinal surgery.* Journal of Morphological Science, 2002. **19**(2): p. 41-47.

67. Gislason, G.T., et al., *A Treatment System for Implementing an Extracorporeal Liver Assist Device.* Artificial Organs, 1994. **18**(5): p. 385-389.

68. Chamuleau, R., T. Deurholt, and R. Hoekstra, *Which Are the Right Cells to be Used in a Bioartificial Liver?* Metabolic Brain Disease, 2005. **20**(4): p. 327-335.

69. Mavri-Damelin, D., et al., *Cells for bioartificial liver devices: the human hepatoma-derived cell line C3A produces urea but does not detoxify ammonia.* Biotechnol Bioeng, 2008. **99**(3): p. 644-51.

70. Kelly, J.H., *Permanent Human Hepatocyte Cell Line and its use in a Liver Assist Device (LAD)*. 1994, Baylor College of Medicine, Houston, TX: USA.

71. Kelly, J.H. and N.L. Sussman, *A fluorescent cell-based assay for cytochrome P-450 isozyme 1A2 induction and inhibition.* J Biomol Screen, 2000. **5**(4): p. 249-54.

72. Sussman, N.L., et al., *The Hepatix Extracorporeal Liver Assist Device: Initial Clinical Experience.* Artificial Organs, 1994. **18**(5): p. 390-396.

73. Ellis, A.J., et al., *Pilot-controlled trial of the extracorporeal liver assist device in acute liver failure.* Hepatology, 1996. **24**(6): p. 1446-1451.

74. Dunn, J.C.Y., R.G. Tompkins, and M.L. Yarmush, *Long-term in vitro function of adult hepatocytes in a collagen sandwich configuration.* Biotechnology Progress, 1991. **7**(3): p. 237-245.

75. Kono, Y. and E.A. Roberts, *Modulation of the Expression of Liver-Specific Functions in Novel Human Hepatocyte Lines Cultured in a Collagen Gel Sandwich Configuration.* Biochemical and Biophysical Research Communications, 1996. **220**(3): p. 628-632.

76. Kono, Y., et al., *Establishment of a human hepatocyte line derived from primary culture in a collagen gel sandwich culture system.* Exp Cell Res, 1995. **221**(2): p. 478-85.

77. Wu, D.Q., et al., *Evaluation of diffusion in gel entrapment cell culture within hollow fibers.* World J Gastroenterol, 2005. **11**(11): p. 1599-604.

78. Anseth, K.S., C.N. Bowman, and L. Brannon-Peppas, *Mechanical properties of hydrogels and their experimental determination.* Biomaterials, 1996. **17**(17): p. 1647-1657.

79. Ponticiello, M.S., et al., *Gelatin-based resorbable sponge as a carrier matrix for human mesenchymal stem cells in cartilage regeneration therapy.* J Biomed Mater Res, 2000. **52**(2): p. 246-55.

80. Rohanizadeh, R., M.V. Swain, and R.S. Mason, *Gelatin sponges (Gelfoam) as a scaffold for osteoblasts.* J Mater Sci Mater Med, 2008. **19**(3): p. 1173-82.

81. Gruber, H., et al., *Three-dimensional culture of human meniscal cells: Extracellular matrix and proteoglycan production.* BMC Biotechnology, 2008. **8**(1): p. 54.

82. Gruber, H.E., et al., *Three-dimensional culture of human disc cells within agarose or a collagen sponge: assessment of proteoglycan production.* Biomaterials, 2006. **27**(3): p. 371-376.

83. Takahashi, Y., M. Yamamoto, and Y. Tabata, *Osteogenic differentiation of mesenchymal stem cells in biodegradable sponges composed of gelatin and [beta]-tricalcium phosphate.* Biomaterials, 2005. **26**(17): p. 3587-3596.

84. Burke, M.D. and R.T. Mayer, *Ethoxyresorufin: direct fluorimetric assay of a microsomal O-dealkylation which is preferentially inducible by 3-methylcholanthrene.* Drug Metab Dispos, 1974. **2**(6): p. 583-8.

85. Doostdar, H., M.D. Burke, and R.T. Mayer, *Bioflavonoids: selective substrates and inhibitors for cytochrome P450 CYP1A and CYP1B1.* Toxicology, 2000. **144**(1-3): p. 31-38.

86. Rodríguez-Antona, C., et al., *Cytochrome P450 expression in human hepatocytes and hepatoma cell lines: molecular mechanisms that determine lower expression in cultured cells.* Xenobiotica, 2002. **32**(6): p. 505-520.

87. O'Brien, J., et al., *Investigation of the Alamar Blue (resazurin) fluorescent dye for the assessment of mammalian cell cytotoxicity.* Eur J Biochem, 2000. **267**(17): p. 5421-6.

88. Gloeckner, H., T. Jonuleit, and H.D. Lemke, *Monitoring of cell viability and cell growth in a hollow-fiber bioreactor by use of the dye Alamar Blue.* J Immunol Methods, 2001. **252**(1-2): p. 131-8.

89. Larson, E.M., et al., *A new, simple, nonradioactive, nontoxic in vitro assay to monitor corneal endothelial cell viability.* Invest Ophthalmol Vis Sci, 1997. **38**(10): p. 1929-33.

90. Nakayama, G.R., et al., *Assessment of the Alamar Blue assay for cellular growth and viability in vitro.* J Immunol Methods, 1997. **204**(2): p. 205-8.

91. Perrot, S., et al., *Resazurin metabolism assay is a new sensitive alternative test in isolated pig cornea.* Toxicol Sci, 2003. **72**(1): p. 122-9.

92. Duarte, M., et al., *A quantitative resazurin assay to determinate the viability of Trichomonas vaginalis and the cytotoxicity of organic solvents and surfactant agents.* Exp Parasitol, 2009. **123**(2): p. 195-8.

93. Scharenberg, C.W., M.A. Harkey, and B. Torok-Storb, *The ABCG2 transporter is an efficient Hoechst 33342 efflux pump and is preferentially expressed by immature human hematopoietic progenitors.* Blood, 2002. **99**(2): p. 507-12.

94. Kim, M., et al., *The multidrug resistance transporter ABCG2 (breast cancer resistance protein 1) effluxes Hoechst 33342 and is overexpressed in hematopoietic stem cells.* Clin Cancer Res, 2002. **8**(1): p. 22-8.

95. Mao, Q. and J.D. Unadkat, *Role of the breast cancer resistance protein (ABCG2) in drug transport.* AAPS J, 2005. **7**(1): p. E118-33.

96. Sarkadi, B., et al., *ABCG2 - a transporter for all seasons.* FEBS Letters, 2004. **567**(1): p. 116-120.

97. McClelland, R.E. and R.N. Coger, *Effects of Enhanced O2 Transport on Hepatocytes Packed within a Bioartificial Liver Device.* Tissue Engineering, 2004. **10**(1-2): p. 253-266.

98. Niu, M., M.G. Clemens, and R.N. Coger, *Optimizing normoxic conditions in liver devices using enhanced gel matrices.* Biotechnology and Bioengineering, 2008. **99**(6): p. 1502-1512.

99. Gordon, J. and A.F. Palmer, *Impact of Increased Oxygen Delivery Via Bovine Red Blood Cell Supplementation of Culturing Media on Select Metabolic and Synthetic Functions of C3A Hepatocytes Maintained within a Hollow Fiber Bioreactor.* Artificial Cells, Blood Substitutes, & Biotechnology, 2005. **33**(3): p. 297-306.

100. Sullivan, J.P., D.R. Harris, and A.F. Palmer, *Convection and Hemoglobin-Based Oxygen Carrier Enhanced Oxygen Transport in a Hepatic Hollow Fiber Bioreactor.* Artificial Cells, Blood Substitutes and Biotechnology, 2008. **36**(4): p. 386-402.

101. Iseki, et al., *Diverse regulations of albumin gene expression by hepatocyte growth factor in HepG2 human hepatoma cells and primary culture of rat hepatocytes*. Vol. 16. 2000, Athens, GRECE: Editorial Academy of the International Journal of Oncology.

102. Sonna, L.A., et al., *Effect of hypoxia on gene expression by human hepatocytes (HepG2).* Physiol. Genomics, 2003. **12**(3): p. 195-207.

103. Nyberg, S.L., et al., *Primary hepatocytes outperform Hep G2 cells as the source of biotransformation functions in a bioartificial liver.* Ann Surg, 1994. **220**(1): p. 59-67.

104. Gomez-Lechon, M.J., et al., *Cell Lines: A Tool for In Vitro Drug Metabolism Studies.* Current Drug Metabolism, 2008. **9**(1): p. 1-11.

105. Wilkening, S., F. Stahl, and A. Bader, *Comparison of Pimary Human Hepatocytes and Hepatoma Cell Line HepG2 with regard to their Biotransformation Properties.* Drug Metabolism and Disposition, 2003. **31**(8): p. 1035-1042.

106. Niu, M., P. Hammond, and R.N. Coger, *The Effectiveness of a Novel Cartridge-Based Bioreactor Design in Supporting Liver Cells.* Tissue Engineering Part A, 2009. **15**(10): p. 2903-2916.

107. Lekas, P., et al., *The Human Cytochrome P450 1A1 mRNA Is Rapidly Degraded In HepG2 Cells.* Archives of Biochemistry and Biophysics, 2000. **384**(2): p. 311-318.

108. Consolo, F., et al., *A Computational Model for the Optimization of Transport Phenomena in a Rotating Hollow-Fiber Bioreactor for Artificial Liver.* Tissue Engineering Part C: Methods, 2009. **15**(1): p. 41-55.

109. Hutmacher, D.W. and H. Singh, *Computational fluid dynamics for improved bioreactor design and 3D culture.* Trends in Biotechnology, 2008. **26**(4): p. 166-172.

110. Kays, W.M., M.E. Crawford, and B. Weigand, *Convective heat and mass transfer*. 2005: McGraw-Hill Higher Education.

111. ANSYS (2010) *FLUENT 13.0 Theory Guide and User's Guide*.

112. Ingham, D.B. and I.I. Pop, *Transport Phenomena in Porous Media II*. 2002: Pergamon.

113. Swartz, M.A. and M.E. Fleury, *Interstitial Flow and Its Effects in Soft Tissues.* Annual Review of Biomedical Engineering, 2007. **9**(1): p. 229-256.

114. Jackson, G.W. and D.F. James, *The permeability of fibrous porous media.* The Canadian Journal of Chemical Engineering, 1986. **64**(3): p. 364-374.

115. Ramanujan, S., et al., *Diffusion and Convection in Collagen Gels: Implications for Transport in the Tumor Interstitium.* Biophysical Journal, 2002. **83**(3): p. 1650-1660.

116. Happel, J., *Viscous flow relative to arrays of cylinders.* AIChE Journal, 1959. **5**(2): p. 174-177.

117. Phillips, R.J., *A Hydrodynamic Model for Hindered Diffusion of Proteins and Micelles in Hydrogels.* Biophysical Journal, 2000. **79**(6): p. 3350-3353.

118. Bozec, L., G. van der Heijden, and M. Horton, *Collagen Fibrils: Nanoscale Ropes.* Biophysical Journal, 2007. **92**(1): p. 70-75.

119. Sung, K.E., et al., *Control of 3-dimensional collagen matrix polymerization for reproducible human mammary fibroblast cell culture in microfluidic devices.* Biomaterials, 2009. **30**(27): p. 4833-4841.

120. Revenko, I., et al., *Atomic force microscopy study of the collagen fibre structure.* Biology of the Cell, 1994. **80**(1): p. 67-69.

121. Mareels, G., et al., *Three-dimensional Numerical Modeling and Computational Fluid Dynamics Simulations to Analyze and Improve Oxygen Availability in the AMC Bioartificial Liver.* Annals of Biomedical Engineering, 2006. **34**(11): p. 1729-1744.

122. Oddou, C., et al., *Hydrodynamics in Porous Media with Applications to Tissue Engineering*, in *Porous Media*. 2010, CRC Press. p. 75-119.

123. Hirt, C.W. and B.D. Nichols, *Volume of fluid (VOF) method for the dynamics of free boundaries.* Journal of Computational Physics, 1981. **39**(1): p. 201-225.

124. Mölder, E., A. Mashirin, and T. Tenno, *Measurement of the Oxygen Mass Transfer Through the Air-Water Interface.* Environmental Science and Pollution Research, 2005. **12**(2): p. 66-70.

125. Patankar, S.V. and D.B. Spalding, *A calculation procedure for heat, mass and momentum transfer in three-dimensional parabolic flows.* International Journal of Heat and Mass Transfer, 1972. **15**(10): p. 1787-1806.

126. Peric, M., *Flow Simulation Using Control Volumes of Arbitrary Polyhedral Shape.* ERCOFTAC Bulletin, 2004. **62**: p. 25-29.

127. Spiegel, M., et al., *Tetrahedral vs. polyhedral mesh size evaluation on flow velocity and wall shear stress for cerebral hemodynamic simulation.* Computer Methods in Biomechanics and Biomedical Engineering, 2010. **14**(1): p. 9-22.

128. Bruckschen, B., et al., *Comparing different porosity measurement methods for characterisation of 3D printed bone replacement scaffolds.* Biomedizinische Technik (Biomedical Technology), 2005. **50**(Supplementary vol. 1 Part 2).

129. Leclaire, P., et al., *Porosity measurement by comparison of air volumes.* Review of Scientific Instruments, 2003. **74**(3): p. 1366-1370.

130. Chernoff, E.A.G. and D.A. Chernoff, *Atomic force microscope images of collagen fibers.* Journal of Vacuum Science & Technology A: Vacuum, Surfaces, and Films, 1992. **10**(4): p. 596-599.

131. Seglen, P.O., *Preparation of isolated rat liver cells.* Methods in cell biology, 1976. **13**: p. 29-83.

132. Perry, R.H., D.W. Green, and J.O. Maloney, *Perry's Chemical Engineers' Handbook.* 1997: McGraw-Hill.

133. Sander, R., *Compilation of Henry's Law Constants for Inorganic and Organic Species of Potential Importance in Environmental Chemistry*, R. Sander, Editor. 1999: Mainz, Germany.

134. Jungermann, K. and T. Kietzmann, *Oxygen: Modulator of metabolic zonation and disease of the liver.* Hepatology, 2000. **31**(2): p. 255-260.

135. Iles, R.A., P.G. Baron, and R.D. Cohen, *The effect of reduction of perfusion rate on lactate and oxygen uptake, glucose output and energy supply in the isolated perfused liver of starved rats.* Biochem J, 1979. **184**(3): p. 635-42.

136. Schumacker, P.T., N. Chandel, and A.G. Agusti, *Oxygen conformance of cellular respiration in hepatocytes.* Am J Physiol, 1993. **265**(4 Pt 1): p. L395-402.

137. Rotem, A., et al., *Oxygen uptake rates in cultured rat hepatocytes.* Biotechnology and Bioengineering, 1992. **40**(10): p. 1286-1291.

138. Yuki, T., et al., *Evaluation of effects of shear stress on hepatocytes by a microchip-based system.* Measurement Science and Technology, 2006. **17**(12): p. 3167.

139. Spiess, B.D., *Perfluorocarbon emulsions as a promising technology: a review of tissue and vascular gas dynamics.* J Appl Physiol, 2009. **106**(4): p. 1444-1452.

140. Mates, E.A., et al., *Shunt and ventilation-perfusion distribution during partial liquid ventilation in healthy piglets.* Journal of Applied Physiology, 1997. **82**(3): p. 933-942.

141. STOLLINGS, et al., *Oxygen therapeutics : Oxygen delivery without blood*. Vol. 26. 2006, Boston, MA, ETATS-UNIS: Pharmacotherapy. 12.

142. Brophy, C.M. and S.L. Nyberg, *Is there a future for the bioartificial liver?* Current Opinion in Organ Transplantation, 2006. **11**(3): p. 219-225 10.1097/01.mot.0000227836.98957.be.

143. Allen, J.W. and S.N. Bhatia, *Engineering Liver Therapies for the Future.* Tissue Engineering, 2002. **8**(5): p. 725-737.

144. Westlake, A., *Japanese scientists use stem cells to create human liver*, in *The Japan Daily Press*. 2012, GiMo Co.: Nagoya, Japan.

145. Cyranoski, D., *Rudimentary liver grown in vitro*, in *Nature*. 2012, Nature Publishing Group: Yokohama.

146. Diekmann, S., A. Bader, and S. Schmitmeier, *Present and Future Developments in Hepatic Tissue Engineering for Liver Support Systems : State of the art and future developments of hepatic cell culture techniques for the use in liver support systems.* Cytotechnology, 2006. **50**(1-3): p. 163-79.

147. von Bahr, C., et al., *Drug metabolism in human liver in vitro: establishment of a human liver bank.* Clin Pharmacol Ther, 1980. **27**(6): p. 711-25.

148. Donato, M.T., J.V. Castell, and M.J. Gomez-Lechon, *Characterization of drug metabolizing activities in pig hepatocytes for use in bioartificial liver devices: comparison with other hepatic cellular models.* J Hepatol, 1999. **31**(3): p. 542-9.

149. Behnia, K., et al., *Xenobiotic metabolism by cultured primary porcine hepatocytes.* Tissue Eng, 2000. **6**(5): p. 467-79.

150. Ekins, S., et al., *Xenobiotic metabolism in rat, dog, and human precision-cut liver slices, freshly isolated hepatocytes, and vitrified precision-cut liver slices.* Drug Metab Dispos, 1996. **24**(9): p. 990-5.

151. Donato, M.T., et al., *Cell lines: a tool for in vitro drug metabolism studies.* Curr Drug Metab, 2008. **9**(1): p. 1-11.

152. Castell, J.V., et al., *Hepatocyte cell lines: their use, scope and limitations in drug metabolism studies.* Expert Opinion on Drug Metabolism & Toxicology, 2006. **2**(2): p. 183-212.

153. Gomez-Lechon, M.J., J.V. Castell, and M.T. Donato, *Hepatocytes--the choice to investigate drug metabolism and toxicity in man: in vitro variability as a reflection of in vivo.* Chem Biol Interact, 2007. **168**(1): p. 30-50.

154. Groneberg, D.A., C. Grosse-Siestrup, and A. Fischer, *In vitro models to study hepatotoxicity.* Toxicol Pathol, 2002. **30**(3): p. 394-9.

155. Tuschl, G., B. Lauer, and S.O. Mueller, *Primary hepatocytes as a model to analyze species-specific toxicity and drug metabolism.* Expert Opin Drug Metab Toxicol, 2008. **4**(7): p. 855-70.

156. Guo, L., et al., *Similarities and differences in the expression of drug-metabolizing enzymes between human hepatic cell lines and primary human hepatocytes.* Drug Metab Dispos, 2011. **39**(3): p. 528-38.

157. Haelssig, J.B., et al., *Direct numerical simulation of interphase heat and mass transfer in multicomponent vapour-liquid flows.* International Journal of Heat and Mass Transfer, 2010. **53**(19-20): p. 3947-3960.

158. Polito, A.L., C.P. Barba, and S.T. Solis, *Collagen Type I Scaffolds for Use in Medicine.* AIP Conference Proceedings, 2006. **854**(1): p. 129-131.

159. Matthews, J.A., et al., *Electrospinning of collagen nanofibers.* Biomacromolecules, 2002. **3**(2): p. 232-8.

160. Boschetti, F., et al., *Prediction of the micro-fluid dynamic environment imposed to three-dimensional engineered cell systems in bioreactors.* Journal of Biomechanics, 2006. **39**(3): p. 418-425.

161. Porter, B., et al., *3-D computational modeling of media flow through scaffolds in a perfusion bioreactor.* Journal of Biomechanics, 2005. **38**(3): p. 543-549.

162. Cioffi, M., et al., *Modeling evaluation of the fluid-dynamic microenvironment in tissue-engineered constructs: A micro-CT based model.* Biotechnology and Bioengineering, 2006. **93**(3): p. 500-510.

APPENDIX A: COURANT-FRIEDRICHS-LEWY CONDITION AND PROPERTY VALUES USED IN SIMULATION

Courant-Friedrichs-Lewy condition is a necessary condition for numerically solving partial differential equations (usually hyperbolic) to obtain correct results. The mathematical form of this condition is stated as:

$$Cou \leq C \qquad (A.1)$$

where C is a constant. Cou is the courant number as quantitative index of CFL condition. In 3D case it is defined as:

$$Cou = \Delta t \cdot \left(\frac{u}{\Delta x} + \frac{v}{\Delta y} + \frac{w}{\Delta z}\right) \qquad (A.2)$$

where Δt is time step, $\Delta x, \Delta y, \Delta z$ are components of computational grid dimension and u, v, w are velocity components at x, y, z direction respectively. Larger Courant number enables faster convergence speed yet less numerical stability, making it essential to choose its value wisely. From Eqn. A.2, with dynamic velocity development (varying u, v, w) in stationary grids (unchanged $\Delta x, \Delta y, \Delta z$), throttling Courant number as constant will make time step an irrational number. It natively lacks precise control in saving data at interested "integral flow time" such as 30 seconds or 5 minutes. The transient mode computation took more than 30 days by three octo-core 2.93GHz Intel® Xeon® X5570 CPUs from a High Performance Computing (HPC). Simulated physical time progressed to 335s yet still failed to converge.

Ideally, the free-surface featured 4QB should incorporate air-medium O_2 exchange for rich O_2 content in air overwhelms O_2 in aqueous medium and endows a strong air-to-medium O_2 boundary condition at the interface. Yet the interfacial O_2 diffusivity across the two phases is not well defined and the direct numerical simulation

of the interfacial mass transport is very complicated [157] in terms of both theory derivation and code development. Even the diffusivity is immediate, continuous air-to-medium O_2 supply renders mass imbalance of the air phase, which pleads special programming treatment to supplement mass loss of air phase in FLUENT. While it remained hard to directly model interfacial diffusion and to calculate dynamic free surface at high computational cost thereof.

Tab.A.1 lists the key values used in model simulation of CHAPTER 4.

TABLE.A.1 Values of key properties used for parameters in simulation model of CHAPTER4.

Symbol	Description	Value	Unit	Source
D_c	rat hepatocytes intracellular O_2 diffusivity	0.25	10^{-9} m^2/s	[121]
D_e	effective O_2 diffusivity in porous collagen	1.48	10^{-9} m^2/s	calculated
D_e	effective O_2 diffusivity in gelatin sponge	2.88	10^{-9} m^2/s	calculated
D_o	O_2 diffusivity in free medium	2.92	10^{-9} m^2/s	[121]
K_c	collagen permeability (1.3mg/mL)	1.536	10^{-14} m^2	[114]
K_g	gelatin sponge Darcy permeability	9.04	10^{-11} m^2	measured
K_M	Michaelis-Menten constant	3	mmHg	[108]
K_m	PTFE membrane Darcy permeability	1.48	10^{-14} m^2	measured
$\dot{M}$	medium mass flow rate	1.00967	10^{-3} kg/s	previous setup[106]
R_h	O_2 hydrodynamic radius	1.695	10^{-7} m	[115]
$\dot{V}$	medium volumetric flow rate	1	cm^3/s	previous setup[106]
k_B	Boltzmann constant	1.38	10^{-23} J/K	-

(Continued)

(Continued)

ρ_m	medium density	1.00967	10^3 kg/m^3	[121]
T	temperature	310.15	K	incubator setup
a	collagen fiber diameter	1~1.5	nm	[158]
a	collagen fiber diameter	6.5	nm	[159]
b	average pore size (collagen gel)	3.5	μm	deduced from [80, 115]
b	average pore size (gelatin sponge)	350	μm	averaged from [80]
g	gravitational acceleration	9.81	m/s^2	-
Δn	PTFE membrane thickness	30	μm	vendor
ε	porosity of collagen gel (1.3 mg/mL), $\varepsilon + \phi = 1$	0.929±0.013	-	measured
ε	porosity of gelatin sponge, $\varepsilon + \phi = 1$	0.956±0.003	-	measured
μ	medium dynamic viscosity	7.02326	10^{-7} kg/(m·s)	measured
ω	saturated O_2 mass fraction in aqueous medium at 37ºC and 1 atm	6.636	ppm (10^{-6})	[21]
ϕ	collagen fiber volume fraction (1.3 mg/mL)	0.0708	-	$1 - \varepsilon = \phi$

APPENDIX B: FLUENT® USER DEFINED FUNCTION (UDF) SOURCE CODE

```
/**********************************************************************
UDF to precisely model oxygen consumption by C3A or primary hepatocytes within the
collagen space of 4QB, cell population 4 million per cartridge
Gengbei Shi, Ph.D dissertation, UNC Charlotte, 2012
**********************************************************************/

 #include "udf.h"
 #include "mem.h"

 #define Km 3.  /*Michaelis-Menten constant, in mmHg*/
 #define n 8.54482e5 /* Hepatocytes cell density, 2million/m^3*/
 #define Vmax 0.7286   /* Maximum hepatocytes O2 uptake rate in nmol/s-million cells
*/
 #define Rho 32e-12 /* Oxygen molar mass in kg/nmol*/
 #define Alpha 3.1385e-5 /*Henry's constant in ml O2/mmHg-ml medium*/

 DEFINE_SOURCE(MM_O2source,c,t,dS,eqn)
 {
        real source;
        real rho_o2 = 4.0625e-5; /* in kg/ml*/
        real rho_medium = 1.00967e-3; /*in kg/ml*/

        source = - Rho * Vmax * 2 * n * C_YI(c,t,0) / (C_YI(c,t,0) + rho_o2/rho_medium
* Alpha * Km);  /* C_YI(c,t,0)is oxygen mass fraction, in kg O2/kg medium */
                                                    /* 4 million each cartridge*/
                                                       /*convert ml o2/ ml medium into kg
o2/ kg medium */

        return source;
 }
```

```
/*********************************************************************
UDF to Define Density of Mixture (medium-dissolved O2)
Gengbei Shi, Ph.D dissertation, UNC Charlotte, 2012
*********************************************************************/

#include "udf.h"



DEFINE_PROPERTY (mix_density, c, t)

{
        real m_O_den = 1009.67;

        return m_O_den;
 }
```

```
/*********************************************************************
UDF to set soluble O2 upper limit in medium, 4 cartridges
Gengbei Shi, Ph.D dissertation, UNC Charlotte, 2012
*********************************************************************/

#include "udf.h"

DEFINE_EXECUTE_AT_END(execute_at_end)
{
        Domain *d = Get_Domain(1);
        Thread *t = Lookup_Thread(d,14);
        cell_t c;
        thread_loop_c(t,d)
        {
            begin_c_loop(c,t)
            if (C_YI(c,t,0)> 6.636e-6)
            C_YI(c,t,0) = 6.636e-6;
            end_c_loop(c,t)
         }
}
```

```
/************************************************************************
UDF to distinct different O2 diffusivity in medium only and in collagen-medium space
with cells presence, cell population 8 million per cartridge, 4 cartridges
Gengbei Shi, Ph.D dissertation, UNC Charlotte, 2012
************************************************************************/

 #include "udf.h"
 #include "mem.h"

 #define FD_MEDIUM  2.92e-9
 #define EFFD_MEDIUM_S 2.89e-9
 #define EFFD_MEDIUM_C 1.48598e-9
 #define DIFF_CELL 0.25E-9                    /*unit m2/s */
 #define PHI 7.5e-9                    /* rat hepatocytes volume per 10^6 cells*/
 #define N 8                           /* rat hepatocytes population in 10^6 */

  DEFINE_DIFFUSIVITY(O2_diffusivity, c, t, i)     /* 0 as O2 index number, define O2
diffusivity in free medium only*/
        {
                real O2_diff = FD_MEDIUM;
                int zone_ID = THREAD_ID (t);
                if (zone_ID == 14)
                O2_diff = FD_MEDIUM;                /* unit m2/s */
                else if (zone_ID == 10 || zone_ID == 11 || zone_ID == 12 || zone_ID ==
13)
                O2_diff = EFFD_MEDIUM_S*(1-(1-
DIFF_CELL/EFFD_MEDIUM_S)*(1.727*PHI*N-
0.8177*PHI*N*PHI*N+0.09075*PHI*N*PHI*N*PHI*N));
                /*define O2 diffusivity in 2nd cell-collagen-medium space, where 0.01 is
collagen hindering correction factor*/
                return O2_diff;
        }
```

APPENDIX C: ANALYSIS OF SHEAR STRESS INTENSITY IN POROUS SCAFFOLD – A SIMPLIFIED APPROACH

Since in any biodevices, increasing flow rate will increase both O_2 supply and shear stress, the balance between these two must be considered under all circumstances and an optimal flow rate is desired. However, due to irregularity and randomness of scaffold microarchitecture, analytical prediction of shear stress of interstitial flow at designated locations is difficult and computational method must be referred. These computations either assumed interconnected and uniformly sized pore [160], or based on actual microcomputer tomography (μCT)-scanned geometry [161, 162], accuracy of both cases is to be yet corroborated.

It would be pertinent to analyze the actual shear stress level in tube device for justifying the flow rate. A simple estimation can be achieved: the 15 mL conical tube has an inner diameter of 16 mm, making the cross-sectional area of the sponge disc inside as 2 cm^2, and the superficial fluid velocity (flow speed assumed uniform on cross-sectional area) through the sponge disc as 3.42×10^{-3} cm/s (given flow rate 0.41 mL/min in experiments).

For simplification, a “straight lumen” model is used to represent tortuous channel in the porous material, and fully developed laminar flow velocity distribution in pipe can be used to estimate the wall shear stress at locations hepatocytes adhere to. (Fig. C.1)

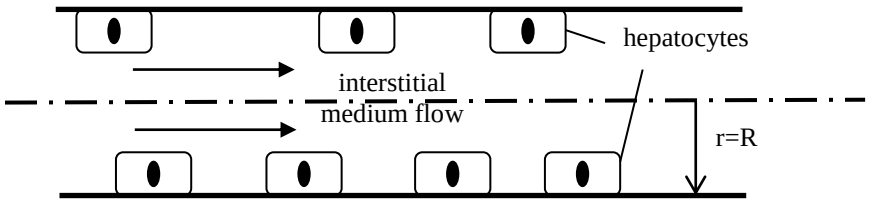

FIGURE C.1. Simplifying cell embedded tortuous channel into straight lumen for stress analysis.

The fully developed laminar flow velocity profile in a pipe is parabolic [110]:

$$u(r) = \frac{1}{4\mu}\frac{\Delta P}{\Delta L}(R^2 - r^2) \quad (C.1)$$

Given constant viscosity, the 3D shear stress tensor is defined as:

$$\boldsymbol{\tau} = \mu\left(\frac{1}{2}\right)(\nabla \boldsymbol{U} + \nabla \boldsymbol{U}^T) \quad (C.2)$$

where $\boldsymbol{U}$ is velocity vector: $\boldsymbol{U} = u\boldsymbol{i} + v\boldsymbol{j} + w\boldsymbol{k}$ and $\nabla \boldsymbol{U}$ is the gradient tensor of velocity:

$\nabla \boldsymbol{U} = \begin{bmatrix} \frac{\partial u}{\partial x} & \frac{\partial u}{\partial y} & \frac{\partial u}{\partial z} \\ \frac{\partial v}{\partial x} & \frac{\partial v}{\partial y} & \frac{\partial v}{\partial z} \\ \frac{\partial w}{\partial x} & \frac{\partial w}{\partial y} & \frac{\partial w}{\partial z} \end{bmatrix}$, $\nabla \boldsymbol{U}^T$ is the transposed matrix of $\nabla \boldsymbol{U}$.

In the simplified axisymmetric lumen, assuming fully developed flow and incompressible fluid, density ρ is constant and dynamic viscosity μ can also be regarded as constant at stable temperature (e.g., incubator chamber temperature 37°C). Thus Eqn. C.2 is simplified to:

$$\tau = -\mu\frac{du}{dr} = -\mu \cdot \frac{1}{4\mu}\frac{\Delta P}{\Delta L}(-2r) = \frac{r}{2} \cdot \frac{\Delta P}{\Delta L} \quad (C.3)$$

where u is the flow velocity through the lumen, and r is lumen radius. Assume local pressure gradient equals to the total pressure gradient, by Darcy's law it is:

$$\frac{\Delta P}{\Delta L} = \frac{\mu}{K} \cdot \frac{Q}{A} = \frac{\mu \bar{u}}{K} \quad \text{(C.4)}$$

In a specified lumen, the minimum and maximum wall shear stresses by plugging in values of μ, $\bar{u}$, R_{max}, R_{min} as well as K acquired from CHAPTER 4, are:

$$\tau_{min} = \frac{R_{min}}{2} \cdot \frac{\mu \bar{u}}{K} = \frac{R_{min}}{2} \cdot \frac{\nu \rho \bar{u}}{K} \quad \text{(C.5)}$$

$$= \frac{15\mu m}{2} \cdot \frac{0.725 \frac{mm^2}{s} \cdot 1.00967 \times 10^3 \frac{kg}{m^3} \cdot 3.42 \times 10^{-3} \frac{cm}{s}}{9.03667 \times 10^{-11} m^2} = 0.002078\ Pa$$

$$\tau_{max} = \frac{R_{max}}{2} \cdot \frac{\mu \bar{u}}{K} = \frac{R_{max}}{2} \cdot \frac{\nu \rho \bar{u}}{K} \quad \text{(C.6)}$$

$$= \frac{350\mu m}{2} \cdot \frac{0.725 \frac{mm^2}{s} \cdot 1.00967 \times 10^3 \frac{kg}{m^3} \cdot 3.42 \times 10^{-3} \frac{cm}{s}}{9.03667 \times 10^{-11} m^2} = 0.0485\ Pa$$

where ν is kinematic viscosity: $\nu = \mu/\rho$.

The maximum stress, from this simplified analysis, did not exceed the shear stress benefit bound (0.5 Pa) with average flow rate at 0.41 mL/min (pump speed: 5 rpm), and moderately higher flow rate is more likely to provide ampler O_2 than disturbing hepatocytes functionalities. However, in real pores due to tortuosity and varying diameters instead of “straight lumen with constant diameter”, the maximum shear stress in gelatin sponge should be higher than estimation above. Therefore, the speculation on flow rate is upon experimental verification.

APPENDIX D: SAMPLES OF CONFOCAL FLUORESCENT IMAGES FOR C3A CELLS VIABILITY STUDY IN CHAPTER 3

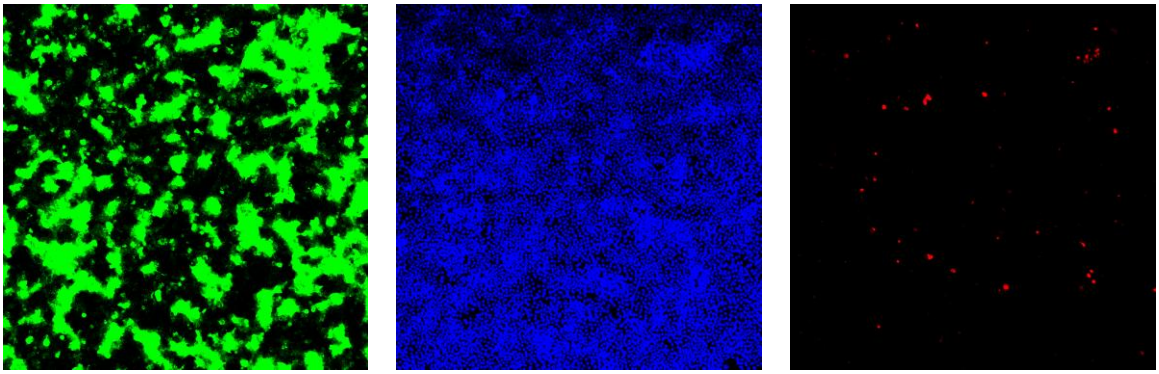

FIGURE D.1 A fluorescently stained sample field of C3A cells sandwich-cultured in 12-well plate using normal medium. LEFT: Calcein-AM stained cells that are effusive and not countable (live cells only); MIDDLE: Hoechst 33324 stained cells that are separated and countable (all cells); RIGHT: Ethidium homodimer stained cells (dead cells only). Objective 10×.

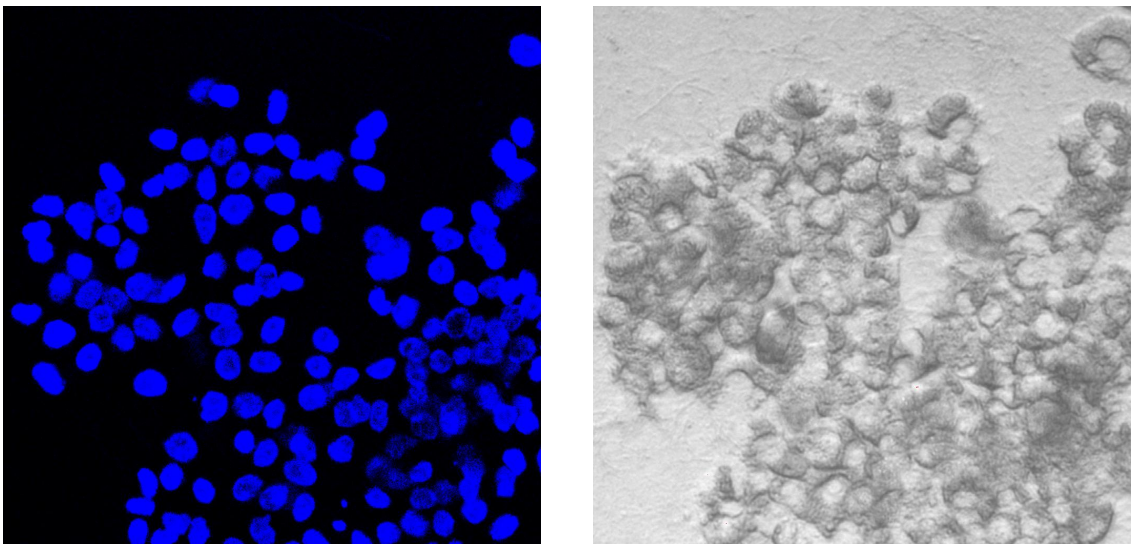

FIGURE D.2 A fluorescently stained sample field of C3A cells sandwich-cultured in 12-well plate using PFC-medium. LEFT: Hoechst 33342 stained cells; RIGHT: cells morphology at same field. Objective 20×, zoom 4×. This field had no ethidium homodimer stain mark (viability close to 100%).

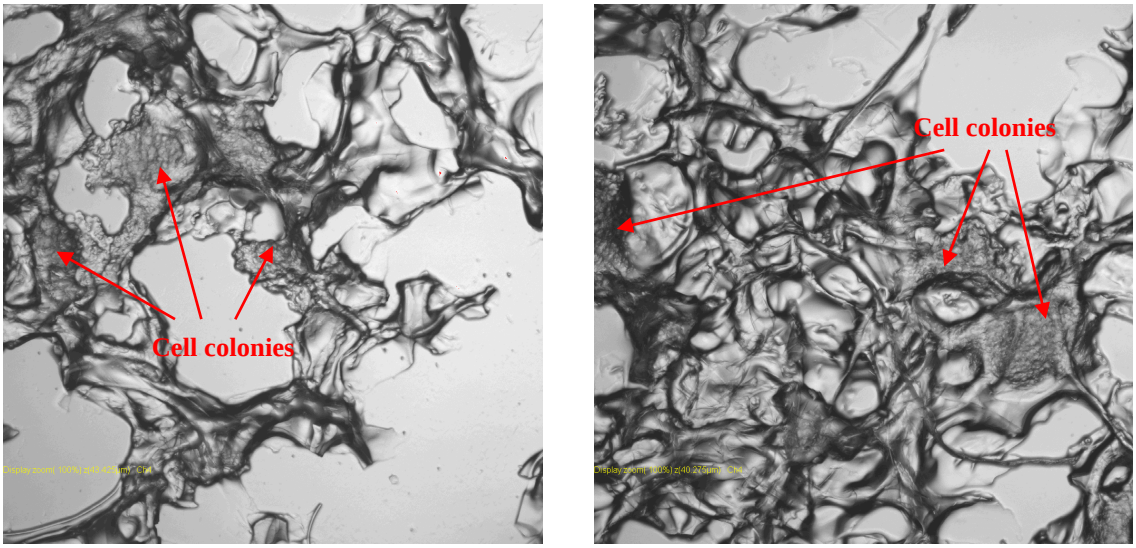

FIGURE D.3 Two random sample fields of 100 μm sliced stained gelatin sponge-C3A cells assembly cultured in flow device using normal medium, where scaffold attached cell colonies can be discerned. LEFT: random field 1; RIGHT: random field 2. Objective: 10×